

Universidade Estadual do Norte Fluminense Darcy Ribeiro

Felipe Figueirôa Moreira

Avaliação da atividade dos compostos de coordenação dinucleares de Fe(III)
em diferentes formas de *Trypanosoma cruzi*

Campos dos Goytacazes, RJ-Brasil

Março de 2023

UNIVERSIDADE ESTADUAL DO NORTE FLUMINENSE DARCY
RIBEIRO

Felipe Figueirôa Moreira

Avaliação da atividade dos compostos de coordenação dinucleares de Fe(III)
em diferentes formas de *Trypanosoma cruzi*

Tese apresentada ao Centro de Biociências e
Biotecnologia da Universidade Estadual do Norte
Fluminense Darcy Ribeiro, como parte das exigências
para obtenção do título de Doutorado em Biociências e
Biotecnologia

Orientador: Dr^o Sergio Henrique Seabra
Co-orientadora: Dr^a Juliana de Araujo Portes

Campos dos Goytacazes, RJ-Brasil

Março de 2023

FICHA CATALOGRÁFICA

UENF - Bibliotecas

Elaborada com os dados fornecidos pelo autor.

M838

Moreira, Felipe Figueirôa.

Avaliação da atividade dos compostos de coordenação dinucleares de Fe(III) em diferentes formas de *Trypanosoma cruzi* / Felipe Figueirôa Moreira. - Campos dos Goytacazes, RJ, 2023.

85 f.

Inclui bibliografia.

Tese (Doutorado em Biociências e Biotecnologia) - Universidade Estadual do Norte Fluminense Darcy Ribeiro, Centro de Biociências e Biotecnologia, 2023.

Orientador: Sergio Henrique Seabra.

1. Doença de Chagas. 2. Metalocomplexos. 3. *Trypanosoma cruzi*. 4. Amastigotas. 5. Epimastigotas. I. Universidade Estadual do Norte Fluminense Darcy Ribeiro. II. Título.

CDD - 570

**AVALIAÇÃO DA ATIVIDADE DOS COMPOSTOS DE
COORDENAÇÃO DINUCLEARES DE FE(III) EM DIFERENTES
FORMAS DE *TRYPANOSOMA CRUZI***

Felipe Figueirôa Moreira

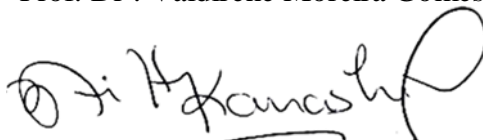
Tese apresentada ao Centro de Biociências e Biotecnologia da Universidade Estadual do Norte Fluminense Darcy Ribeiro, como parte das exigências para obtenção do título de Doutorado em Biociências e Biotecnologia

Aprovada em 20 de março de 2023

Comissão Examinadora



Prof. Dr^a. Valdirene Moreira Gomes



Prof. Dr^o. Milton Masahiko Kanashiro



Prof. Dr^o. Kildare Rocha de Miranda



Prof. Dr^a. Juliana de Araujo Portes

(Coorientadora)



Prof. Dr^o. Sergio Henrique Seabra

(Orientador)

“Dream on. Dream until your dreams come true”
(Steven Tyler)

AGRADECIMENTOS

Agradeço primeiramente à Deus por ter me dado saúde e força para superar todas as dificuldades.

À minha família e amigos por toda ajuda e confiança, pelo apoio incondicional em todas as minhas decisões desde sempre, pelos cuidados e por acreditarem na minha capacidade, por entenderem meus horários incertos e por todo amor dispensado a mim. Ninguém é nada se não tiver uma boa base sólida o suficiente para que lhe sirva de alicerce.

À todos os professores que tive ao longo de minha vida acadêmica, por uma formação de qualidade, apesar de tantas dificuldades enfrentadas pelas universidades públicas nos últimos anos. Sempre solícitos a ensinar e nos passar o máximo de conhecimento. Vocês são e sempre serão exemplos.

Ao professor Sergio Henrique Seabra pelo esforço, otimismo ímpar, por me dar a oportunidade de ingressar no meio científico e me ensinar muito do que sei hoje. Como seu aluno, agradeço por todas as oportunidades confiadas a mim e pela experiência adquirida.

À minha co-orientadora Juliana de Araujo Portes agradeço por me abrir as portas do mundo científico, me encorajando e mostrando como superar as adversidades com leveza e se fazendo presente em todas as etapas. Quero um dia poder ser tão dedicado e competente quanto você.

Ao professor Renato Augusto DaMatta, pelo amparo em todas as etapas, mesmo se desdobrando dentre tantas tarefas diárias e dedicação em manter o nosso laboratório de pesquisa. Por ter me recebido de braços abertos no laboratório, pelo incentivo e pela confiança, obrigado.

Gostaria também de agradecer a todos os integrantes e companheiros de bancada do Laboratório de Biologia Celular e Tecidual da UENF, grandes profissionais que me ensinaram a ser crítico, competente e a fazer ciência de qualidade. Em especial Pedro, Tâmara, Frederico, Ana Carolina, Saulo e Lara, que além de tornarem agradável o convívio no ambiente de trabalho, estiveram sempre que possível, dispostos a me ajudar, isso faz a diferença. Ainda por outros ensinamentos, muitas vezes involuntários, que poderiam passar despercebidos e levarei para minha vida.

Às técnicas do LBCT - Adriana, Darli, Beatriz e Giovana, pelo excelente trabalho de apoio.

À Universidade Estadual do Norte Fluminense Darcy Ribeiro - UENF e à Coordenação de Aperfeiçoamento de Pessoal de Nível Superior - CAPES, pela estrutura e concessão de bolsa.

Agradeço a todos que tiveram participação, direta ou indireta, na elaboração desta tese.

RESUMO

A doença de Chagas é uma doença negligenciada, causada pelo protozoário *Trypanosoma cruzi*, afetando de 6 e 7 milhões de pessoas em todo o mundo, principalmente na América Latina. A atual terapia utiliza Nifurtimox ou Benznidazol que geram radicais livres e provocam graves efeitos colaterais aos pacientes. Portanto, novos compostos contra este parasito são necessários. Metalocomplexos já foram testados e se mostraram ativos contra *Leishmania* spp. e *Toxoplasma gondii*, sendo uma alternativa interessante contra *T. cruzi*. Aqui avaliou-se o efeito *in vitro* de dois complexos dinucleares de Fe(III) contra epimastigotas (cepa Y) em cultivo axênico e amastigotas (cepa Dm28c) de *T. cruzi* em células epiteliais LLC-MK2. Também avaliamos a citotoxicidade dos compostos em células LLC-MK2 usando o método MTT. Possíveis alterações morfofuncionais dos parasitos foram analisadas por microscopia eletrônica de transmissão e confocal com o marcador JC-1. Os menores valores de IC₅₀ foram obtidos após tratamento de epimastigotas com complexo (1) sendo de 99,0 ± 3,0; 97,0 ± 2,0 e 110,0 ± 39,0 nM, após 48, 72 e 120 h de tratamento, respectivamente. Complexo (2) resultou em valores de IC₅₀ de 118,0 ± 5,0; 122,0 ± 6,0 e 104,0 ± 29,0 nM para os mesmos tempos de tratamento. Tratamento de amastigotas com complexo (1) gerou valores de IC₅₀ similares, de 61,3 ± 4,2 e 107,5 ± 6,6 nM para 72 e 96 h de tratamento, respectivamente. Complexo (2) gerou valores de IC₅₀ de 50,6 ± 2,2 e 173,00 ± 5,6 nM, para os mesmos tempos de tratamento. Os complexos resultaram em baixa citotoxicidade para LLC-MK2 rendendo índices de seletividade impressionantes de 167,3, complexo (1), e 454,3, o complexo (2), após 96 h de tratamento. Tratamento com os complexos resultou em epimastigotas e amastigotas com inchaço de mitocôndrias visto pela disposição anormal de sua membrana externa ao redor do cinetoplasto; epimastigotas apresentaram reservossomos alterado com espículas anormais, amastigotas apresentaram estrutura nuclear alterada, com heterocromatina concentrada no envelope nuclear. O tratamento com os complexos reduziu o potencial de membrana mitocondrial do parasito. Os complexos foram ativos contra as duas formas de *T. cruzi* apresentando IC₅₀ na faixa de nanomolar, alto índice de seletividade e afetando organelas essenciais para o parasito. Portanto, os complexos podem atuar como novos protótipos de drogas contra *T. cruzi* podendo ajudar no desenvolvimento de terapias para o tratamento da doença de Chagas.

Palavras-chave: Doença de Chagas. Metalocomplexos. *Trypanosoma cruzi*. Amastigotas. Epimastigotas.

ABSTRACT

Chagas disease is a neglected disease caused by the protozoan *Trypanosoma cruzi*, affecting between 6 and 7 million people worldwide, mainly in Latin America. Current therapy uses Nifurtimox or Benznidazole which generates free radicals and causes severe side effects to patients. Therefore, new compounds against this parasite are needed. Metallocomplexes have already been tested and appreciated as active against *Leishmania* spp. and *Toxoplasma gondii*, being an interesting alternative against *T. cruzi*. Here we evaluated the *in vitro* effect of two Fe(III) dinuclear complexes against epimastigotes (Y strain) in axenic culture and amastigotes (Dm28c strain) of *T. cruzi* in LLC-MK2 epithelial cells. We also evaluated the cytotoxicity of the compounds in LLC-MK2 cells using the MTT method. Possible morphofunctional alterations of the parasites were analyzed using transmission electron microscopy and confocal with the JC-1 marker. The lowest IC₅₀ values were obtained after treatment of epimastigotes with complex (1) being 99.0 ± 3.0; 97.0 ± 2.0 and 110.0 ± 39.0 nM after 48, 72 and 120 h of treatment, respectively. Complex (2) resulted in IC₅₀ values of 118.0 ± 5.0; 122.0 ± 6.0 and 104.0 ± 29.0 nM for the same treatment times. Treatment of amastigotes with complex (1) generated similar IC₅₀ values of 61.3 ± 4.2 and 107.5 ± 6.6 nM for 72 and 96 h of treatment, respectively. Complex (2) generated IC₅₀ values of 50.6 ± 2.2 and 173.00 ± 5.6 nM, for the same treatment times. The complexes resulted in low cytotoxicity for LLC-MK2 yielding impressive selectivity scores of 167.3 for complex (1) and 454.3 for complex (2) after 96 h of treatment. Treatment with the complexes in epimastigotes and amastigotes resulted in extension of mitochondria seen by the abnormal arrangement of their outer membrane around the kinetoplast; epimastigotes had altered reservosomes with abnormal spicules, amastigotes had altered nuclear structure, with heterochromatin concentrated in the nuclear envelope. Treatment with the complexes reduced the mitochondrial membrane potential of the parasite. The complexes were active against both forms of *T. cruzi*, presenting IC₅₀ in the nanomolar range, high selectivity index and affecting essential organelles for the parasite. Therefore, the complexes may act as new prototype drugs against *T. cruzi* and may help in the development of therapies for the treatment of Chagas disease.

Keywords: Chagas disease. Metallocomplexes. *Trypanosoma cruzi*. Amastigotes. Epimastigotes.

SUMÁRIO

1. INTRODUÇÃO	1
1.1. Doença de Chagas	2
1.2. Classificação taxonômica	2
1.3. Ciclo Biológico	3
1.4. Morfologia dos tripanosomatídeos	5
1.4.1. Flagelo	5
1.4.2. Microtúbulos subpeliculares	6
1.4.3. Mitocôndria	6
1.4.4. Cinetoplasto	7
1.4.5. Reservossomo	7
1.4.6. Núcleo	8
1.5. Meios de transmissão e sintomatologia	8
1.6. Epidemiologia	9
1.7. Estratégias atuais de tratamento contra doença de Chagas	10
1.8. Metalocomplexos	12
2. OBJETIVOS	15
2.1. Objetivo geral	15
2.2. Objetivos específicos	15
3. TRABALHOS	16
3.1. Trabalho I - Development of new dinuclear Fe(III) coordination compounds with <i>in vitro</i> nanomolar antitrypanosomal activity	16
3.2. Trabalho II - Dinuclear Fe(III) coordination compounds at nanomolar concentration reduce the <i>in vitro</i> growth and changes the structural organization of <i>Trypanosoma cruzi</i> amastigotes	40
4. DISCUSSÃO	61
5. CONCLUSÃO	66
6. REFERÊNCIAS BIBLIOGRÁFICAS	67

1. INTRODUÇÃO

A doença de Chagas (DC) representa um problema para saúde pública, por sua grande distribuição geográfica e por gerar impacto socioeconômico (WHO, 2015). Protozoários da família Trypanosomatidae são agentes causadores de doenças parasitárias que têm uma incidência elevada e representam um impacto econômico negativo nos países em desenvolvimento. A Leishmaniose, por exemplo, causada por várias espécies de *Leishmania*, afeta dezesseis milhões de pessoas na África, Ásia, partes da Europa e América Latina. A doença do sono, causada pelo *Trypanosoma brucei*, acomete cerca de três milhões de pessoas na África. Em relação à DC, causada pelo protozoário parasito *Trypanosoma cruzi*, estima-se que cerca de 6 a 7 milhões de pessoas em todo o mundo, principalmente na América Latina, estejam infectadas (WHO, 2016). No passado, a DC era restrita principalmente a países não desenvolvidos de clima tropical, como os da América do Sul. Atualmente a doença acomete também países desenvolvidos como Canadá e EUA, além de muitos países europeus e africanos, do Mediterrâneo Oriental e do Pacífico Ocidental devido a migração de pacientes infectados (WHO, 2022).

A principal forma de transmissão da DC é a vetorial, através de insetos triatomíneos hematófagos como a espécie *Rhodnius prolixus*, conhecidos popularmente como barbeiros. Outros mecanismos de transmissão possíveis são: transfusão de sangue oriundo de um doador contaminado, transplante de órgãos e transmissão vertical (NUNES *et al.*, 2013).

A DC apresenta duas fases da infecção: a aguda (fase inicial) e a crônica. A maioria dos casos na fase aguda são assintomáticos, e quando os pacientes apresentam sintomas, estes são: hepatomegalia, edema subcutâneo (sinal de Romaña) e, em casos de transmissão via vetor, são observados sinais da picada, por onde o parasito acessa o organismo (TEIXEIRA *et al.*, 2006).

Atualmente, existem apenas dois fármacos para tratamento na fase aguda da DC, sendo estes Nifurtimox e Benznidazol. Ambos requerem acompanhamento prolongado e extremamente cauteloso, pois conferem altos riscos e efeitos adversos aos pacientes. O principal efeito citotóxico de ambos está relacionado à atividade enzimática da redução do grupamento nitro que resulta na geração de radicais livres. Para tratar a fase crônica ainda não existem opções específicas de fármacos. Com isto, a busca por novas alternativas terapêuticas, que ofereçam tratamento para ambas as fases, com riscos baixos de efeitos colaterais, se faz necessária (CHAMOND *et al.*, 2002). Os metalocomplexos vem se apresentando como uma promissora alternativa em terapias antiparasitárias, e neste contexto,

nosso grupo vem descrevendo esses complexos como alternativas promissoras para o desenvolvimento de novos tratamentos de algumas doenças (PORTES *et al.*, 2018; MOREIRA *et al.*, 2021; CARDOSO *et al.*, 2022).

1.1. Doença de Chagas

A DC é uma doença crônico-degenerativa descrita pela primeira vez em 1909 pelo pesquisador brasileiro Carlos Ribeiro Justiniano Chagas (CHAGAS, 1909) e recebeu este nome em homenagem ao médico e pesquisador que a descreveu. Durante o projeto de erradicação da malária em Minas Gerais, Chagas observou a existência de uma doença causada por um protozoário flagelado. Chagas primeiro detectou estes protozoários no intestino de insetos conhecidos como barbeiros. Pesquisando possíveis hospedeiros vertebrados para este parasito, encontrou Berenice, uma criança de dois anos que se tornou o primeiro caso registrado de infecção aguda causada por este protozoário flagelado em humanos. O parasito recebeu o nome, *Trypanosoma cruzi*, em homenagem à Oswaldo Cruz, cientista pioneiro em medicina experimental no Brasil (RASSI JÚNIOR *et al.*, 2010).

A DC é também conhecida como a tripanossomíase americana, sendo uma doença potencialmente fatal. A principal forma de transmissão da doença é através do inseto vetor, conhecido como barbeiro. Estes insetos geralmente habitam rachaduras de paredes de casas de barro ou de madeira em áreas rurais ou suburbanas. O vetor normalmente se esconde durante o dia e se torna ativo à noite, quando vai à busca de alimentos como o sangue humano. Os insetos costumam picar uma área exposta da pele, como a face, e no momento do repasto sanguíneo, defecam em área próxima à da picada. Os parasitos entram no organismo quando a pessoa instintivamente coça o local da picada, ferindo a derme e assim espalhando as fezes no local da picada, podendo o parasito também alcançar os olhos, a boca ou qualquer outra parte com rupturas ou pequenas lesões na pele como a própria picada (TONG *et al.*, 1998; COURA, 2007).

1.2. Classificação taxonômica

T. cruzi pertence ao reino Protista, filo Euglenozoa, classe Zoomastigophora, ordem Kinetoplastidiae, família Trypanosomatidae, gênero Trypanosoma, subgênero Schizotrypanum, espécie *Trypanosoma cruzi*. O inseto vetor da doença, pertence ao reino

Animalia, filo Arthropoda, classe Insecta, ordem Hemiptera, família Reduviidae, gêneros *Triatoma*, *Panstrongylus* e *Rhodnius* (NEVES, 2005).

O gênero *Trypanosoma* é um dos mais importantes dentro da família Trypanosomatidae, por albergar espécies de importância etiológica, uma vez que provocam diversas doenças tanto em humanos quanto em outros animais. Entre os parasitos deste gênero está *T. cruzi*, *T. brucei rhodesiense* (causador da doença do sono da África oriental), *T. brucei gambiense* (agente etiológico da doença do sono da África ocidental), *T. equinum* (causador do mal das cadeiras em equinos), *T. equiperdum* (Durina - Equinos e asininos), entre outros (BRENNER *et al.*, 2000).

1.3. Ciclo Biológico

O parasito exibe um ciclo biológico complexo do tipo heteróxico envolvendo estágios morfológicos distintos no hospedeiro vertebrado (homem e mamíferos) como tripomastigotas e amastigotas e no inseto vetor (triatomíneos) como epimastigotas e tripomastigotas metacíclicos. Entre os tripanosomatídeos, *T. cruzi* apresenta um dos ciclos de vida mais complexos, que envolve vários estágios de desenvolvimento do parasito encontrados nos hospedeiros invertebrados e nos vertebrados (LIMA *et al.*, 2008; NEVES, 2005) (Figura 1).

O ciclo se inicia quando o inseto da família Reduviidae suga o sangue de vertebrados infectados com formas tripomastigotas que circulam na corrente sanguínea, e são por isso conhecidos como tripomastigotas sanguíneos. Uma vez ingerido o sangue, os tripomastigotas são lisados no estômago do inseto (CASTRO *et al.*, 2007). Após poucos dias, os tripomastigotas sobreviventes diferenciam-se em epimastigotas e migram para o intestino, onde se dividem intensamente e aderem às membranas perimicrovilares, que são secretadas por células do intestino médio posterior do inseto (ALVES *et al.*, 2007; NOGUEIRA *et al.*, 2007). Esta etapa é importante para desencadear o processo de diferenciação dos epimastigotas, não-infectivos, em tripomastigotas metacíclicos, que são altamente infectivos. O processo de adesão de epimastigotas à membrana perimicrovilar envolve a participação de glicoconjugados expostos à superfície, e proteínas encontradas na membrana perimicrovilar parecem estar envolvidas nesse processo (ALVES *et al.*, 2007). Após a metaciclogênese, os tripomastigotas metacíclicos permanecem na ampola retal até que ocorra um novo repasto sanguíneo, momento em que essas formas serão liberadas junto com as fezes do inseto (GARCIA *et al.*, 2007).

Os tripomastigotas metacíclicos infectam várias espécies de mamíferos, incluindo humanos. Normalmente, a infecção de mamíferos ocorre no momento do repasto sanguíneo do inseto, e os tripomastigotas liberados nas fezes tem acesso ao organismo do hospedeiro vertebrado ao penetrar na pele lesionada ou via mucosas e invadem as células no local da picada como fibroblastos, macrófagos e células epiteliais. Dentro da célula hospedeira, os tripomastigotas metacíclicos são inicialmente envolvidos por um vacúolo endocítico conhecido como o vacúolo parasitóforo, mas logo conseguem escapar para o citosol, onde se diferenciam em formas amastigotas, de modo que as formas amastigotas no citosol entram em contato direto com as organelas das células hospedeiras. Após várias divisões celulares, os amastigotas se diferenciam em tripomastigotas sanguíneos, que rompem a célula hospedeira e são liberados para o meio extracelular, alcançando novos tecidos através da corrente sanguínea podendo ser ingeridos por um triatomíneo novamente durante um novo repasto sanguíneo completando assim o ciclo de *T. cruzi* (CARVALHO & DE SOUZA, 1989).

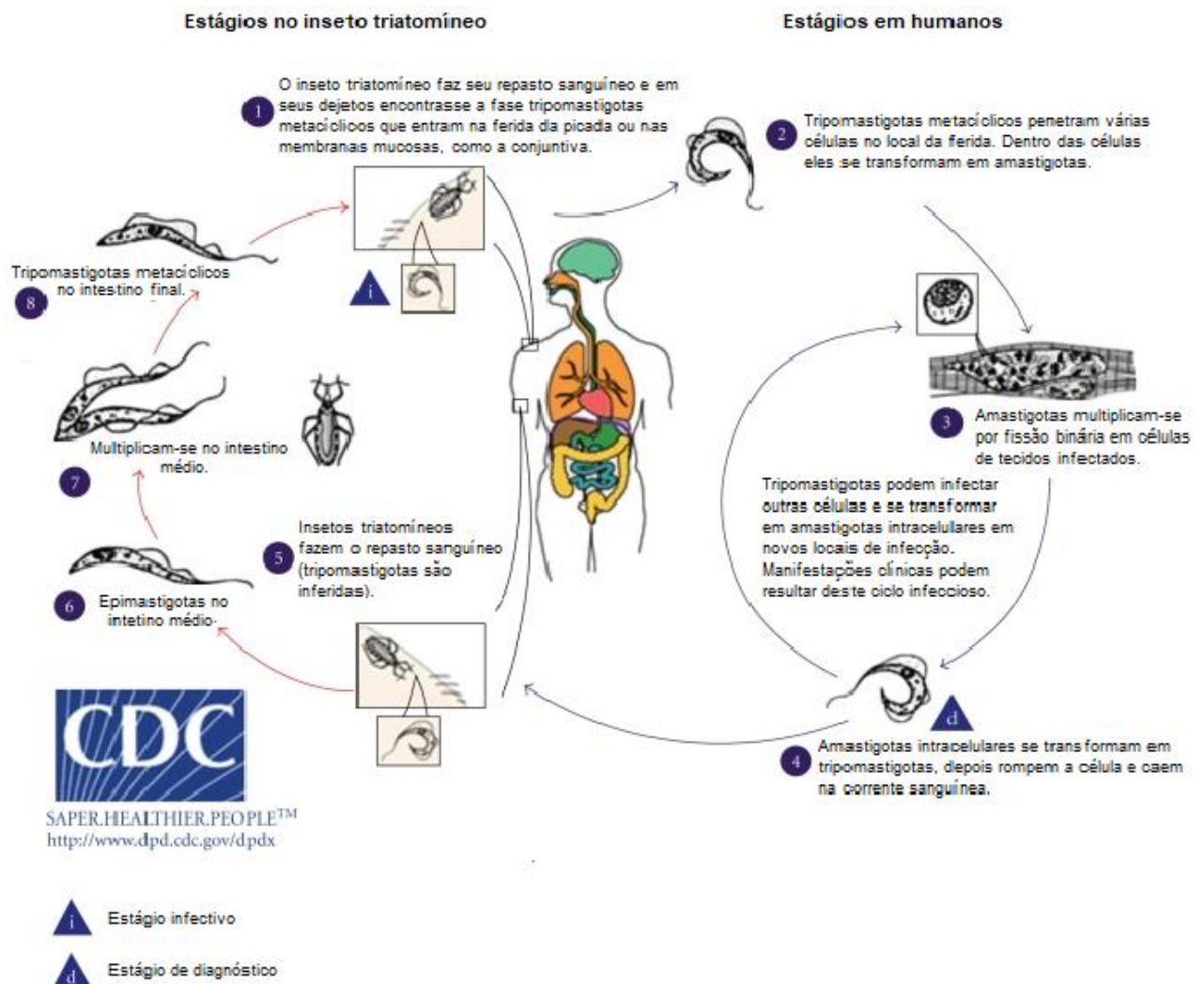


Figura 1 - Ciclo biológico do *Trypanosoma cruzi*. São apresentadas diferentes formas evolutivas do parasito em hospedeiros invertebrados (triatomíneos) e vertebrados (mamíferos). Tripomastigotas metacíclicos ganham o organismo do hospedeiro vertebrado através do repasto sanguíneo do inseto vetor (1), posteriormente tripomastigotas metacíclicos penetram em diferentes tipos celulares e se diferenciam em amastigotas (2). Amastigotas se multiplicam (3) e se diferenciam em tripomastigotas sanguíneos, durante esse processo as células infectadas rompem liberando as duas formas (4). Tripomastigotas e amastigotas infectam novas células, mas a primeira forma pode chegar ao sangue na circulação periférica. O inseto vetor faz novo repasto sanguíneo e com isso ingere tripomastigotas sanguíneos (5); no intestino do vetor essas formas se diferenciam em epimastigotas (6). Epimastigotas se multiplicam (7) e se diferenciam novamente em tripomastigotas metacíclicos no reto do vetor (8), completando o ciclo (Reproduzida a partir da homepage do *Center for Diseases Control*).

1.4. Morfologia dos tripanosomatídeos

Por serem eucariotos, os tripanosomatídeos apresentam características encontradas nas células eucarióticas típicas. *T. cruzi* possui variações morfológicas e funcionais, alternando entre formas proliferativas, epimastigotas e amastigotas, e infectantes, tripomastigotas (ZUMA *et al.*, 2021) (Figura 2). Dentre as diversas organelas, nessa seção destacaremos algumas de maior relevância a este trabalho.

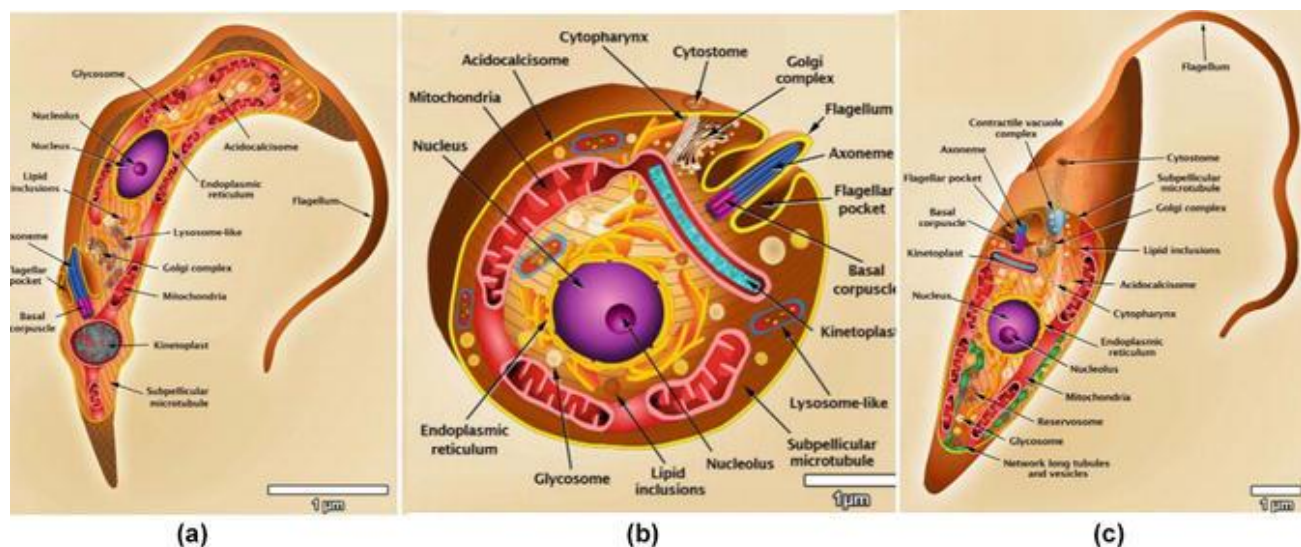


Figura 2. Representações esquemáticas das organelas do *T. cruzi*. (a) tripomastigota, (b) amastigota e (c) epimastigota). Essas imagens foram feitas com base em micrografias de microscopia de luz, bem como microscopia eletrônica de varredura e transmissão (Adaptado de Teixeira *et al.*, 2012).

1.4.1. Flagelo

O flagelo é uma organela característica de todos os membros da família Trypanosomatidae. Existe apenas um flagelo por célula, mas em uma célula em divisão,

podem ser observados dois flagelos. O flagelo de *T. cruzi* tem seu comprimento variável de acordo com o estágio de desenvolvimento que se encontra. É mais curto e internalizado em amastigotas, que tem sua proliferação no interior da célula do hospedeiro. O aumento no comprimento do flagelo ocorre durante a diferenciação de amastigotas em epimastigotas ou tripomastigotas. Nessas duas últimas etapas, o flagelo se apresenta aderido ao corpo do protozoário, terminando livremente na porção anterior. Estudos anteriores mostraram que a membrana flagelar é pobre em proteínas, mas apresenta alguns agregados que ajudam no estabelecimento da típica zona de fixação do corpo da célula flagelar. Esta organela se apresenta sempre associada à bolsa flagelar e desempenha diversos papéis fisiológicos em processos como locomoção, fixação, detecção e até produção de vesículas extracelulares e nanotúbulos que podem ser liberados para o meio extracelular. Durante o ciclo biológico, o flagelo não se desprende da célula, é encurtado durante a diferenciação tripomastigota-amastigota e cresce novamente durante a diferenciação amastigota-tripomastigota (DE SOUZA & SOUTO-PADRÓN, 1980).

1.4.2. Microtúbulos subpeliculares

Os denominados microtúbulos subpeliculares se apresentam como uma rede de túbulos formada por um arranjo longitudinal de heterodímeros de α e β tubulina, formando um padrão helicoidal ao longo do longo eixo do corpo do protozoário. Esses microtúbulos se originam na região anterior e se projetam para a região posterior. Além disso, existem outros microtúbulos citoplasmáticos como um grupo de quatro microtúbulos, conhecido como “quarteto de microtúbulos”, que se origina na região onde está localizado o corpo basal e se estende para a região anterior da célula, intimamente associado ao zona de fixação do flagelo, que aparece como uma estrutura filamentosa (DE SOUZA & SOUTO-PADRÓN, 1980).

1.4.3. Mitocôndria

A mitocôndria é uma organela que converte energia necessária para o crescimento, diferenciação e homeostase do cálcio nos tripanosomatídeos. A mitocôndria desta família é peculiar entre as células eucarióticas, visto que possuem apenas uma unidade, diferente das múltiplas cópias presentes nas células dos mamíferos, que nesse caso possibilitam que uma compense a função da outra quando danificada (CASSOLA, 2011). Além da quantidade, outra característica especial das mitocôndrias dos tripanossomatídeos é sua localização especificamente distribuída ao longo do corpo celular, próximo à membrana e sob os microtúbulos subpeliculares (FIDALGO & GILLE, 2011). A biogênese da mitocôndria

nesses parasitos é coordenada com a divisão da célula inteira, diferente do que é observado em células de mamíferos. A primeira observação da mitocôndria dos tripanossomatídeos sugeriu que havia apenas uma organela por célula, o que foi confirmado posteriormente usando reconstrução 3D (CASSOLA, 2011; VAN HELLEMOND *et al.*, 2005; DE SOUZA *et al.*, 2009). Essa organela é geralmente afetada durante tratamentos variados, apresentado um inchamento que pode ser detectado pela análise ultraestrutura do cinetoplasto (MENNA-BARRETO *et al.*, 2014; MOREIRA *et al.*, 2021, ROCHA *et al.*, 2023).

1.4.4. Cinetoplasto

O cinetoplasto se apresenta no interior da mitocôndria sendo constituído pelo DNA mitocondrial, conhecido como kDNA que é composto por uma rede única de DNA circular exclusivo de organismos da ordem Kinetoplastida. O cinetoplasto se encontra próximo à bolsa flagelar, perpendicular ao flagelo, e está conectado ao corpo basal por filamentos de proteínas (MORRIS *et al.*, 2001). O arranjo do kDNA varia entre os membros da família, bem como entre os estágios de vida de uma mesma espécie. Por exemplo, tripanossomatídeos que contêm uma bactéria endossimbiótica no citoplasma, como *Strigomonas culicis* e *Angomonas deanei*, possuem um cinetoplasto arredondado e a rede é mais frouxa em comparação com as formas epimastigota e amastigota do *T. cruzi*, cujo kDNA é mais compactado e se apresenta em formato de barra. Por outro lado, tripomastigotas de *T. cruzi* apresentam um cinetoplasto globular com fibras frouxamente arranjadas (DE SOUZA, 1984).

1.4.5. Reservossomo

O destino final do material internalizado pelos tripanosomatídeos são os reservossomos, grandes organelas capazes de acumular as macromoléculas ingeridas pelo parasito por meio do processo de endocitose (GRUENBERG, 2001). Presentes em grande número na porção posterior do corpo do parasito, eles têm uma matriz densa, membranas internas e inclusões lipídicas (MONTEIRO *et al.*, 2001; SANTOS *et al.*, 2005). Essas inclusões lipídicas são compostas, em sua maioria, por colesterol e ésteres de colesterol, derivados da endocitose de componentes séricos. Em condições de privação de nutrientes, as epimastigotas podem mobilizar essas reservas lipídicas para manter suas funções fisiológicas (PARUSSINI *et al.*, 2003). Reservossomos têm um pH ácido em torno de 6,0, sendo inicialmente comparado aos endossomos tardios de células de mamíferos (GRUENBERG, 2001). No entanto, organelas semelhantes aos lisossomos foram

recentemente considerados devido à sua intensa atividade proteolítica e capacidade de armazenamento de nutrientes (SOARES & DE SOUZA, 1988).

1.4.6. Núcleo

O núcleo dos tripanossomatídeos ocupa um grande espaço no citoplasma. É facilmente visto por microscopia de luz e a microscopia eletrônica de transmissão mostra uma morfologia típica com bastante heterocromatina. Como em outros eucariotos, o núcleo dos tripanossomatídeos inclui o envoltório nuclear provido de poros, intermediando a comunicação entre a matriz nuclear e o citoplasma, e uma membrana externa, que é contínua com o retículo endoplasmático. Porém, nesses protozoários, essa organela se diferencia pelo menor tamanho e pela ausência de cromossomos condensados (DE SOUZA, 2002). Além disso, nesses organismos, a divisão do núcleo é altamente coordenada com outras estruturas, como o cinetoplasto, o corpo basal e o flagelo (ELIAS *et al.*, 2002). Vale ressaltar que nos tripanossomatídeos o nível de condensação da cromatina varia de acordo com a fase do ciclo biológico do parasito, como observado nos epimastigotas e tripomastigotas do *T. cruzi*. A cromatina da forma proliferativa é menos condensada em comparação com a do estágio infeccioso (ALSFORD *et al.*, 2004; JANZEN *et al.*, 2006). A condensação da cromatina na periferia nuclear, retração do citoplasma, fragmentação DNA, inchaço mitocondrial e ativação de caspases são características típicas de morte celular programada similar a apoptose (SALVESEN & DIXIT, 1997; DEOLINDO *et al.*, 2010)

1.5. Meios de transmissão e sintomatologia

Além da transmissão pelo inseto vetor, outros importantes mecanismos de transmissão devem ser considerados, como a transfusão de sangue, transmissão vertical e através de transplante de órgãos. Atualmente estes mecanismos são muito menos frequentes devido a programas de controle de vetores e maior segurança biológica em processos de doação de sangue. *T. cruzi* pode também ser transmitido, em menores ocorrências, através do consumo de alimentos contaminados pelas fezes do barbeiro e acidentes laboratoriais (DIAS *et al.*, 2008). No entanto, mostrou-se que o parasito pode ser transmitido por via oral (YOSHIDA, 2009), ocasionada principalmente pela ingestão de caldo de cana, açaí e palmito de açaizeiro contaminados e não pasteurizados (NÓBREGA *et al.*, 2009).

T. cruzi induz uma infecção aguda que dura menos de 90 dias, com elevada parasitemia no sangue e sintomas geralmente brandos ou não específicos, o que faz com que o

diagnóstico muitas vezes seja falho. No entanto, em alguns casos, a fase aguda pode ser fatal, ou ainda levar a quadros de miocardite e meningoencefalite (BERN *et al.*, 2008). No local da entrada do parasito pode haver formação de uma lesão inflamatória, conhecida como Chagoma de inoculação. Se o local da infecção for a mucosa ocular, o chagoma é chamado de Sinal de Romaña, um edema unilateral e bipalpebral. Dentro das células do organismo hospedeiro, o parasito começa a se multiplicar em ciclos assíncronicos, promovendo destruição tecidual. Em muitos indivíduos a fase aguda apresenta sintomas bem discretos. No entanto, quando há manifestações, estas ocorrem em um período de 7 a 14 dias e incluem febre, hepatoesplengomegalia, náuseas, vômito, diarreia, anorexia, irritação da meninge e conjuntivite. Um pequeno número de pacientes desenvolve miocardite, podendo apresentar taquicardia, cardiomegalia e falência cardíaca. A fase aguda é seguida por uma fase crônica na qual a parasitemia diminui, atingindo níveis baixos que impedem a detecção do parasito por exames de sangue direto (TANOWITZ *et al.*, 1992).

Na fase crônica da doença, os parasitos estão alojados principalmente no coração e músculo liso do sistema digestivo. Até 30% dos pacientes sofrem de distúrbios cardíacos e até 10% sofrem de problemas no sistema digestivo (tipicamente alargamento do esôfago ou do cólon), ou alterações neurológicas mistas. Nos anos posteriores à infecção, pode ocorrer morte súbita ou insuficiência cardíaca causada por destruição progressiva do músculo cardíaco e do seu sistema nervoso periférico (COURA, 2007).

1.6. Epidemiologia

A doença é encontrada principalmente em áreas endêmicas de 21 países da América Latina, incluindo o Brasil. No entanto, nas últimas décadas, tem sido cada vez mais detectados casos da doença nos Estados Unidos da América, Canadá, em muitos países europeus e alguns países do Pacífico Ocidental. Isto pode ser facilitado principalmente devido à mobilidade da população entre a América Latina e os outros países (WHO, 2022). Segundo estimativas da Organização Mundial de Saúde (OMS), aproximadamente oito milhões de pessoas estão cronicamente infectadas com *T. cruzi* e cerca de 10.000 – 14.000 mortes por ano são causadas por DC (Revisto por RASSI JÚNIOR *et al.*, 2012). Nas áreas endêmicas, a doença acomete mais frequentemente indivíduos residentes em áreas rurais devido à coabitação entre insetos vetores infectados, animais domésticos e o próprio homem (DIAS, 2007).

Em países anteriormente considerados livres da doença, tais como Japão e Austrália, desde 2018 novos casos são cada vez mais relatados (Figura 3). Em 2006, o Brasil foi certificado pela OMS como uma área livre de DC em relação à transmissão vetorial por *Triatoma infestans* (RASSI, 2010; SILVEIRA & DIAS, 2011), e embora a prevalência da DC tenha diminuído nas últimas décadas no Brasil, cerca de 2,4% ou 4,6 milhões de brasileiros estão infectados por *T. cruzi*, dados de 2012 (MARTINS-MELO *et al.*, 2014). Dados recentes mostram que entre 2003 e 2018, foram notificados 4.556 novos casos de DC, tendo maior incidência relatada na região Norte do país (BRASIL, 2019).

Global distribution of cases of Chagas disease, based on official estimates, 2018

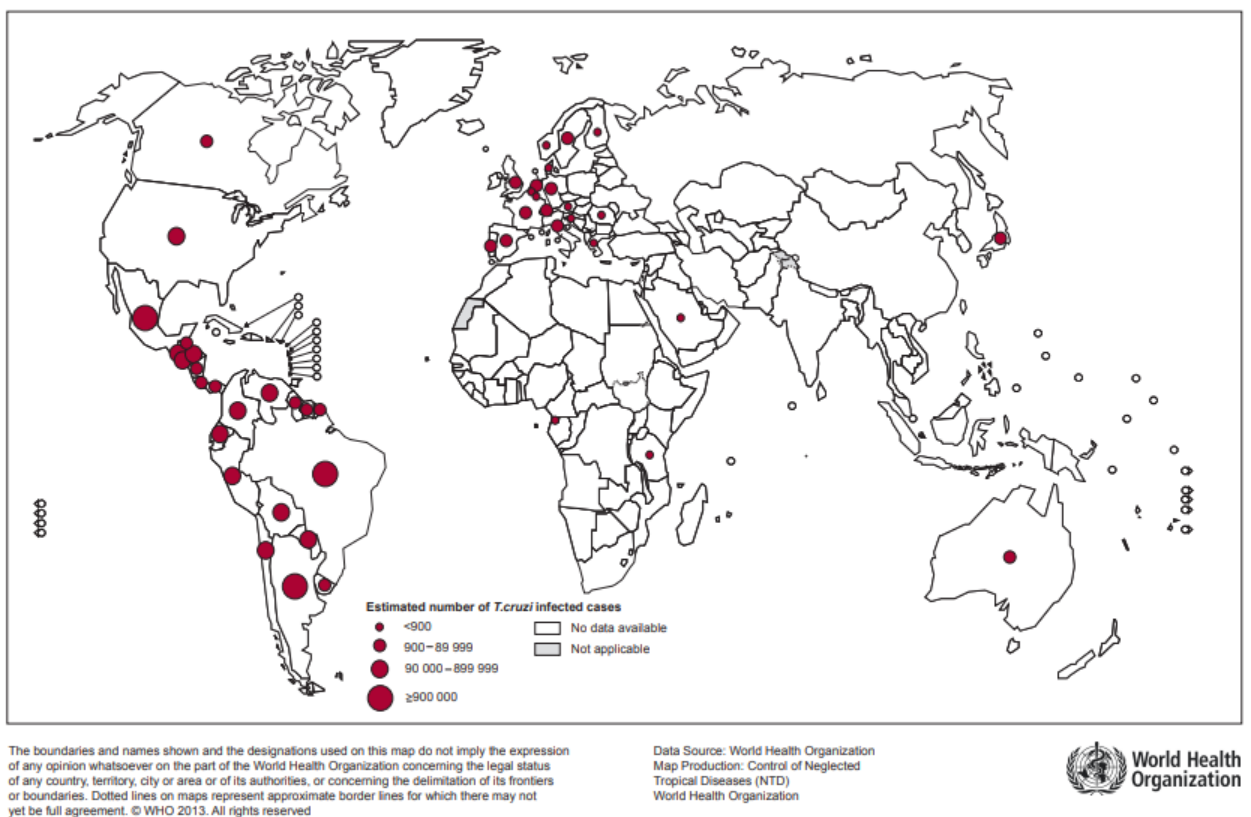


Figura 3 - Distribuição global de casos de DC. A propagação da DC em diferentes países anteriormente considerados livres da doença é problemática devido à presença de vetores nativos que podem propiciar a transmissão de infecção (Adaptado de WHO - 2018).

1.7. Estratégias atuais de tratamento contra DC

Atualmente, o tratamento utilizado é mais focado nos sintomas do que na eliminação dos parasitos no organismo do hospedeiro. Assim, do ponto de vista sintomático, procura-se amenizar as diversas manifestações da doença, através da administração de diuréticos para o tratamento da insuficiência cardíaca congestiva. Do ponto de vista etiológico, o Nifurtimox (Lampit®, Bayer) e Benznidazol (Rochagan®, Roche) são os fármacos indicados há mais

de três décadas (DIAS & SCHOFIELD, 1999) (Figura 4). Entretanto, esses fármacos são ativos somente na fase aguda da doença, e o Nifurtimox não é mais comercializado no Brasil, Argentina, Chile e Uruguai. No Brasil, o benznidazol é produzido pelo Laboratório Farmacêutico do Estado de Pernambuco (Lafepe) (FAIRLAMB, 1999; SCHOFIELD *et al.*, 2006).

O Nifurtimox (Nif, 3-metil-4-(5'-nitrofurfurilidenoamina) tetrahydro-4H-1,4-tiazina-1,1-dióxido) é um nitrofurano que foi desenvolvido pela Bayer em 1967 e comercializado como Lampit®. Age reduzindo o grupamento nitro para gerar nitro-ânions que posteriormente reagem com oxigênio molecular para produzir superóxido e peróxido de hidrogênio, responsáveis por provocar efeitos citotóxicos às células (DOCAMPO & STOPPANI, 1979). Hoje, Nifurtimox é produzido pela Bayer HealthCare na Corporación Bonima em El Salvador.

O Benznidazol (Bz, N-benzil-2-nitroimidazol acetamida) é um nitroimidazol que foi desenvolvido pela Roche em 1972 e foi anteriormente comercializado como Rochagan® ou Radanil® (COURA & BORGES-PEREIRA, 2011). Assim como o Nifurtimox, o principal efeito citotóxico do Benznidazol está relacionado à atividade enzimática da redução do grupamento nitro que resulta em radicais livres (VIOTTI *et al.*, 2009).

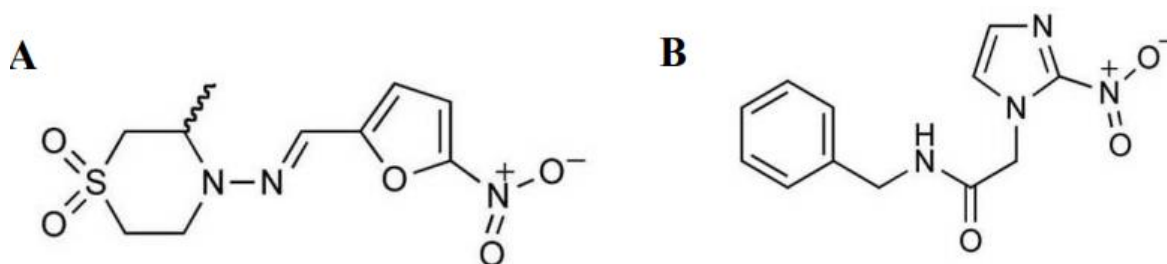


Figura 4 – Estrutura química dos compostos Nifurtimox (A) e Benznidazol (B). (Retirado de BOSCARDIN *et al.*, 2009).

O tratamento também é indicado para aqueles em que a infecção foi reativada devido à imunossupressão. Para adultos infectados, especialmente em casos assintomáticos, também deve ser oferecido o tratamento antiparasitário, pois pode prevenir a progressão da doença. Apesar dos benefícios potenciais da medicação para prevenir ou retardar o desenvolvimento da DC, deve se considerar a longa duração do tratamento, de até 2 meses, e as possíveis reações adversas, que ocorrem em até 40% dos pacientes tratados (MOREL, 1999).

Tanto o Benznidazol como o Nifurtimox provocam sérios efeitos colaterais como hiporexia, perda de peso, náuseas, vômitos, alergia cutânea e neuropatia periférica. Além disso, esses medicamentos apresentam baixa eficácia, uma vez que algumas cepas estudadas apresentam diferentes níveis de resistência para esses fármacos (VERONESI, 1991; CINQUE *et al.*, 1998; BUCKNER *et al.*, 2001).

O Benznidazol e o Nifurtimox não devem ser utilizados para tratamento de mulheres grávidas ou de pessoas com insuficiência renal ou hepática. O Nifurtimox também é contraindicado para pessoas com histórico de distúrbios neurológicos ou psiquiátricos (MONCAYO & ORTIZ YANINE, 2006).

Com base no conhecimento atual das características biológicas do parasito e do hospedeiro, um fármaco ideal para tratar a DC deveria apresentar os seguintes atributos: atividade contra as diferentes formas evolutivas do parasito presentes nos hospedeiros mamíferos e nos diferentes reservatórios do parasito, necessidade de administração oral de poucas doses, baixa toxicidade e um perfil de segurança melhorado (incluindo possibilidade de tratamento para crianças e mulheres em idade reprodutiva), baixo custo e estabilidade adequada para manutenção em temperaturas tropicais e que apresente níveis elevados de acúmulo nos tecidos e com meia-vida longa (NWAKA & HUDSON, 2006).

1.8. Metalocomplexos

Os metais de transição oferecem mais vantagens quando comparados a outros fármacos comuns baseados em compostos orgânicos. Estas vantagens se devem ao fato de os metais possuírem diferentes possibilidades de coordenação e geometria com o ligante de interesse, o fármaco, além de grande diversidade estrutural (VAN RIJT & SADLER, 2009). Podem também apresentar diferentes estados de oxidação, além de interagirem e se coordenarem comumente com moléculas ricas em elétrons, como proteínas e DNA (ORVIG & ABRAMS, 1999).

A coordenação dos metais com os ligantes resulta em uma configuração tridimensional, onde a molécula pode reconhecer alvo molecular e realizar a interação de forma mais estável e específica (FRICKER, 2007). Esta coordenação pode alterar as características dos compostos utilizados, revertendo perfis de resistência da célula-alvo ao composto utilizado. Esta reversão do perfil de resistência pode ocorrer pelo fato de que os mecanismos normalmente utilizados pelas células podem não ser ativados quando o

composto está ligado a um metal. Com isso, alguns efeitos colaterais gerados pelos compostos não coordenados podem ser reduzidos após a adição de um metal. Em alguns casos há sinergismo entre o metal e o ligante, levando à diminuição das concentrações necessárias para obter a ação biológica desejada (MENDES *et al.*, 2005; PÉREZ-REBOLLEDO *et al.*, 2005). Os metais podem possibilitar o aumento da lipofilicidade do fármaco após sua coordenação ao mesmo, facilitando a difusão através das membranas biológicas (BRUIJNINCX & SADLER, 2010).

Estes complexos metálicos têm sido estudados em diferentes aplicações biológicas para combater os mecanismos de resistência desenvolvidos por alguns agentes causadores de doenças (WRIGHT & SUTHERLAND, 2007). Dentre estes estudos, encontra-se a conjugação destes complexos a antibióticos, os quais demonstram propriedades terapêuticas mais eficazes quando comparado ao fármaco não coordenado. Complexos formados com o metal de transição Pd e o antibiótico tetraciclina apresentaram atividade antibacteriana contra linhagem resistente de *Escherichia coli*. O composto coordenado à tetraciclina mostrou atividade 16 vezes maior do que a droga não coordenada (GUERRA *et al.*, 2005).

Estudos prévios relatam metalocomplexos como alternativa à terapia anticâncer (BRUIJNINCX & SADLER, 2010). Um composto de coordenação de Cu (II) com diferentes ligantes provocaram uma inibição de 92,4% do crescimento do tumor em testes *in vivo* (BORGES *et al.*, 2016). Compostos de coordenação também de Cu (II), com diferentes ligantes, mostraram efeitos antiproliferativos contra linhagens celulares de leucemia, sendo quase 4 vezes menos tóxicos às células não cancerígenas do que a cisplatina (FERNANDES *et al.*, 2015).

Os metalocomplexos também se apresentam como alternativa na busca por compostos que ofereçam atividade antiparasitária. Nos últimos anos, nosso grupo vem desenvolvendo, caracterizando e testando compostos de coordenação contendo íons de metais de transição de primeira linha (Cu(II), Co(II), Zn(II) e Fe(III)) como uma classe química promissora com potencial para ser aplicado na quimioterapia de doenças distintas, incluindo doenças negligenciadas como toxoplasmose (PORTES *et al.*, 2015) e leishmaniose (ROCHA *et al.*, 2023). Relatamos atividade anti-*Toxoplasma gondii* e análises ultraestruturais de dois complexos de Cu(II) (PORTES *et al.*, 2017). Estes complexos também exibiram atividade antitumoral relevante (FERNANDES *et al.*, 2015). Ambos os complexos, que não apresentam Sulfadiazina (SDZ-) coordenada ao centro Cu(II), controlam de forma irreversível o crescimento *in vitro* do parasito *T. gondii* causador da toxoplasmose,

resultando em valores de IC₅₀ de 3,57 e 0,78 µM, após 48h de tratamento. Observou-se que esses compostos induzem a conversão de parte dos parasitos da forma taquizoíta para bradizoíta. A comparação entre os valores de IC₅₀ para os compostos sob investigação indica melhor eficiência quando comparado com SDZ isoladamente, sugerindo um efeito da natureza do metal e do ligante na atividade anti-*Toxoplasma* (PORTES *et al.*, 2017). Complexos de Zn e Fe(III), contendo SDZ- coordenado ao centro metálico, também exibiram atividade anti-*Toxoplasma in vitro* (BATISTA *et al.*, 2015; PORTES *et al.*, 2018). Recentemente, relatamos a atividade anti-*Toxoplasma* e estudos DFT de complexos hidrossolúveis (Fe, Cu, Zn), que facilitam a absorção e transporte intracelular, contendo o ligante N-2[(piridina-2-ilmetil)amino)etanol. Dentre todos os compostos investigados, o complexo Fe(III) [Fe(HL1)Cl₃] apresentou a melhor atividade anti-*Toxoplasma* (CARDOSO *et al.*, 2022).

Também avaliamos os efeitos de dois compostos de coordenação Co(II) na atividade antiproliferativa *in vitro* contra a forma promastigota da *L. amazonensis*, causadora das leishmanioses, mostrando um valor de IC₅₀ para o complexo (1) de 4,90 (24 h), 3,50 (48 h) e 3,80 µM (72 h), e para o complexo (2) de 2,09, 4,20 e 2,80 µM, respectivamente. O complexo (1) foi capaz de elevar o potencial de membrana mitocondrial dos parasitos após o tratamento. A microscopia eletrônica de transmissão revelou condensação apoptótica típica da cromatina, estruturas alteradas de cinetoplastos e mitocôndrias, sugerindo que a morte celular do protozoário semelhante à apoptose é provavelmente mediada por um mecanismo apoptótico associado à disfunção mitocondrial (ROCHA *et al.*, 2023).

Baseado nos dados expostos sobre metalocomplexos mostrando vantagens quando comparados a fármacos comuns e assim destacando suas propriedades químicas e atividades biológicas, os compostos metalocomplexos são possíveis alternativas para o desenvolvimento de uma nova estratégia de tratamento para a DC.

2. OBJETIVO

2.1. Objetivo geral

- Analisar os efeitos *in vitro* de compostos dinucleres de Fe (III) contra epimastigotas e amastigotas de *T. cruzi*

2.2. Objetivos específicos

- Avaliar o crescimento da população de epimastigotas em cultivo axênico e amastigotas de *T. cruzi* infectando células hospedeiras após tratamento com os compostos de Fe (III) em diferentes tempos de desenvolvimento dos parasitos.
- Avaliar as alterações na morfologia e ultraestrutura de epimastigotas e amastigotas de *T. cruzi* e viabilidade das células hospedeiras após tratamento com os compostos de Fe (III).
- Avaliar o efeito dos compostos de Fe (III) sobre o metabolismo mitocondrial do parasito, utilizando marcador específico.

3. TRABALHOS

3.1. Trabalho I

PAPER

Cite this: *Dalton Trans.*, 2021, **50**, 12242Development of new dinuclear Fe(III) coordination compounds with *in vitro* nanomolar antitrypanosomal activity†Felipe Figueirôa Moreira,^{a,b} Juliana de Araujo Portes,^c Nathália Florência Barros Azeredo,^d Christiane Fernandes,^{e,†} Adolfo Horn Jr.,^{d,‡} Cristina Pinheiro Santiago,^d Bruna Barriquel Segat,^e Giovanni Finoto Caramori,^e Leticia Maria Pequeno Madureira,^e Dalber Ruben Sanchez Candela,^f Marcelo Monteiro Marques,^g Jackson Antônio Lamounier Camargos Resende,^h Wanderley de Souza,^c Renato Augusto DaMatta^b and Sergio Henrique Seabra^{a,b}

Chagas disease is a neglected tropical disease caused by the protozoan pathogen *Trypanosoma cruzi*. The disease is a major public health problem affecting about 6 to 7 million people worldwide, mostly in Latin America. The available therapy for this disease is based on two drugs, nifurtimox and benznidazole, which exhibit severe side effects, including resistance, severe cytotoxicity, variable efficacy and inefficiency in the chronic phase. Therefore, new drugs are urgently needed. Coordination compounds may be an interesting alternative for antiparasite therapy against *Leishmania* spp., *Toxoplasma gondii* and *T. cruzi*. Herein, we tested the *in vitro* effect on *T. cruzi* epimastigotes (Y strain) of two new μ -oxo Fe(III) dinuclear complexes: [(HL1)(Cl)Fe(μ -O)Fe(Cl)(HL2)](Cl)₂·(CH₃CH₂OH)₂·H₂O (**1**) and [(HL2)(Cl)Fe(μ -O)Fe(Cl)(HL2)](Cl)₂·H₂O (**2**) where HL1 and HL2 are ligands which contain two pyridines, amine and alcohol moieties with a naphthyl pendant unit yielding a N₃O coordination environment. Complexes (**1**) and (**2**), which are isomers, were completely characterized, including X-ray diffraction studies for complex (**1**). Parasites were treated with the complexes and the outcome was analyzed. Complex (**1**) exhibited the lowest IC₅₀ values, which were 99 ± 3, 97 ± 2 and 110 ± 39 nM, after 48, 72 and 120 h of treatment, respectively. Complex (**2**) showed IC₅₀ values of 118 ± 5, 122 ± 6 and 104 ± 29 nM for the same treatment times. Low cytotoxicity to the host cell LLC-MK2 was found for both complexes, resulting in impressive selectivity indexes of 106 for complex (**1**) and 178 for (**2**), after 120 h of treatment. Treatment with both complexes reduced the mitochondrial membrane potential of the parasite. Ultrastructural analysis of the parasite after treatment with complexes showed that the mitochondria outer membrane presented swelling and abnormal disposition around the kinetoplast; in addition, reservosomes presented anomalous spicules and rupture. The complexes showed low nanomolar IC₅₀ values affecting mitochondria and reservosomes, essential organelles for the survival of the parasite. The low IC₅₀ and the high selectivity index show that both complexes act as a new prototype of drugs against *T. cruzi* and may be used for further development in drug discovery to treat Chagas disease.

Received 29th March 2021.

Accepted 11th July 2021

DOI: 10.1039/d1dt01048d

rsc.li/dalton

^aLaboratório de Tecnologia em Bioquímica e Microscopia, Centro Universitário Estadual da Zona Oeste (UEZO), Rio de Janeiro, RJ, Brazil.

E-mail: seabrash@gmail.com

^bLaboratório de Biologia Celular e Tecidual, Centro de Biociências e Biotecnologia, Universidade Estadual do Norte Fluminense Darcy Ribeiro (UENF), Campos dos Goytacazes, RJ, Brazil^cLaboratório de Ultraestrutura Celular Hertha Meyer, Instituto de Biofísica Carlos Chagas Filho,

Universidade Federal do Rio de Janeiro (UFRJ), RJ, Brazil

^dLaboratório de Ciências Químicas, Centro de Ciência e Tecnologia, Universidade Estadual do Norte Fluminense Darcy Ribeiro (UENF), Campos dos Goytacazes, RJ, Brazil. E-mail: christiane.horn@ufsc.br^eDepartamento de Química, Universidade Federal de Santa Catarina (UFSC), Florianópolis, SC, Brazil^fDepartamento de Física, Universidade Federal Fluminense (UFF), Niterói, RJ, Brazil^gColégio Universitário Geraldo Reis, Universidade Federal Fluminense (UFF), Niterói, RJ, Brazil^hInstituto de Ciências Exatas e da Terra, Campus Universitário do Araguaia, Universidade Federal de Mato Grosso (UFMT), Barra do Garças, MT, Brazil† Electronic supplementary information (ESI) available: The Cartesian coordinates of all optimized geometries. CCDC 1998387 for complex (**1**). For ESI and crystallographic data in CIF or other electronic format see DOI: 10.1039/d1dt01048d

‡ Current address: Departamento de Química, Universidade Federal de Santa Catarina (UFSC), Florianópolis, SC, Brazil.

1. Introduction

Chagas disease (CD), also known as American trypanosomiasis, was first described in 1909 by the Brazilian researcher Carlos Chagas. It is caused by the intracellular obligate parasite *Trypanosoma cruzi*.¹ *T. cruzi* is a hemoflagellate protozoan of the Trypanosomatidae family, Kinetoplastida order. CD is one of the 20 neglected tropical diseases (NTDs) according to the World Health Organization.² It can be transmitted through the faeces of sucking insects belonging to the Triatominae subfamily, blood transfusions, organ transplantation, oral contamination, through laboratory accidents, congenital routes and oral infection.³ Endemic Chagas disease shows similarities to a situation in both Latin America and the US between today's global Chagas disease epidemic and the first two decades of the HIV/AIDS epidemic.⁴

The parasite exhibits a complex life cycle involving distinct morphological stages during its passage through vertebrate and invertebrate hosts, as epimastigotes and metacyclic trypomastigotes in the insect vector, and as trypomastigotes and amastigotes in the vertebrate host.^{5,6}

CD presents high morbidity and mortality load in endemic countries.^{7–9} This disease is a major public health burden because about 6 to 7 million people worldwide, mostly in Latin America, are estimated to be infected.^{10,11} The geographic distribution of the disease prevails in Latin American countries due to the presence of more than 140 species of insect vectors (Triatominae, Hemiptera, Reduviidae); hence, it is also called American trypanosomiasis.¹² Because of human migration, CD has also led to the appearance of several cases in nonendemic areas and current major concerns related to the mechanisms of transmission in these countries include transmission by the transfusion with infected blood and congenital transmission from mother-to-child during pregnancy.¹³

This disease presents an acute and a chronic phase. The former is short and marked by non-specific symptoms, complicating the diagnosis. The chronic stage of CD may generate severe intestinal and heart lesions. There is no vaccine for preventing the infection, and the only drugs that are currently used for the treatment of CD are two nitroheterocycles: nifurtimox (Lampit, Bayer) and benznidazole (Rochagan, Roche). These drugs were empirically developed in the early 1960s and have limited efficacy and induce several adverse effects, ranging from abdominal discomfort to leukopenia or peripheral neuropathy.¹⁴ Both available drugs for CD are ineffective in the chronic phase and teratogenic, causing severe side effects such as anorexia, insomnia, nausea, headache, dizziness, asthenia, peripheral neuritis, exfoliative dermatitis, thrombocytopenia, allergic purpura, nervousness, hallucinations and convulsions; and as a consequence, forcing treatment withdrawal.^{15,16}

The mechanism of action of nifurtimox and benznidazole is still being discussed, although they have been in clinical use

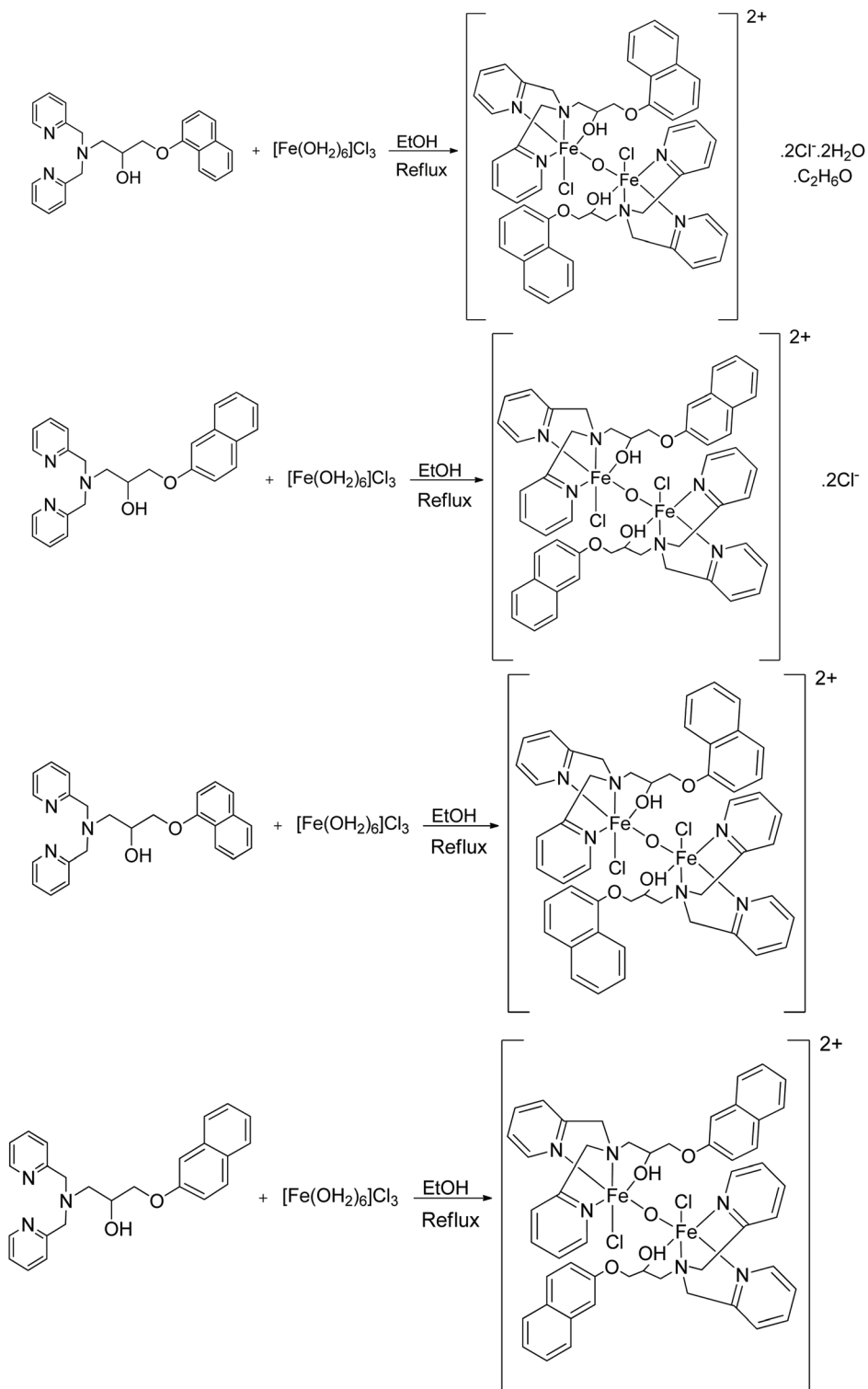
for more than 5 decades.^{17–20} Both act through the formation of free radicals and electrophilic metabolites by the reduction of their nitro group to an amino group by nitroreductases. These free radicals damage lipids, proteins, and DNA.²¹ The efficacy of this treatment is limited to the acute phase, although most patients are not treated at this stage, resulting in great economic impact related to CD.^{22,23} Furthermore, some *T. cruzi* strains have exhibited drug resistance in *in vitro* and experimental infections.²⁴ These limitations have stimulated research on novel therapeutic strategies and different classes of compounds to improve the treatment of this disease.^{25–28}

All these factors frame CD among the NTDs, and it is known that in the period from 2009 to 2018, only 0.67% of the total applied for all NTDs was addressed for CD.²⁹ Thus, there is a need to identify new active compounds against *T. cruzi*. In view of that, there is an agreement that the development of new therapeutics is urgent because parasitic diseases are among the most prevalent illnesses worldwide, emerging as a global health problem with no clinical drugs available to treat the chronic stage.³⁰

Coordination compounds have only recently emerged as a promising class of chemicals with potential to be applied in the chemotherapy of distinct disease including CD. Copper(II) complexes with ligands 1-(bis(pyridin-2-ylmethyl)amino)-3-(naphthalen-1-yloxy)propan-2-ol (HL1) and 1-(bis(pyridin-2-ylmethyl)amino)-3-(naphthalen-2-yloxy)propan-2-ol (HL2) (Scheme 1) have an antiproliferative effect inducing apoptosis-like effect against leukemia cell lines.³¹ The palladium and platinum complexes of the bioactive ligand pyridine-2-thiol *N*-oxide showed high *in vitro* growth inhibition activity (IC₅₀ of 67–200 nM) against epimastigotes of the Tulahuen 2 strain.³² The antichagasic activity of Cu(II) complexes was evaluated against the amastigote forms of CL Brener strain and the IC₅₀ ranged from 0.3 to 418 μM.³³

Metallic compounds based on palladium were able to generate morphological changes such as shortening of the cell body and inducing necrosis in *T. cruzi* epimastigotes.³⁴ A gold(III) complex was effective against both the trypomastigote and amastigote forms of *T. cruzi*. Despite its limited reduction of the parasite load in the acute phase the *in vivo* assays demonstrated reduction of the tissue parasitism in addition to protecting the liver and heart from tissue damage, leading to the survival of treated mice during the acute phase.³⁵

Toward developing new metallodrugs to tackle NTDs, we have described several coordination complexes with action against *T. gondii*, the agent that causes toxoplasmosis, inhibiting the proliferation and inducing cystogenesis.^{36–38} To contribute in the compound search against CD, as well as, to expand our understanding to changes within *T. cruzi* epimastigotes after treatment with coordination compounds, we have synthesized two iron(III) complexes (Scheme 1): [(HL1)(Cl)Fe(μ-O)Fe(Cl)(HL2)](Cl)₂·(CH₃CH₂OH)₂·H₂O (**1**) and [(HL2)(Cl)Fe(μ-O)Fe(Cl)(HL2)](Cl)₂·H₂O (**2**), in which HL1 = 1-(bis(pyridin-2-



Scheme 1 Syntheses of complexes (1) prepared with ligand HL1 and (2) prepared with ligand HL2. The proposed structures are based on X-ray diffraction data recorded for complex (1) and theoretical calculations.

ylmethyl)amino)-3-(naphthalen-1-yloxy)propan-2-ol and HL2 = 1-(bis(pyridin-2-ylmethyl)amino)-3-(naphthalen-2-yloxy)propan-2-ol. As can be seen in Scheme 1, both ligands are isomers. While HL1 contains the α -naphthoyl group, ligand HL2 con-

tains the β -naphthoyl unit. These complexes were active against *T. cruzi* epimastigotes presenting IC_{50} values in the nanomolar range, acting on mitochondria and reservosomes, essential organelles for the survival of the parasite.

2. Experimental

2.1. Materials and methods

The ligands and their respective iron(III) complexes were synthesized using commercial grade reagents. UV-Vis, electrochemical and ESI(+)-MS investigations were carried out employing spectroscopic, HPLC or MS grade solvents. All chemicals and reagents were purchased from Sigma-Aldrich and used as such. ^1H and ^{13}C NMR spectra were recorded with an NMR AS 400 spectrometer. Chemical shifts (δ) are given in ppm, and the spectra were recorded in appropriate, deuterated solvents, as indicated. TMS (0 ppm) was employed as the standard. The elemental analysis (CHN) for the complexes was performed with a PerkinElmer 2400 CHN analyzer. Infrared spectra were recorded with a Shimadzu FT-IR 8300 spectrophotometer. The solid samples were prepared in a KBr pellet and the spectra were recorded over the frequency range of 400–4000 cm^{-1} . UV-Vis spectra for the ligands and iron(III) complexes were recorded in methanol, and stability studies were performed in aqueous medium with 1% of DMSO, both in a UV-Vis Varian, Cary 50 Bio. Full scan mass spectra (MS mode) were obtained with a MicroTOF LC Bruker Daltonics spectrometer equipped with an electrospray source operating in positive ion mode. Samples were dissolved in a MeOH/H₂O (50/50) solution and were injected into the apparatus by direct infusion. The determination of melting points was performed in the Microquimica MQAPF – 307 apparatus. Thermogravimetric analyses (TGA) were performed by using a Shimadzu TGA-50 instrument. In summary, 5 mg of each sample were placed in a platinum crucible and heated from 10 to 1000 °C at a heating and a volumetric flow rate of nitrogen close to 10 °C min^{-1} and 50 mL min^{-1} , respectively.

Cyclic voltammograms (CVs) were recorded with an Autolab PGSTAT 10 potentiostat/galvanostat in acetonitrile containing 0.1 mol dm^{-3} tetrabutylammonium perchlorate (TBAClO₄) as the supporting electrolyte under an argon atmosphere at room temperature. The electrochemical cell employed was a standard three-electrode configuration: a glassy carbon working electrode, a platinum-wire auxiliary electrode and a commercial Ag/AgCl electrode immersed in a salt bridge containing 0.1 mol dm^{-3} TBAClO₄. The formal potential of the ferrocene/ferrocene couple was 0.426 V vs. the reference electrode Ag/AgCl, being established as 0.400 V vs. NHE.³⁹ Mössbauer spectroscopy of ^{57}Fe was performed at room temperature in transmission geometry. The spectra were taken with the Co-57 Rh-matrix source and the powdered sample maintained at the same temperature, moving in a sinusoidal mode. The isomer shift (δ) values are in relation to metallic iron. All the spectra were fitted with only one paramagnetic component (doublet) and the quadrupole splitting ΔE_{q} , isomer shift δ , the linewidth Γ and the absorption area were the free fitting parameters.

2.2. Synthesis

2.2.1. Synthesis of the ligands. The ligands HL1 and HL2 (Scheme 1) were synthesized as described by us in the literature.³¹

2.2.2. Synthesis of [(HL1)(Cl)Fe(μ -O)Fe(Cl)(HL2)](Cl)₂·(CH₃CH₂OH)₂·H₂O (1) and [(HL2)(Cl)Fe(μ -O)Fe(Cl)(HL2)](Cl)₂·H₂O (2). Complex (1) was prepared by the reaction between the ligand HL1 (1 mmol, 400 mg) and [Fe(H₂O)₆]Cl₃ (1 mmol, 270 mg) in ethanol (20 ml). The mixture was refluxed for 10 h. A brown solid was formed which was filtered off, washed with cold propan-2-ol and recrystallized in ethanol, affording complex (1) as red crystals. Yield: 240 mg (20%). M. p. 192 °C. Anal. calcd for [(HL1)(Cl)Fe(μ -O)Fe(Cl)(HL1)](Cl)₂·(CH₃CH₂OH)₂·H₂O (1) (C₅₄H₆₄Fe₂Cl₄N₆O₈, MW = 1178.64 g mol^{-1}): C, 55.03; H, 5.47; N, 7.13. Found: C, 55.08; H, 5.50; N, 7.22%.

Complex (2) was prepared by using the same procedure employed for (1), but only an amorphous brown solid was isolated. Yield: 121 mg (10%). M. p. 183 °C. Anal. calcd for [(HL2)(Cl)Fe(μ -O)Fe(Cl)(HL2)](Cl)₂·H₂O (2) (C₅₀H₅₂Fe₂Cl₄N₆O₆, MW = 1085.55 g mol^{-1}): C, 55.32; H, 4.82; N, 7.74. Found: C, 55.34; H, 4.85; N, 7.85%.

2.3. X-ray crystallography

Single crystals of the complex (1) were selected and X-ray diffraction measurements were performed using a Bruker D8 Venture diffractometer equipped with an INCOATEC Mo micro source at room temperature. The unit cell parameters and data integration of the reflections were performed with the APEX3.⁴⁰ All collected data were corrected for Lorentz and polarization effects and for absorption using the SADABS semi-empirical multi-scan method.⁴⁰ The structure was solved using SHELXT by intrinsic phasing methods.⁴¹ The structural model was refined by full-matrix least-squares on F^2 using SHELXL,⁴² embedded in Olex2.⁴³ The non-hydrogen atoms of the solvent molecules and the chloride ion were found in the Fourier maps. All non-hydrogen atoms were refined with anisotropic displacement parameters. Hydrogen atoms bonded to C atoms were placed at their idealized positions using standard geometric criteria. The hydrogen atoms linked to O atoms were located from Fourier maps, analyzing the geometries of the hydrogen bonds. The U_{iso} values for the hydrogen atoms were fixed at 1.2 times (for aromatic complexes and methylene) and 1.5 times (for methyl and OH) the U_{eq} of the carrier atom. The crystallographic data for the complex are given in Table 1, and the relevant structural parameters are listed in Table 3.

2.4. Computational details

Since the crystallographic structure of (1) is available, it has been used as a reference model structure (Fig. 1), and in order to simplify such a model, all counter-ions or solvent coordinated molecules have been removed. The structure was optimized with an extended-tight-binding method called xTB^{44,45} under vacuum. A preliminary systematic conformational search of complex (1) was then carried out using the conformational search workflow called iMTD-GC, as implemented in CREST software,⁴⁶ which includes functionalities such as parallel optimization and screening functions for GFNN-xTB.

Table 1 Crystallographic data for complex (1)

Chemical formula	[Fe ₂ O(C ₂₅ H ₂₅ N ₂ O ₂) ₂ (Cl) ₂] ₂ Cl ₂ (H ₂ O) ₂ (C ₂ H ₅ OH) ₂ Fe ₂ C ₅₄ H ₆₆ N ₆ O ₉ Cl ₄
MW	1196.62
Crystal system, space group	Monoclinic, <i>P</i> 2 ₁ / <i>n</i>
<i>a</i> /Å	12.292(5)
<i>b</i> /Å	19.974(9)
<i>c</i> /Å	12.365(6)
β /°	110.669(18)
Volume/Å ³	2840(2)
<i>Z</i>	2
ρ_{calc} /g cm ⁻³	1.399
μ /mm ⁻¹	0.758
Crystal size/mm ³	0.02 × 0.12 × 0.18
2 θ range for data collection/°	4.506 to 50.7
Index ranges	-14 ≤ <i>h</i> ≤ 14, -24 ≤ <i>k</i> ≤ 20, -14 ≤ <i>l</i> ≤ 14
Reflections collected	30 857
Independent reflections	5188 [<i>R</i> _{int} = 0.0540, <i>R</i> _{sigma} = 0.0347]
Data/restraints/parameters	5188/3/348
Goodness-of-fit on <i>F</i> ²	1.081
Final <i>R</i> indexes [<i>I</i> ≥ 2 σ (<i>I</i>)]	<i>R</i> ₁ = 0.0457, <i>wR</i> ₂ = 0.1003
Final <i>R</i> indexes [all data]	<i>R</i> ₁ = 0.0711, <i>wR</i> ₂ = 0.1107
Largest diff. peak/hole/e Å ⁻³	0.56/-0.36

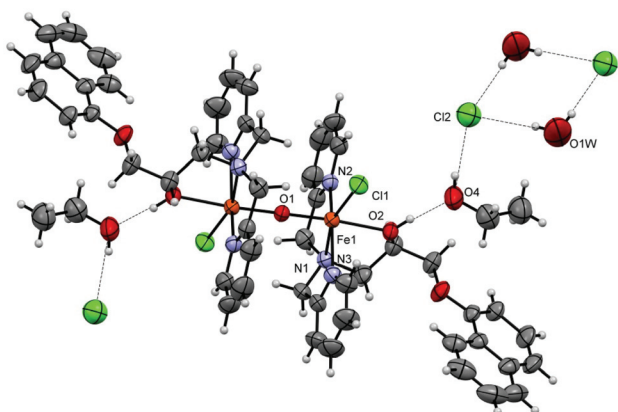


Fig. 1 Representation of the unit cell of iron(III) complex (1) (ellipsoids drawn at 50%).

Afterwards, the most stable conformers were selected for full geometry optimization with the functional BP86,⁴⁷ in conjunction with the def2-TZVP⁴⁸ basis set, D3BJ dispersion correction, and ZORA (Zero Order Regular Approximation)⁴⁹ as a relativistic approach in the ORCA program.^{50,51} The obtained structures have been checked as corresponding to minima on the potential energy surfaces, since no imaginary eigenvalues in the hessian matrix have been obtained. Additionally, the calculated normal modes are totally in line with the experimental infrared values (Tables S1 and S2†). The same procedure employed for the geometry optimization of (1) was extended to complex (2). It is worth mentioning that no crystallographic data are available for (2). In this case, the most stable conformer of (1) has been selected as the reference structure and the relative positions of naphthoyl groups changed using Chemcraft software accordingly and the entire structure was reoptimized by employing the same level of theory as described above.

2.5. Antitrypanosomal activity

2.5.1. Culture of parasite. Epimastigotes of *T. cruzi* from the virulent Y strain were grown in 25 cm² culture flasks (SPL Life Sciences) in Liver Infusion Tryptose culture medium (LIT) supplemented with 10% fetal bovine serum (FBS) at 28 °C. Culture passages were performed every 3 or 4 days by passing 0.5 mL of the culture to 5 mL of new LIT supplemented with FBS.

2.5.2. *In vitro* antitrypanosomal assay. For *in vitro* studies, iron(III) complexes were dissolved in dimethyl sulfoxide and Roswell Park Memorial Institute (RPMI) 1640 medium and stored at -22 °C. The final concentration of DMSO in the medium never exceeded 0.01% (v/v) and had no effect on the proliferation of parasites. Parasites (1×10^5) were added into culture flasks containing LIT supplemented with FBS. After 24 h, complexes were added at different concentrations and parasites were quantified every 24 h up to 120 h of treatment. Quantification of the parasites was performed by direct count through a phase light microscope in a Neubauer chamber in triplicate. Parasites were first treated with 20 μ M of the complexes; in a second series of experiments the concentration of the complexes varied from 10 nM to 200 nM and parasites were treated up to 72 h; in a third series of experiments the concentration of the complexes varied from 20 nM to 100 nM and parasites were counted after 120 h of treatment.

Results are shown as the percentage of parasite growth at different concentrations of the complexes in a distinct treatment time period. The percentage of parasite growth allows a clear observation of the treatment effect between early and late treatment time points. To calculate the percentage of parasite growth the number of the parasites of the non-treated control was set to 100% and the values of treated parasites with distinct complex concentrations were derived proportionally. For the calculations of the concentration that inhibits parasite growth by 50% (IC₅₀), the percentage of parasite growth was plotted as a function of the used concentration of the com-

plexes and a non-linear regression curve was calculated. The regression analyses were performed using Sigma Plot 8.0 software (Systat Software Inc., Chicago, IL, USA). Eventually in the longest treatment times the IC_{50} number was extrapolated⁵² based on the regression curves calculated with Sigma Plot 8.0 software (Systat Software Inc., Chicago, IL, USA). The results of the IC_{50} calculations are presented as means \pm SD of three independent biological replicates.

2.5.3. Culture of LLC-MK2 cells. LLC-MK2 kidney epithelial cells (Rhesus monkey, *Macaca mulata*) were cultured in 25 cm² culture flasks with RPMI medium (Sigma Aldrich, EUA) supplemented with 10% FBS at 37 °C under a 5% CO₂ atmosphere. Every 48 h or after the formation of confluent monolayers, cultures were treated with trypsin/EDTA solution (Sigma-Aldrich, USA) to obtain subcultures. Cell viability assay was performed in subconfluent cultures in 96-well tissue culture plates (SPL Life Sciences).

2.5.4. Cell viability assay. The effects of the complexes on LLC-MK2 host cells were evaluated based on the reduction of 3-(4,5-dimethylthiazol-2-yl)-5-(3-carboxymethoxyphenyl)-2-(4-sulfophenyl)-2H-tetrazolium (MTS). MTS (CellTiter 96® Aqueous One Solution) is bioreduced by living cells into a formazan product soluble in culture medium.⁵³ For this assay, 1×10^5 cells were seeded per well into 96-well plates and cultured with RPMI medium supplemented with 5% FBS. After 24 h the cells were washed with RPMI medium and subjected to treatment with the Fe(III) complexes at different concentrations ranging from 100 nM to 10 μ M. As a negative control, cells were cultured without the addition of the complexes in RPMI medium supplemented with 5% FBS. As a positive control, cells were cultured with 10% Triton X-100 in RPMI medium. After 24 h, 72 h and 120 h of treatment, cells were incubated with 20 μ L of MTS One solution recently prepared in RPMI medium (0.33 mg mL⁻¹) for 4 h at 37 °C and 5% CO₂, protected from light. The absorbance of the formazan product at 490 nm was determined using a Versamax microplate reader (Molecular Devices). To calculate the percentage of cell growth the absorbance value obtained with the cells of the control (no compound) was set to 100% and the values of treated cells after distinct complex concentrations were derived proportionally. The data presented were representative of at least three independent experiments. When at least 25% toxicity in relation to the non-treated control was detected, the CC_{50} was obtained by calculating the non-linear regression curve after plotting the absorbance readings of live cells by the concentration of the complex. The CC_{50} number was extrapolated⁵² based on the regression curves calculated with Sigma Plot 8.0 software (Systat Software Inc., Chicago, IL, USA). The selective index was calculated by dividing the CC_{50} by the IC_{50} .³⁷ The results of the CC_{50} calculations are presented as means \pm SD of three independent biological replicates.

2.5.5 Mitochondrial membrane potential by fluorescence microscopy. The mitochondrial membrane potential of non-treated and treated parasites (3 μ M of complexes for 120 h) was investigated using the fluorescent marker JC-1. Differential interference contrast (DIC) microscopy images

were used to visualize parasites. The parasites were incubated with 10 μ g mL⁻¹ of JC-1 in LIT for 20 min at 28 °C,⁵⁴ and were analyzed using a Zeiss LSM-710 confocal laser scanning microscope. Quantification of the mitochondrial membrane potential was performed using the fluorescence microscope by directly counting 100 parasites for each experimental condition in triplicate of three independent experiments. Parasites presenting green fluorescence labeled mitochondria were considered "inactive/altered mitochondrial membrane potential" while parasites with red labeled mitochondria were considered with active mitochondrial membrane potential.

2.5.6. Electron microscopy analysis. For analysis of the parasite ultrastructure, non-treated and treated parasites (100 nM or 1 μ M of complexes for 24 h up to 120 h) were fixed for 1 h in a solution containing 2.5% glutaraldehyde and 4% recently prepared formaldehyde in 0.1 mol L⁻¹ sodium cacodylate buffer, pH 7.4. After these procedures, the parasites were washed twice with phosphate buffered saline (PBS) for 10 min and post-fixed for 1 h in the dark with a solution containing 1% osmium tetroxide (OsO₄) and 1.6% ferrocyanide in 0.1 M sodium cacodylate buffer. Subsequently, the parasites were washed in the same buffer, dehydrated in acetone, and embedded in Epon. Ultrathin sections were stained with uranyl acetate and lead citrate and observed under a FEI Tecnai Spirit 120 kV transmission electron microscope at UEZO and at the National Center for Structural Biology and Bioimaging (CENABIO) multiuser unit of UFRJ.

2.5.7. Data analysis. Means were analyzed by two-way ANOVA with a Bonferroni multiple comparison post-test, using GraphPad Prism Software, Version 5.0 (San Diego, CA, USA).

3. Results and discussion

3.1. Synthesis and characterization

Ligands HL1 and HL2 show a N₃O coordination set provided by two pyridyl, one tertiary amine and one alcohol groups. These ligands were employed before in order to obtain copper (II) complexes which induced apoptosis in leukemia cell lines.³¹ We have observed that the presence of naphthoyl groups has improved the biological activity of coordination complexes, as was observed in the evolution of anticancer activity of a family of platinum complexes.⁵⁵

The reactions between the ligands HL1 and HL2 and the [Fe(OH₂)₆]Cl₃ resulted in red or brown complexes, which were characterized and identified as dinuclear μ -oxo iron(III) complexes. Both are stable in air and soluble in solvents such as DMF, DMSO, CH₃CN, ethanol, methanol and chloroform. They are insoluble in pure water. This behavior is different from that previously observed for iron complexes synthesized with a similar ligand 1-(bis-pyridin-2-ylmethyl-amino)-3-chloropropan-2-ol, in which there is a chloro instead of the naphthoyl group and also results in dinuclear μ -oxo iron(III) complexes.^{56,57} This suggests that the lipophilicity of these new complexes has increased due to the incorporation of the naphthoyl group into the ligand structure. The CHN elemental and TGA analyses confirm the nuclearity of the complexes. ESI

(+)-MS data confirm that the dinuclear μ -oxo core is stable in solution.

Despite the attempts, no quality diffraction data were available for complex (2), so the proposal made here is based on physico-chemical data and comparison to complex (1) which was characterized by X-ray diffraction. Complexes (1) and (2) are isomers and represent our first results obtained against *T. cruzi*. So, our aim is to investigate the effect of these complexes containing naphthoyl groups and the additional effect of the isomerism on the antichagasic activity.

3.2. Description of the crystal structure of complex (1)

The single-crystal X-ray data revealed that (1) is a centrosymmetric dinuclear Fe(III) complex. The Fe(III) ions are hexacoordinated and connected through a linear oxo bridge (Fig. 1). Each Fe(III) centre is also coordinated to three nitrogens atoms (N1, N2 and N3), and an oxygen of the ligand HL1. One chloride ligand (Cl1) completes the coordination environment. The Fe(III) centers have distorted octahedral geometries. The coordination environment is exactly the same as that observed for the complex [Cl(L)Fe(μ -O)Fe(L)Cl]2Cl·2H₂O (L = 1-(bis-pyridin-2-ylmethyl-amino)-3-chloropropan-2-ol.⁵⁶

The complex crystallizes in space group $P2_1/n$. The oxygen bridge (μ -oxo) is located in a special position $(0, \frac{1}{2}, \frac{1}{2})$. Thus, the asymmetric unit is formed by half of the molecular unity. The molecular units are connected in the crystal by hydrogen bonds through a C₆_h(16) chain motif⁵⁸ that extends along the direction [010].

The formation of a 180° angle on the Fe(1)–O–Fe(1)' is associated with the formation of a dinuclear complex, in which the oxo group is acting as a bridge, linking two mononuclear complexes. Table 2 presents the hydrogen bonds for complex (1).

Table 3 presents bond lengths and angles for complex (1). A wide range of Fe–O–Fe bond angles (from 115 to 180°) have been reported for (μ -oxo)di-iron(III) species.⁵⁹ The Fe1–O1 and Fe1'–O1 bond lengths of 1.7924(8) Å and the Fe1–O1–Fe1' angle of 180.00(2) are in the region normally found for other oxygen bridged di-iron species.⁵⁶ All other Fe–N and Fe–Cl bond lengths are also in the expected regions.

3.3. DFT study

Concerning the conformational search performed with CREST, the structure (2a) is the nearby conformer from molecule (1),

Table 2 Hydrogen bonds in complex (1)

D–H ... A	$d(\text{D–H})/\text{\AA}$	$d(\text{H}\cdots\text{A})/\text{\AA}$	$d(\text{D–A})/\text{\AA}$	D–H...A/ $^\circ$
O(4)–H(4A)⋯Cl(2)	0.82	2.24	3.051(4)	172.1
O(2)–H(2)⋯O(4)	0.85	1.77	2.616(4)	172.6
O(1 W)–H(1WA)⋯Cl(2) ⁱ	0.85	2.29	3.136(4)	173.3
O(1 W)–H(1WB)⋯Cl(2) ⁱⁱ	0.85	2.40	3.233(4)	166.8

Symmetry: (i) $\frac{1}{2} + x, \frac{1}{2} - y, -\frac{1}{2} + z$; (ii) $\frac{1}{2} - x, \frac{1}{2} + y, \frac{1}{2} - z$.

Table 3 Selected geometric parameters for the isomeric complexes (1) and (2) and the comparisons with the available crystallographic data of complex (1)

	(1)	(2)	(1) (Crystal structure)
Fe(1)–O(1)	1.728	1.720	1.7924 (8)
Fe(1)–O(2)	2.062	2.069	2.204(2)
Fe(1)–Cl(1)	2.120	2.118	2.273(1)
Fe(1)–N(1)	1.960	1.958	2.206(3)
Fe(1)–N(2)	1.933	1.946	2.145(3)
Fe(1)–N(3)	1.928	1.922	2.152(3)
O(1)–Fe(1)–O(2)	173.33	174.34	169.20(7)
O(1)–Fe(1)–Cl(1)	87.23	93.87	86.01(7)
O(1)–Fe(1)–N(1)	94.94	95.08	94.04(8)
O(1)–Fe(1)–N(2)	86.04	94.55	89.68(7)
O(1)–Fe(1)–N(3)	92.44	95.22	94.10(8)
Fe(1)–O(1)–Fe(2)	171.71	174.33	180.00

as showed at superposed molecules in Fig. 2. Schematic representation of optimized geometries of iron(III) complexes (1) and (2) at the BP86 level of theory is presented^{60,61} in Fig. 3 and the energy scale of isomer (2) most stable conformers is shown in Fig. 4. It is possible to conclude that the group with more degrees of freedom in the molecule is the naphthoyl moiety, which rotates in some directions, changing the molecular stability. The conformer (2a) has more stabilizing hydrogen bonds and less steric repulsion, since the naphthoyl groups are spatially arranged so that they are further away from the remaining molecular structure. Structure (2b) has no hydrogen bonds, and structure (2c) has hydrogen repulsion caused by the torsional angle in the naphthoyl group. Conformer (2e) is the most unstable because of the decrease of the naphthoyl group angle.

The calculated structure of complex (1) reveals an excellent agreement with the available crystallographic data for this complex (Table 3). For instance, the Fe–O–Fe calculated bond angle of the oxo-bridge is very close to 180° degrees (171.1°). The optimized structure of (1) recovers the main features of the X-ray structure of (1), in which the Fe(III) metallic centres are hexacoordinated and connected by an oxo bridge. The overlay of both calculated and crystallographic structures for complex (1) (Fig. 2a) reveals that root-mean-square distance (RMSD) values between both structures are smaller than 0.015, and for some individual groups of atoms as Fe, Cl, O, and N, are even smaller (0.003; 0.008; 0.05; and 0.005, respectively), confirming that the level of theory employed for geometry optimizations is totally adequate. Similarly, the calculated structure of isomer (2) shows slightly larger RMSDs for the same groups of atoms Fe, Cl, O, and N (0.45; 0.42; 0.96; and 0.53, respectively), indicating that it differs more significantly from (1) (Fig. 2b). For instance, the C–O–C angles of the naphthoyl group in the crystallographic structure and optimized structures of complexes (1) and (2) are, respectively, 114.31°, 117.21° and 121.03°, but in isomer (2), the naphthoyl group is 90° rotated in relation to the same group in (1), as it is possible to see in Fig. 2. Such differences are also confirmed in terms of the difference of electronic energy between

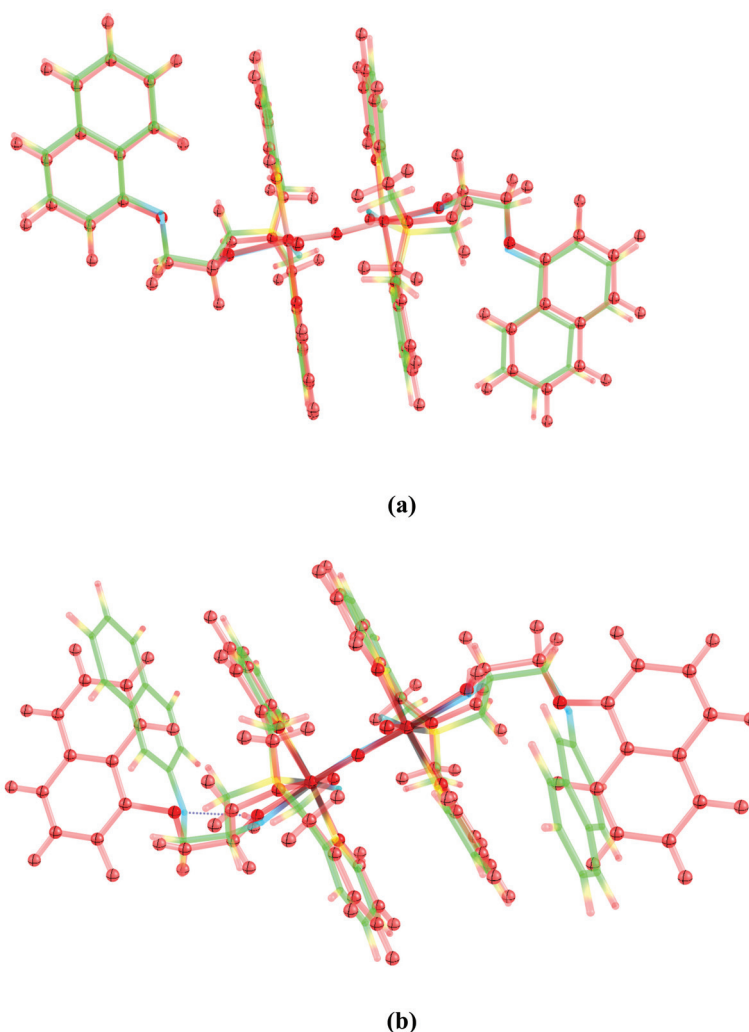


Fig. 2 Comparison scheme of superposition between the crystallographic structure of complex (1) (red ball-stick) and the optimized structures (colorful sticks) of (1) (a) and (2) (b), using the BP86/def2-TZVP level of theory.

isomers (1) and (2), complex (1) being 37.65 kcal mol⁻¹ more stable than complex (2). Table 3 presents selected geometric parameters for the isomeric complexes (1) and (2) and the comparisons with the available crystallographic data of complex (1).

3.4. Infrared, UV-Vis and TGA analyses

The IR spectra of the complexes exhibit similar bands around 3600–3100 (ν OH), 3059 (ν CH), ν (CH₂), 2936 (ν CH₂), ν (CH₂), 2877 (ν CH₂), (C=C and C=N), 1504 (s), 1485 (s), 1458 (s) and 1448 (s) (ν C=C and C=N), ν (C–O–C), 1269 (s) (ν C–O–C), γ (CH), 762 and 803 (γ CH), 828 cm⁻¹ (ν_{as} Fe–O–Fe) for complex (1) and ν (OH), 3600–3100; ν (CH), 3059; ν (CH₂), 2926; ν (CH₂), 2872; (C= and C=N), 1514 (s), 1482 (s), 1465 (s) and 1443 (s); ν (C–O–C), 1257 (s); γ (CH), 762 and 818; ν_{as} (Fe–O–Fe), 839 cm⁻¹ for complex (2) (Fig. S1†). The similarity between both IR spectra shows the similarity between the complexes. The presence of a band at 820–840 cm⁻¹ is evidence of the presence of the oxo bridge in both complexes, resulting in

dinuclear μ -oxo Fe(III) complexes, which is in agreement with the structure solved by X-ray diffraction and the theoretical calculation.

The electronic spectrum obtained in DMSO reveals that complex (1) presents absorptions at 307 nm ($\epsilon = 2 \times 10^3$ M⁻¹ cm⁻¹) attributed to intraligand $\pi \rightarrow \pi^*$ and at 355 nm ($\epsilon = 8 \times 10^3$ M⁻¹ cm⁻¹) which is attributed to LMCT Cl \rightarrow Fe(III) and oxo \rightarrow Fe(III) (LMCT = ligand to metal charge transfer) in comparison with similar complexes previously reported by us.⁵⁶ Complex (2) presents a similar spectrum, with absorption bands at 281 ($\epsilon = 2 \times 10^3$ M⁻¹ cm⁻¹), 375 ($\epsilon = 9 \times 10^3$ M⁻¹ cm⁻¹), and 329 ($\epsilon = 1.3 \times 10^3$ M⁻¹ cm⁻¹) nm (Fig. 5A and B).

The study of the stability in the medium employed in the biological investigation is very relevant to understand the behavior of a metal-based drug. In order to detect any changes after diluting the complexes in the aqueous medium (RPMI), electronic spectra of both complexes were obtained in DMSO and in H₂O (the complexes are insoluble in water; then they were dissolved previously in DMSO (0.01%). Fig. 5 shows the

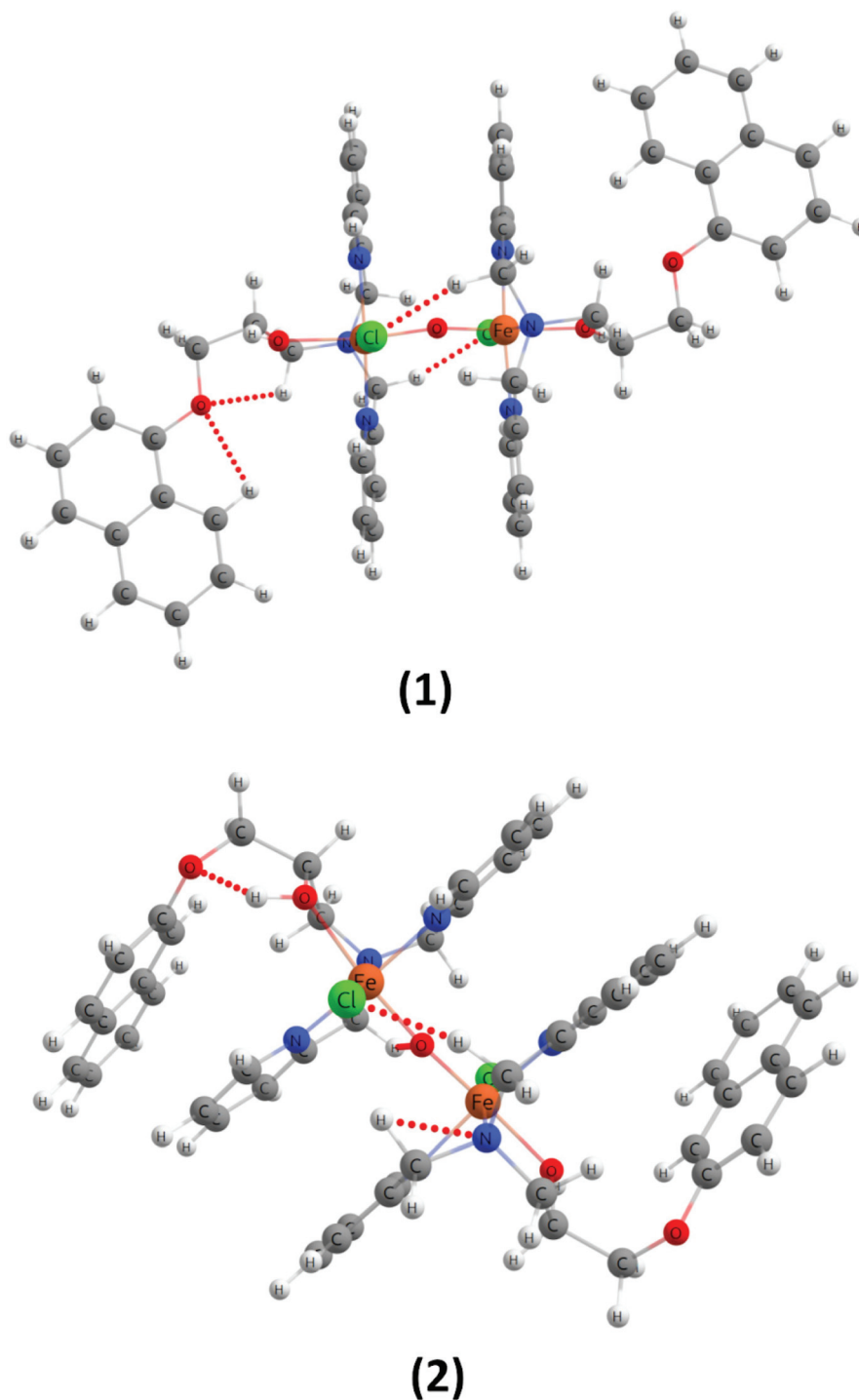


Fig. 3 Schematic representation of optimized geometries of iron(III) complexes (1) and (2) at the BP86 level of theory. Color code: green: chloride ions; grey: carbon atoms; blue: nitrogens; red: oxygens. H atoms are suppressed for the sake of clarity. The dotted red lines depict the hydrogen bonds.

spectra obtained for both complexes in the range of 300–800 nm.

The comparison between the electronic spectra obtained in DMSO (Fig. 5A and B), H₂O (containing 0.01% DMSO) (Fig. 5C and D) and in the RPMI medium (containing 0.01% DMSO)

(Fig. 5E and F) indicates that there are changes in the spectral behavior, depending on the solvent used.

In water (with 0.01% DMSO) and in the RPMI medium (containing 0.01% DMSO), changes in the spectral behavior were verified with time and the bands differ from those

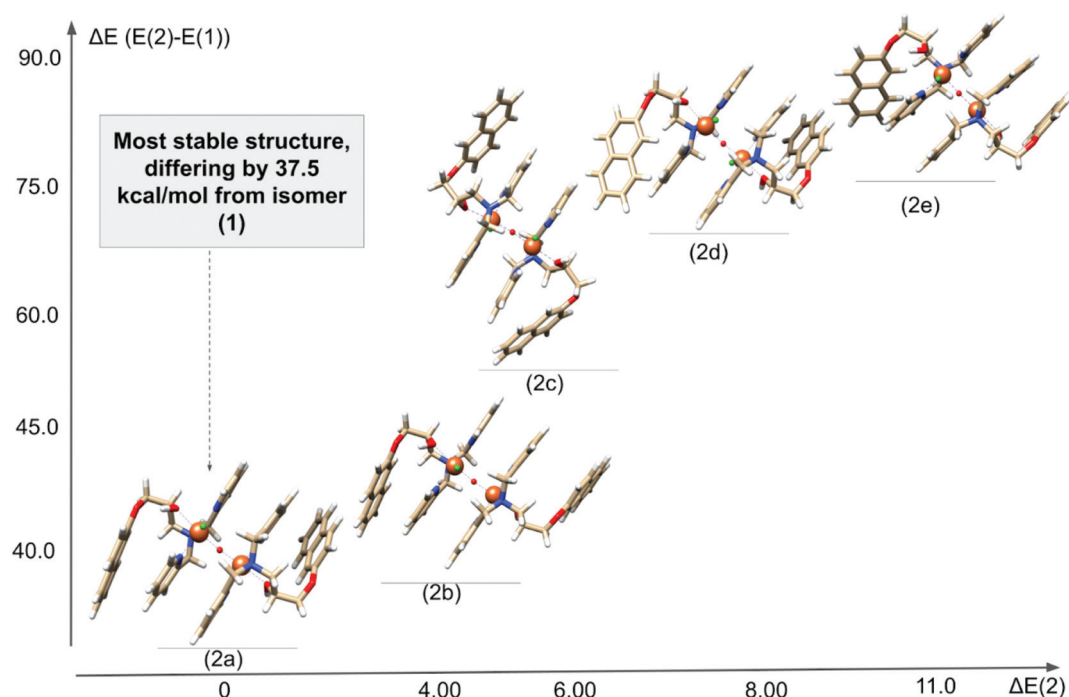


Fig. 4 Energy scale of the five most stable conformers of isomers related to complex (2). In x axis is the relative energy of the conformers compared to (2a), the most stable. In y axis, it is shown the scale of molecular energy values of conformers of complex (2) in comparison with complex (1).

obtained when only DMSO was used as a solvent, indicating that changes may be occurring in the coordination spheres of the compounds with time.

The spectrum of RPMI medium presents an absorption band at 520 nm, which is attributed to the phenol-red, one of the components of this medium. Interestingly, when in the presence of the iron(III) complexes (1) and (2), this band is shifted to 557 and 554 nm, respectively. Such effect indicates that phenol-red is interacting with the iron(III) centers promoting changes in the coordination spheres of the complexes which can result in higher solubility.

The TGA analyses were performed for both complexes and the results are presented in Table S3 and Fig. S2, in the ESI.† Below 200 °C, three mass loss processes (2 CH₃CH₂OH and 1 H₂O) are observed in compound (1), which agrees with one water and two ethanol molecules. In the X-ray analysis, two ethanol and two water molecules were observed. On the other hand, the CHN analysis, performed with the same sample used for TGA analysis, indicates the presence of two ethanol molecules and one water molecule. So, there is a small discrepancy involving the X-ray and TGA analyses concerning the number of crystallization solvents. The most intense peak in the TGA analysis for compound (1) was observed between 205 and 505 °C, with a mass loss of 35.7%. Such mass loss agrees with the oxidation of the two naphthoyl (C₁₂H₁₀O) and two chlorides. Three other oxidation processes observed from 505 to 1000 °C are related to the oxidation of the ligand molecules. In the end, a residue of 16.5% of the initial mass was obtained, which agrees with the species Fe₂Cl₂O (17.2%). This

result means that during the burn, the iron(III) centers were reduced to iron(II). Although complex (2) is a structural isomer of (1), it showed a different TGA behavior, mainly about the oxidation of the ligand and the formed residue. While compound (1) showed a mass loss of 35.7% in the range of 211–505 °C, showing an intense but broad signal in the first derivative, compound (2) had a more significant mass loss (43.4%) in the same temperature range and the first derivative evidenced the presence of three successive burn steps. Therefore, the mass loss above 500 °C was less intense in compound (2) than in (1). Another discrepancy is related to the formed residue, which was bigger for compound (2) (19.9%), in agreement with the formation of the species Fe₂Cl₂O₂, indicating that the iron centers were not reduced during the combustion. A small signal was also observed below 130 °C for (2), indicating the presence of one water molecule. The presence of this water molecule was also confirmed in the CHN analysis.

3.5. ESI(+)-MS and ESI(+)-MS/MS

ESI(+)-MS and ESI(+)-MS/MS of [(HL1)(Cl)Fe(μ-O)Fe(Cl)(HL2)](Cl)₂·CH₃CH₂OH·2H₂O (1) present a characteristic set of isotopologue ions due to mainly the presence of iron and chlorine atoms (Fig. 6). As complex (2) presents the same peaks observed in the ESI(+)-MS spectra of complex (1), as a consequence of the isomerism, just data concerning the characterization of complex (1) will be presented. Data for complex (2) are presented in the MS (Fig. S3 and S4†).

The proposals for the main peaks, based on isotopic distribution and MS/MS investigations of complex (1), are: [H2L1]⁺

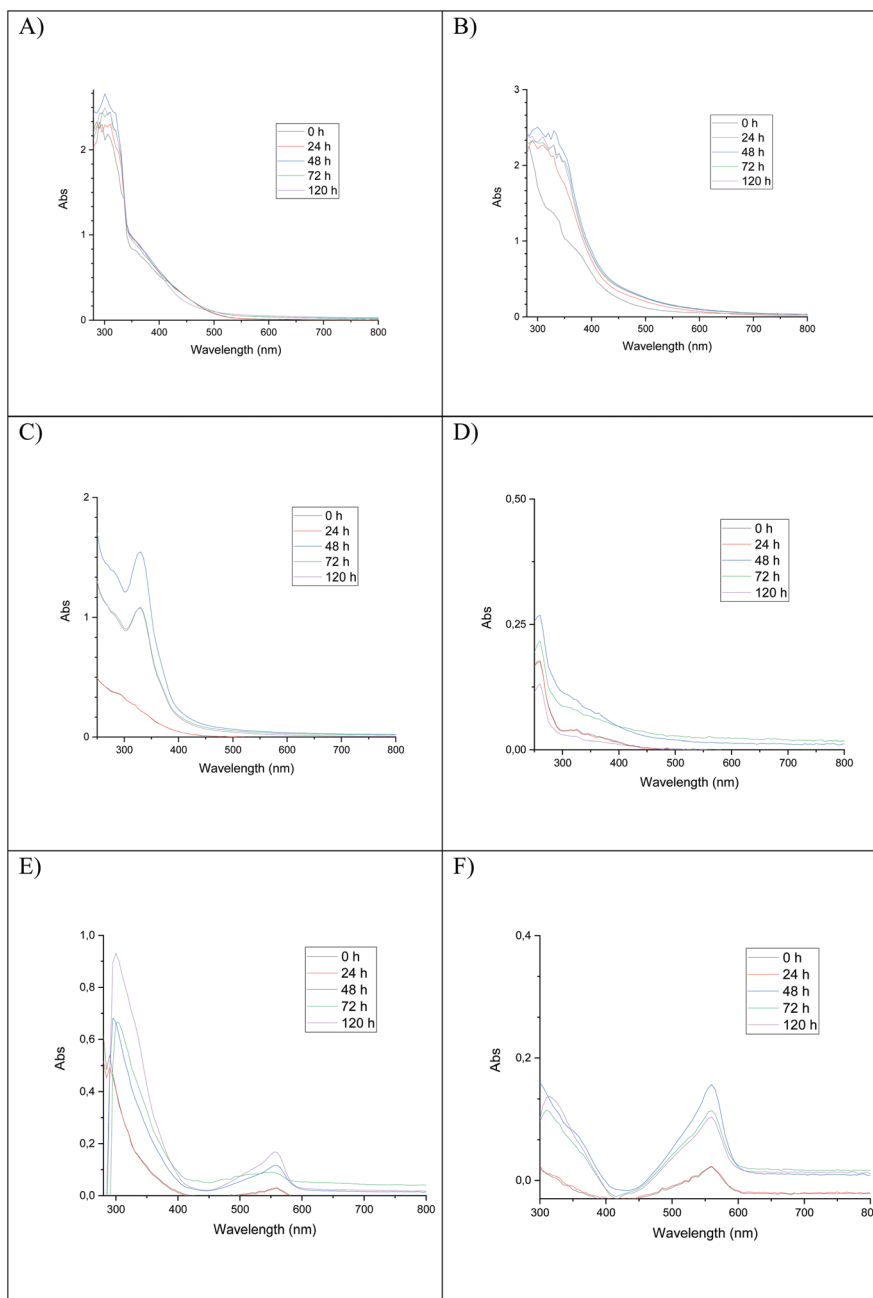


Fig. 5 (A and B) Electronic spectra of complexes (1) and (2) in DMSO (100 μM). (C and D) Electronic spectra of complexes (1) and (2) in H_2O (10 μM –0.01% in DMSO). (E and F). Electronic spectra of complexes (1) and (2) in RPMI medium (10 μM –0.01% in DMSO).

(m/z 400), $[(\text{L1})\text{Fe}(\text{III})(\mu\text{-O})\text{Fe}(\text{III})(\text{L1})]^{2+}$ (m/z 462), $[\text{Fe}(\text{III})(\text{L1})(\text{OH})]^+$ (m/z 471), $[\text{Fe}(\text{III})(\text{L1})(\text{Cl})]^+$ (m/z 489), $[\text{Fe}(\text{III})(\text{HL1})(\text{Cl})_2]^+$ (m/z 525) $[(\text{Cl})(\text{L1})\text{Fe}(\text{III})(\mu\text{-O})\text{Fe}(\text{III})(\text{L1})]^+$ (m/z 959), and $[(\text{Cl})(\text{L1})\text{Fe}(\text{III})(\mu\text{-OH})\text{Fe}(\text{III})(\text{L1})(\text{Cl})]^+$ (m/z 995). MS/MS data for the species with m/z 995 yield the species with m/z 959, 852, 562, 471 and 454 (Fig. S4[†]).

3.6. Electrochemical characterization

Complexes (1) and (2), as a result of their structural similarity, presented similar cyclic voltammograms. Fig. 7

shows the cyclic voltammogram of complex (1) at a scan rate of 25 mV s^{-1} . Complex (1) presents two irreversible redox processes with $E_{\text{pc}} = -0.28$ and at -1.00 V vs. Fc^+/Fc (A and B) attributed to $\text{Fe}(\text{III})/\text{Fe}(\text{II})$ and $\text{Fe}(\text{III})\text{Fe}(\text{II})/\text{Fe}(\text{II})\text{Fe}(\text{II})$ redox couples, respectively. The anodic process at 0.73 V vs. Fc^+/Fc can be attributed to the oxidation of chloride.

Complex (2) presents two irreversible redox processes with $E = -0.27$ and at -0.61 V vs. Fc^+/Fc (A and B) attributed to $\text{Fe}(\text{III})/\text{Fe}(\text{II})$ and $\text{Fe}(\text{III})\text{Fe}(\text{II})/\text{Fe}(\text{II})\text{Fe}(\text{II})$ redox couples, respectively.

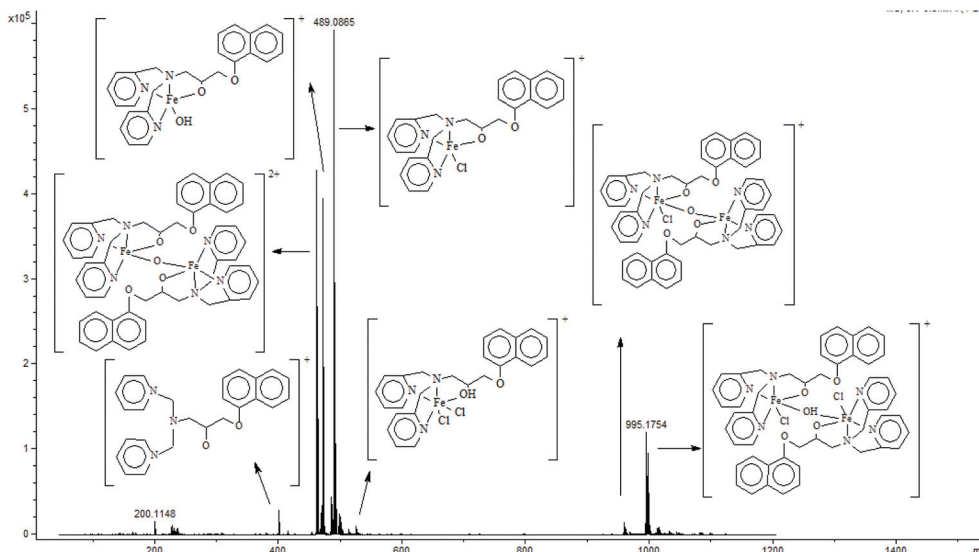


Fig. 6 ESI(+)-MS in water/methanol (1 : 1) for iron(III) complex (1) and proposals of the chemical structure for the main peaks.

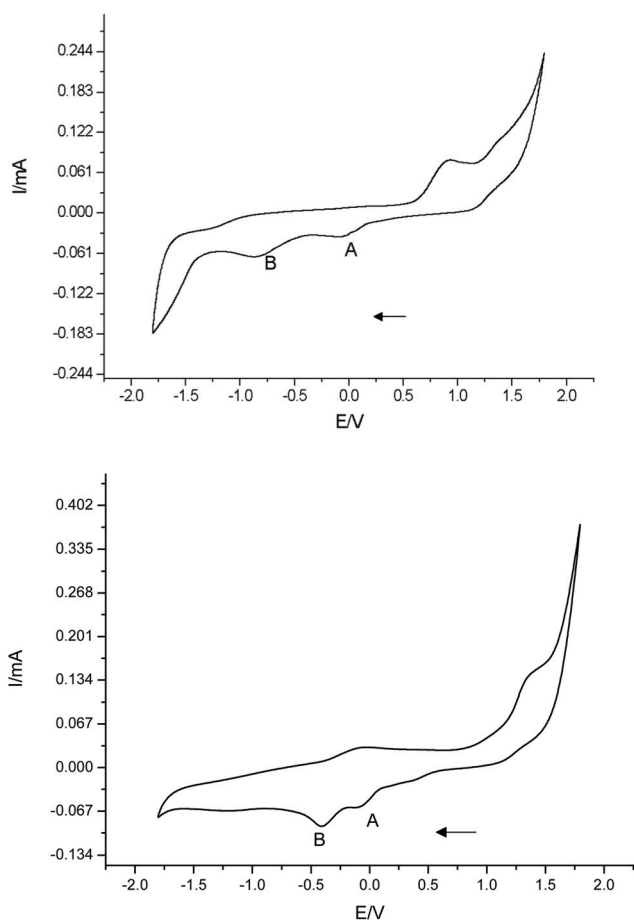


Fig. 7 Cyclic voltammogram of iron(III) complexes (1) (top) and (2) (bottom). Working electrode: platinum; pseudoreference electrode: platinum; counter electrode: platinum; supporting electrolyte: tetrabutylammonium hexafluorophosphate 0.1 mol dm^{-3} ; solvent CH_3CN , internal reference $\text{Fc}^+/\text{Fc}^\ominus$. Scan rate: 100 mV s^{-1} .

respectively. The anodic process at $1.16 \text{ V vs. Fc}^+/\text{Fc}$ can be attributed to the oxidation of chloride, as observed for complex (1).

The presence of two redox processes supports the presence of two iron(III) centers, in agreement with the X-ray data for complex (1) and ESI(+)-MS data for both complexes, suggesting the maintenance of the dinuclear arrangement in solution (acetonitrile). These processes were attributed to the successive one electron reduction $2\text{Fe(III)} + 1\text{e}^- \rightarrow \text{Fe(II)Fe(III)}$ and $\text{Fe(II)Fe(III)} + 1\text{e}^- \rightarrow 2\text{Fe(II)}$ redox couples, respectively (A and B, respectively, see Fig. 5). The presence of low current intensity and the irreversibility of the processes suggests that a partial decomposition took place after the reduction of one Fe(III) site. In this sense, it should be mentioned that the complex is unstable in solution in its mixed-valence state (Fe(III)Fe(II)) or in its totally reduced form (Fe(II)Fe(II)).

3.7. Mössbauer spectroscopy

The presence of iron(III) centers in both complexes was also confirmed by ^{57}Fe Mössbauer spectroscopy. Only one doublet was observed for each sample, indicating that iron(III) centers are equivalent, with the same coordination environment, in good agreement with our proposal. Fig. 8 shows the Mössbauer spectra of complexes (1) and (2), at room temperature. The spectrum for complex (1) was fitted with a single doublet with parameters $\delta = 0.36$ (relative to alpha-iron) and $\Delta E_{\text{q}} = 1.11 \text{ mm s}^{-1}$. For complex (2) the spectrum was fitted with two doublets with the parameters: $\delta = 0.37$ (relative to alpha-iron) and $\Delta E_{\text{q}} = 1.14 \text{ mm s}^{-1}$ (96% of Fe(III)) and $\delta = 0.35$ (relative to alpha-iron) and $\Delta E_{\text{q}} = 0.48 \text{ mm s}^{-1}$ (4% of Fe(III)). The second doublet with a lower percentage (4%) could be related to impurities since this complex is amorphous. Comparing the Mössbauer parameters for complex (1) and those relative to the higher percentage of Fe(III) in complex (2),

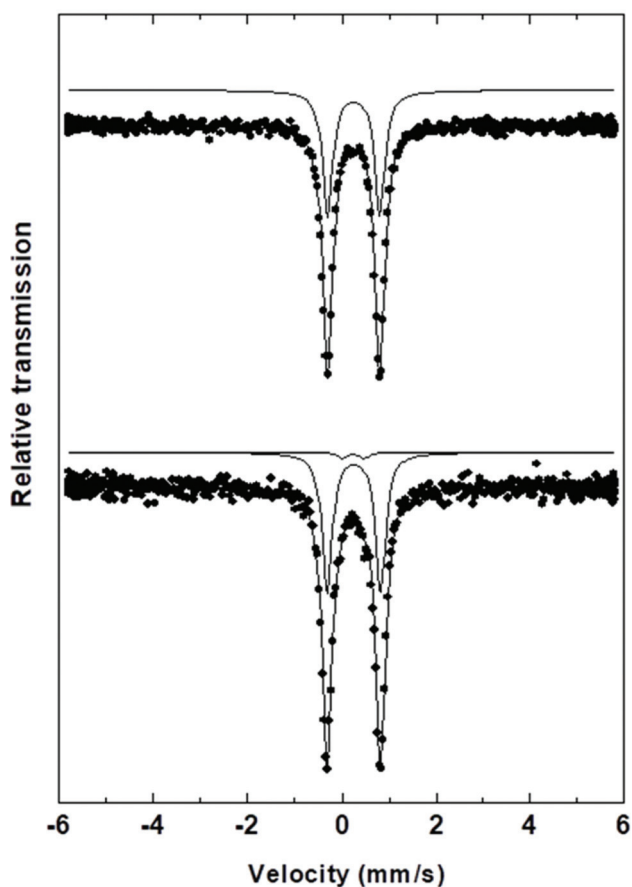


Fig. 8 Mössbauer spectra of iron(III) complexes (1) and (2), at 300 K.

it is possible to infer that the electron densities on the iron centers are similar and typical of high spin iron(III). Furthermore, these parameters are similar to those fitted for similar dinuclear μ -oxo Fe(III) complexes to $[(\text{SO}_4)(\text{L})\text{Fe}(\mu\text{-O})\text{Fe}(\text{L})(\text{SO}_4)]6\text{H}_2\text{O}$ ($\delta = 0.34$ and $\Delta E_{\text{q}} = 1.67 \text{ mm s}^{-1}$) and $[\text{Cl}(\text{L})\text{Fe}(\mu\text{-O})\text{Fe}(\text{L})\text{Cl}]\text{Cl}_2 \cdot 2\text{H}_2\text{O}$ ($\delta = 0.32$ and $\Delta E_{\text{q}} = 0.98 \text{ mm s}^{-1}$) where $\text{L} = 1$ -(bis-pyridin-2-ylmethylamino)-3-chloropropan-2-ol.⁵⁶ The values for quadrupole splitting of 1.11 and 1.14 mm s^{-1} , respectively, for complexes (1) and (2) indicate that the iron centre in complex (2) is slightly more distorted than in complex (1), reflecting the isomerism of the ligand, since complex (1) contains the ligand with the α -naphthoyl unit and complex (2) contains the ligand with the β -naphthoyl unit. Furthermore this distortion can be related to the difficulty in getting good quality crystals for this complex, despite our efforts. Then, the results of Mössbauer spectroscopy indicate that the chemical environments for the Fe(III) centres in both complexes are similar and that small differences in the quadrupole splitting values can be attributed to distortions in the coordination environment of the metal center, which are more prominent for complex (2). DFT calculations reveal substantial differences in the arrangements of the two complexes, reinforcing this analysis.

3.8. *In vitro* antiproliferative activity

Possible parasite growth inhibition was initially accessed employing 20 μM of the complexes. While non-treated parasites showed an exponential growth, parasites treated with complexes (1) and (2) were eliminated from the cultures (Fig. 9). Not even ghost cells, derived from treated parasites, were observed after 72 h of treatment.

Based on the employed concentration of both complexes which have eliminated the parasites, two sets of lower concentrations of the compounds were used to determine the IC_{50} . The percentage of parasite growth was plotted over the used concentrations of both complexes during the distinct treatment periods (Fig. 10 and 11). After 48 h of treatment with complex (1), parasite growth was lower than the control for all concentrations tested; reduction in parasite growth was from 20 to 80% when the control was compared to parasites treated with minimal and maximal concentrations, respectively; similar values were observed for 72 h (Fig. 10a) and 120 h (Fig. 10b). This shows that complex (1) was active after 48 h of treatment and sustained its effect up to 120 h. A similar trend was observed for complex (2) (Fig. 11), indicating that the nature of the isomer (α or β) presented slight influence on the antitrypanosomal activity.

Complex (1) presented the lowest IC_{50} values of 99 ± 3 , 97 ± 2 and $110 \pm 39 \text{ nM}$ for 48, 72 and 120 h of treatment, respectively. Complex (2) also presented low IC_{50} values of 118 ± 5 , 122 ± 6 and $104 \pm 29 \text{ nM}$ for the same treatment times. The IC_{50} values of complexes (1) and (2) are promising when compared to some other metal complexes reported in the literature. For example, other metal complexes (24.4 μM –31.2 μM) and the medicine benznidazole (15.8 μM) present IC_{50} values in the micromolar range after 72 h of treatment for epimastigotes of Maracay strain;⁶² the values observed for vanadium-based agents are in the range of 6.2 μM –10.5 μM while the IC_{50} observed for nifurtimox is 2.8 μM after 120 h of treatment for epimastigotes of CL Brener strain.⁶³

Some other complexes of metallic nature were active with IC_{50} values in the nanomolar range, similar to the compounds we are reporting. The palladium and platinum complexes showed IC_{50} of 67–200 nM against epimastigotes of Tulahuen 2 strain³² and copper complexes against the amastigote forms of CL Brener strain showed IC_{50} ranging from 0.3 to 418 μM .³³

Studies with compounds of a non-metallic chemical nature also show high activity, such as new 4-minopyridine derivatives, azoles and imidazoles 1 and 3–5 derivatives, which presented IC_{50} values in the low nanomolar concentration range (5.0 to 36.0 nM) against amastigotes from Tulahuen C2C4 strain. The (*S*)-1, (*S*)-3, and (*S*)-5 enantiomers showed (up to) a thousand-fold higher activity than the reference drug benznidazole.⁶⁴ Several studies have revealed the trypanocidal activity of alkaloids. In this context, quinoline derivatives have received great attention; thus 4'-odemethylancistrocladinium A, a naphthylisoquinoline alkaloid isolated from the bark and leaves of *Ancistrocladus cochinchinensis*, displayed an excellent effect against the amastigote of

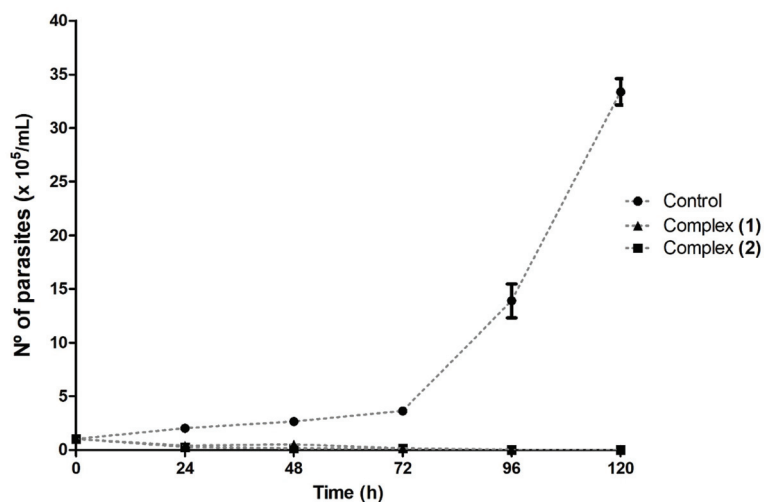


Fig. 9 Effect of iron(III) complexes (1) and (2) against epimastigote forms of *Trypanosoma cruzi* at 20 μ M for 120 h.

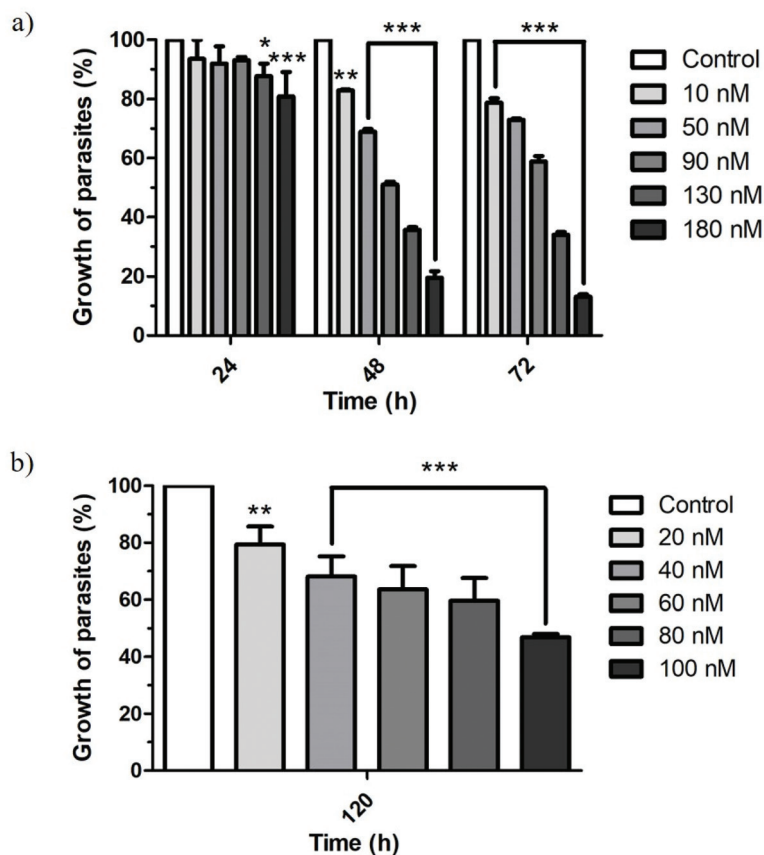


Fig. 10 Antiproliferative effects of the iron(III) complex (1) on the epimastigote of *Trypanosoma cruzi*. Percentage of growth of epimastigotes of *T. cruzi* after treatment with the complex at different concentrations for (a) 24 h, 48 h, and 72 h, (b) 120 h. After 24 h of culture, different concentrations of complex (1) were added to the cultures and parasite growth was evaluated every 24 h up to 120 h. The average of three independent experiments and standard deviation is represented for each point. * $P \leq 0.05$, ** $P \leq 0.01$ and *** $P \leq 0.001$ in relation to the control.

T. cruzi, presenting an IC_{50} equal to 0.03 μ M, being about 70-fold more potent than benznidazole.⁶⁵ Therefore, these complexes may have potential as antitrypanosomal drugs.

Another positive feature that must be highlighted is that both complexes presented low cytotoxicity to LLC-MK2 host cells. Complex (1) (Fig. 12a) and complex (2) (Fig. 12b) did not

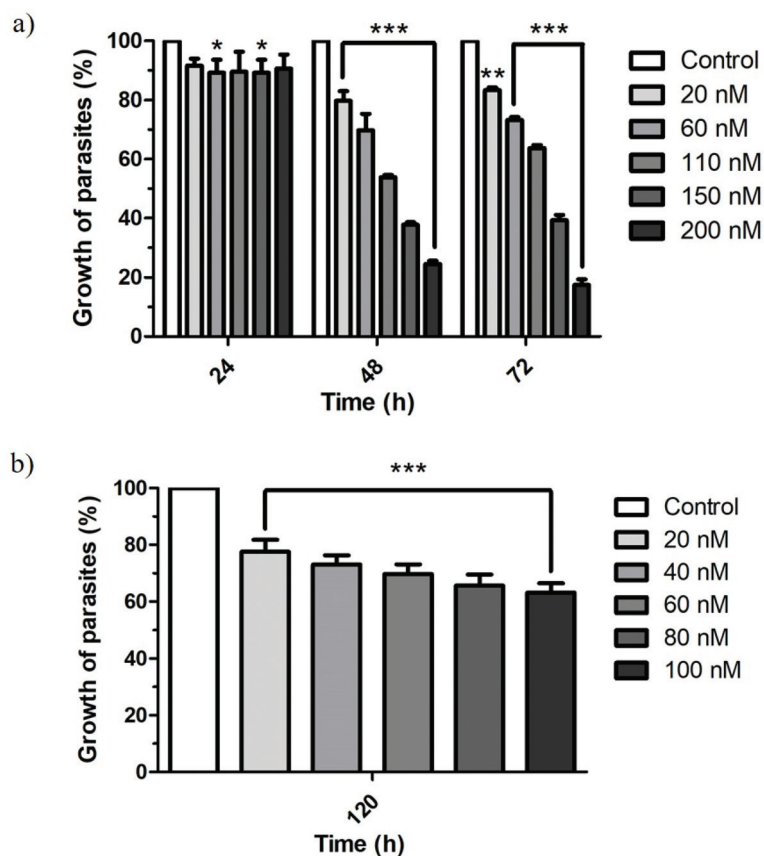


Fig. 11 Antiproliferative effects of the iron(III) complex (2) on epimastigote forms of *Trypanosoma cruzi*. Percentage of growth of epimastigotes of *T. cruzi* after treatment with the complex at different concentrations for (a) 24 h, 48 h, and 72 h, (b) 120 h. After 24 h of culture, different concentrations of complex (2) were added to the cultures and parasite growth was evaluated every 24 h up to 120 h. The average of three independent experiments and standard deviation is represented for each point. * $P \leq 0.05$, ** $P \leq 0.01$ and *** $P \leq 0.001$ in relation to the control.

show cell toxicity at 24 and 72 h of treatment. However, a reduction of 28% and 26% in cell viability was observed after 120 h of treatment with 10 μM of complexes (1) and (2), respectively (Fig. 12). Complex (1) and complex (2) presented CC_{50} values of $12 \pm 1 \mu\text{M}$ and $18 \pm 2 \mu\text{M}$ for 120 h of treatment, respectively. The selective index for 120 h was 106 for complex (1) and 178 for complex (2). For benznidazole, the selective index value obtained may vary from 1⁶² to 11.26,⁶⁶ depending on cell lines. Thus, complexes were more selective than benznidazole against the parasites, demonstrating that they are more safe than this current drug. While complex (1) is slightly more active against the parasite, complex (2) shows a better selective index.

Mitochondria are essential organelles involved in energy conversion, cell cycle, signaling and cell death.⁶⁷ Due to differences between mammalian and trypanosomatids mitochondria, this organelle is an excellent target for therapeutic interventions.⁶⁸ Thus, possible mitochondria impairment after treatment with the complexes was analyzed by first assaying the membrane potential of this organelle, employing staining with JC-1, a lipophilic cationic fluorescent mitochondrial viability marker. Mitochondria concentrate JC-1 according to their

inner membrane potential. In low concentrations JC-1 is a monomer that emits green fluorescence (530 nm). At higher concentrations JC-1 forms J-aggregates in the mitochondria, emitting red fluorescence (590 nm), indicating the mitochondrial energized state.⁵⁴ Non-treated parasites presented normal mitochondrial function (Fig. 13A and B). Reduction in membrane potential was observed in parasites treated with the complexes (Fig. 13C–F). In addition, treatment with both complexes caused structure deformation and rounding of the parasite (Fig. 13C–F).

Parasites with damaged mitochondria were quantified after JC-1 labeling. In non-treated cells, 22% of the parasites showed a reduction in their mitochondrial membrane potential, possibly due to the normal parasite's cell cycle (Fig. 13G). Reduction in mitochondrial membrane potential reached 66% and 55% of the parasite populations after treatment with complexes (1) and (2), respectively, after 120 h at a concentration of 3 μM . Both complexes were capable of affecting a central organelle of the parasite possibly impairing energy metabolism and other functions of the mitochondria.

The parasite ultrastructure was evaluated to find possible *T. cruzi* cellular targets affected by the treatment with the iron

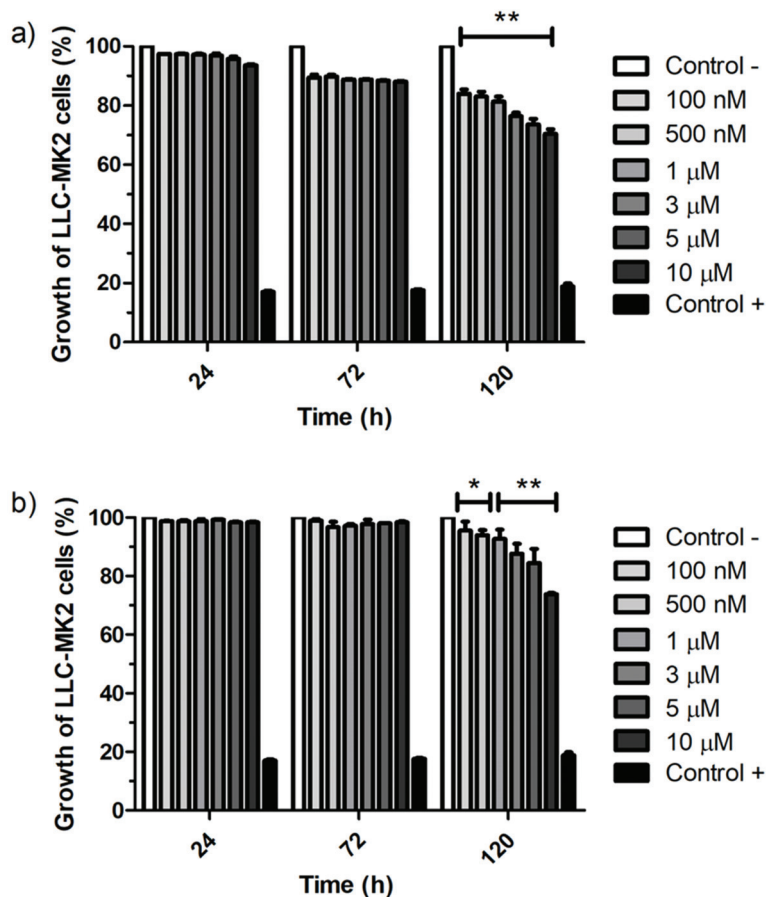


Fig. 12 Cytotoxic effects of iron(III) complexes on LLC-MK2 cells. Percentage of growth of LLC-MK2 cells treated with different concentrations of (a) complex (1) and (b) complex (2). Negative control: cells were cultured in RPMI medium with FBS without complexes. Positive control: cells were cultured with 10% Triton X-100 in RPMI medium. * $P \leq 0.05$ and ** $P \leq 0.001$ in relation to the control (-).

(III) complexes. Although both complexes were capable of reducing mitochondrial membrane potential of the parasite, only complex (2) promoted morphological changes which were seen in mitochondria and their kinetoplast (mitochondrial DNA). Non-treated parasites presented characteristic morphology, with well arranged and preserved organelles, such as plasma membrane, nucleus, kinetoplast and mitochondria; a clear outer mitochondrial membrane around a well organized kinetoplast was seen (Fig. 14A and B). After treatment with complex (2) (1 μM for 120 h), mitochondria presented swelling and abnormal disposition in the kinetoplast region (Fig. 14C–F). The kinetoplast also presented changes in its arrangement (Fig. 14D and F) including lower condensation in its extremities (Fig. 14F). Complex (2) was capable of affecting the parasite organelle that produces ATP; however, complex (1) did not alter or changes were not found in mitochondria. Thus, functional and ultrastructural assays corroborate the effect of complex (2) on the mitochondria, possibly altering its function.

Another organelle that presented ultrastructural changes was reservosomes. Reservosomes are endo-lysosomal essential organelles that store proteins and lipids for future use, which

are present in the posterior end of *T. cruzi* epimastigotes.⁶⁹ Non-treated parasites showed characteristic reservosome morphology (Fig. 15A and B). However, parasites treated with both complexes at a low concentration (100 nM) revealed ultrastructural alterations in the reservosomes, which presented spicules inside after treatment with complex (1) (Fig. 15C and D) and complex (2) (Fig. 15E and F). Interestingly, it was not possible to observe reservosomes in most parasites treated with 1 μM of the complexes, suggesting that at higher concentration these organelles were totally degraded, suggesting that endocytosis stopped in most treated parasites. These organelles are round membrane structures with lipid reserves in their dense electron lumen.^{70,71} Lysosome proteases, such as cruzipain, the main *T. cruzi* cysteine protease,⁷² are concentrated in the reservosomes and digest endocytosed material, although the reservosomes are also capable of storing macromolecules such as cholesterol for future mobilization when necessary.⁷³ The changes in reservosomes caused by the treatment with the iron complexes possibly caused an imbalance in nutrient endocytosis, digestion and reserve, consequently affecting the energy metabolism of the parasite. Thus, these complexes have potential as antitrypanosomal drugs.

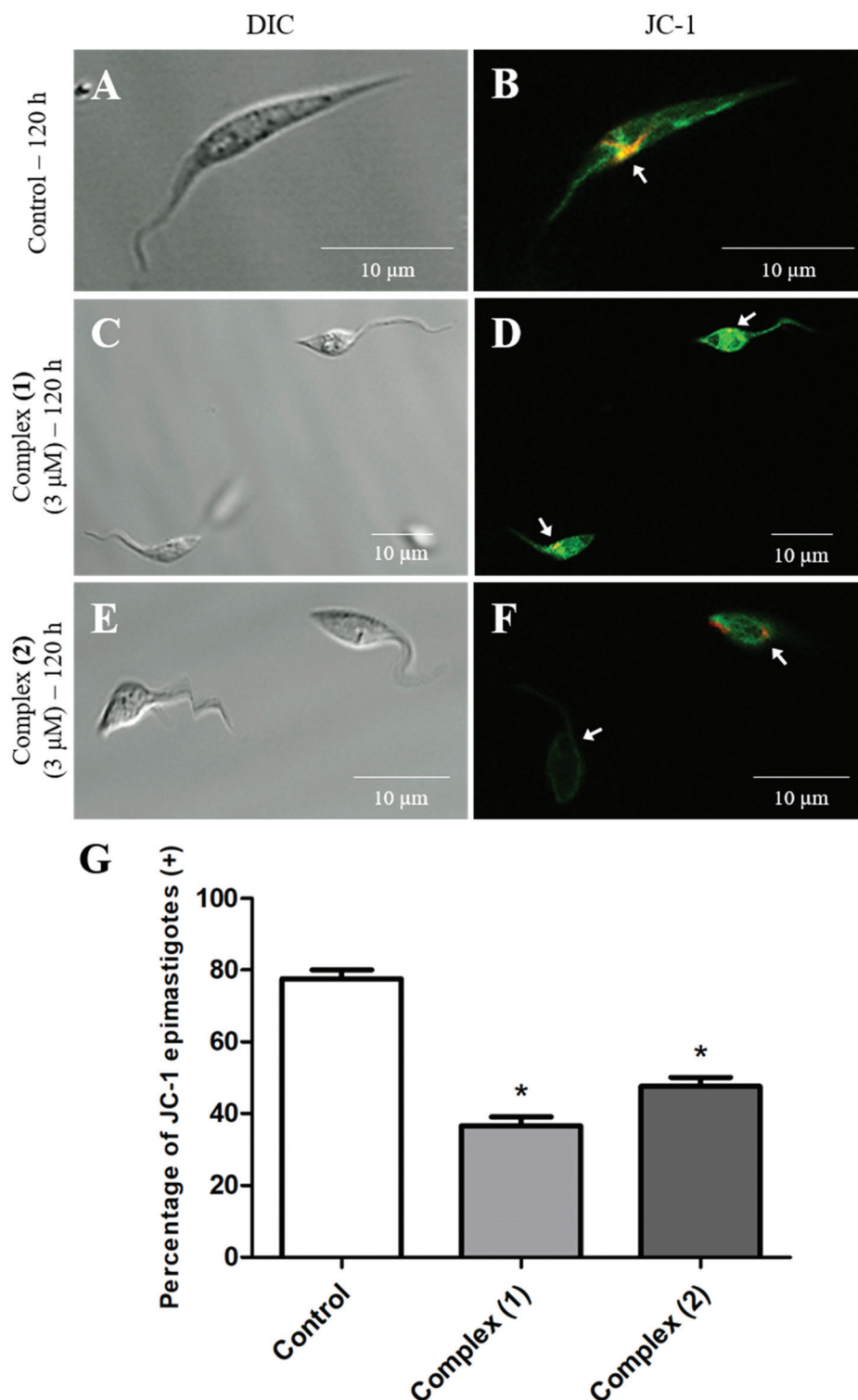


Fig. 13 Mitochondrial membrane potential, revealed by JC-1 labeling, of epimastigote forms of *Trypanosoma cruzi* treated or not with iron(III) complexes (1) and (2). Parasites were treated for 120 h with complexes (1) and (2) at 3 μM and were visualized using confocal microscopy. (A, C and E) Differential interference contrast (DIC) microscopy images. (B, D and F) Fluorescence microscopy after JC-1 labeling. Non-treated parasites show normal mitochondrial membrane potential (A and B) (red fluorescence) and parasites treated with complex (1) (C and D) or complex (2) (E and F) lost mitochondrial membrane potential. Note also that treated parasites become rounded. Bars: 10 μm. (G) Quantification of epimastigote with normal mitochondrial membrane potential after treatment with complexes (1) and (2) at 3 μM and JC-1 labeling. The data are representative of three independent experiments. * $P \leq 0.001$ in relation to the control.

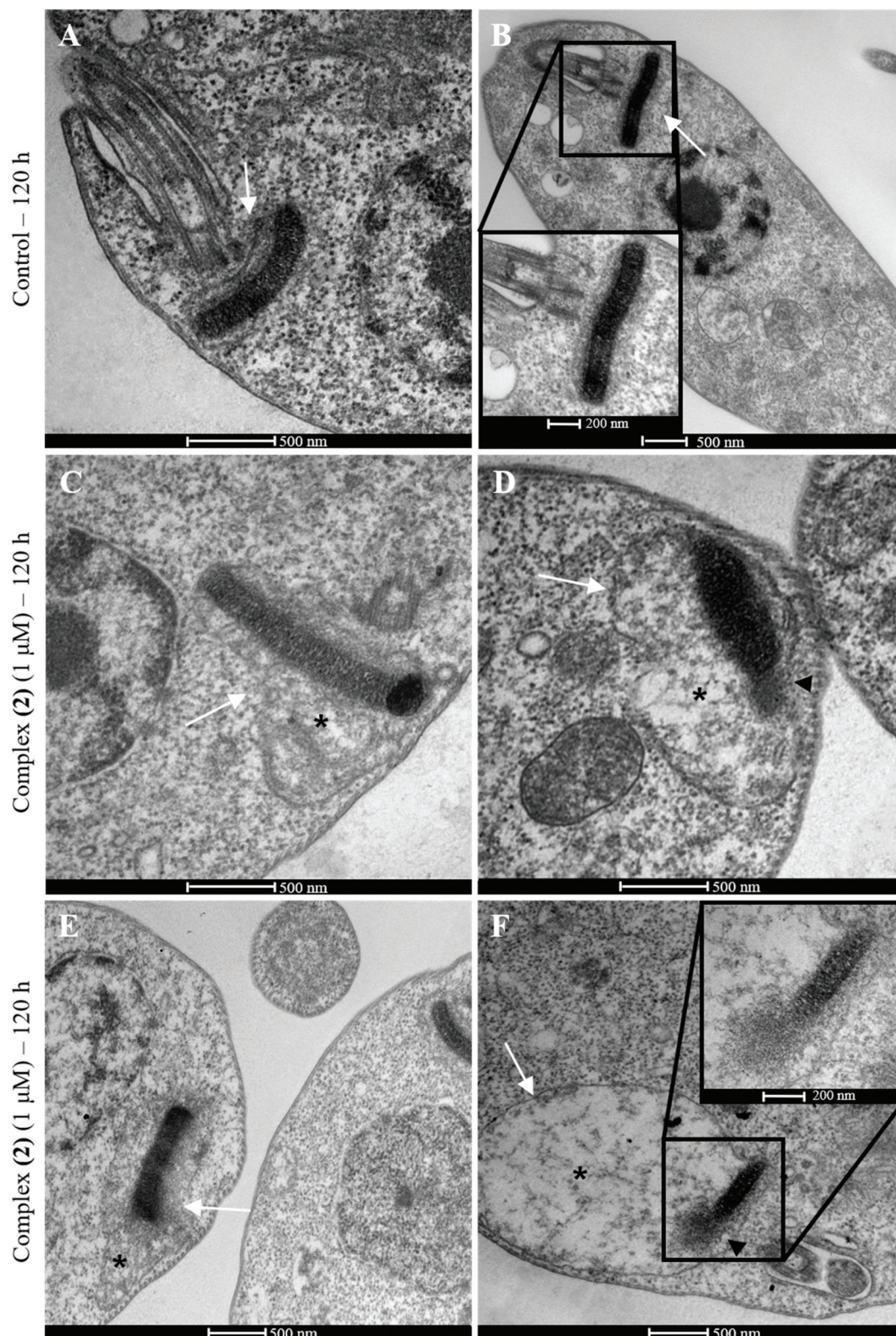


Fig. 14 Transmission electron microscopy of epimastigote forms of *Trypanosoma cruzi* treated or not with iron(III) complex (2). (A and B) Untreated parasites present a normal ultrastructure of organelles such as kinetoplast and nucleus. (C–F) Parasites treated with the complex (2) at 1 μ M for 120 h. Note that the parasite's mitochondria (arrows) shows changes on its membrane, with swelling and abnormal disposition around the kinetoplast (asterisk). Kinetoplast also presented changes in its arrangement (arrowhead). Bars: 500 nm and 200 nm.

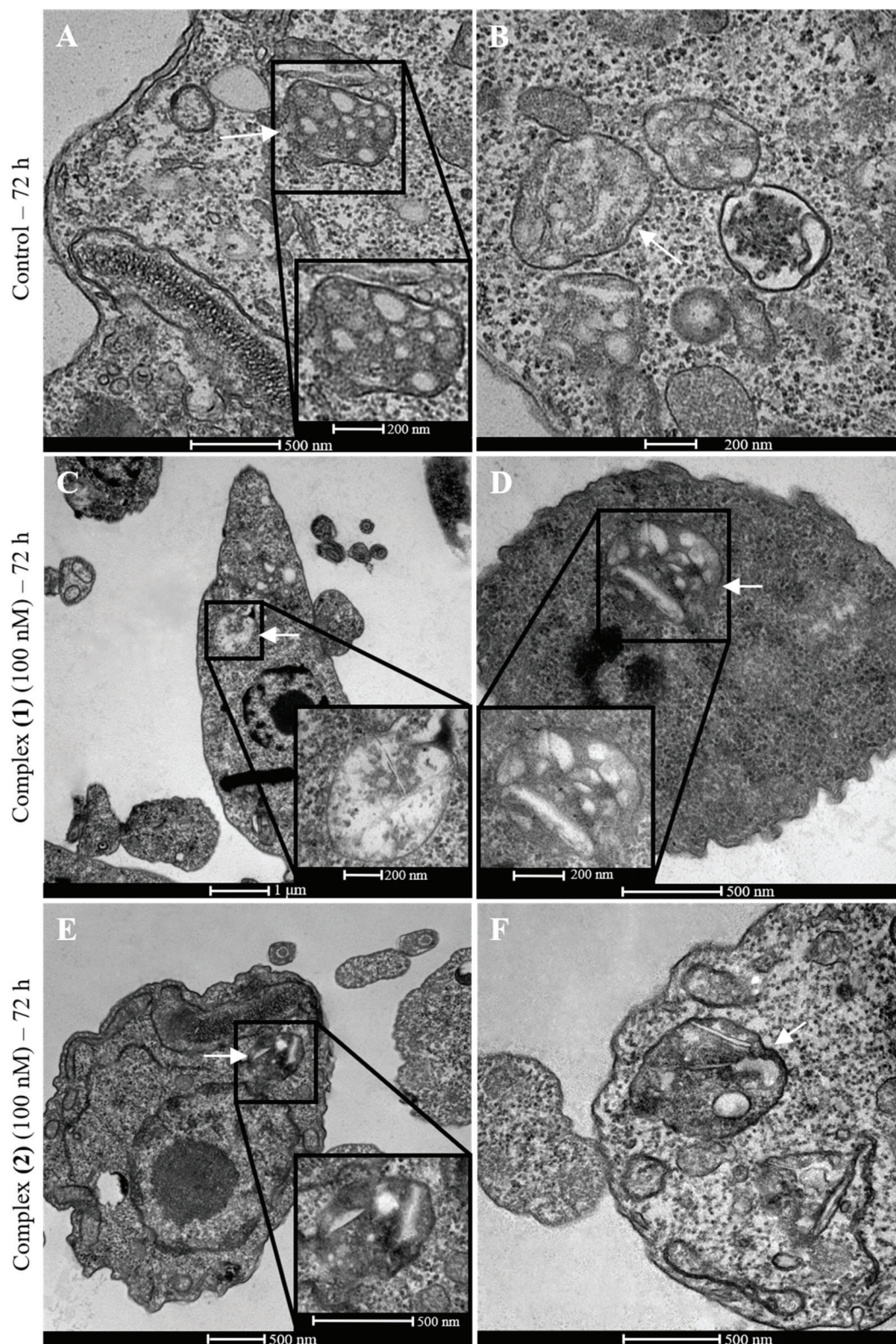


Fig. 15 Transmission electron microscopy of epimastigote forms of *Trypanosoma cruzi* treated or not with iron(III) complexes (1) and (2). Non-treated parasites (A and B) were cultured for 72 h. Parasites were treated for 72 h with complex (1) (C and D) and complex (2) (E and F), both at 100 nM. Reservosomes of the treated parasites present spicules and degradations in their structure (arrows in C–F). Bars: 1 μ m, 500 nm and 200 nm.

4. Conclusions

Two new μ -oxo-diiron(III) complexes have been prepared and successfully characterized using tripodal tetradentate ligands that show N_3O coordination sets. The ligands are isomers: the ligand HL1 has an α -naphthoyl pendent group while the ligand HL2 possesses a β -naphthoyl unit. The physical and chemical properties of the iron(III) centres are similar since the coordination environment is the same, as observed by X-ray diffraction studies performed for complex (1) and theoretical calculations. Both complexes were active against *T. cruzi* epimastigotes at concentrations in the nanomolar range ($IC_{50} = 97\text{--}122$ nM), showing low cytotoxicity to the host cells LLC-MK2, resulting in a high selectivity index for both complexes (106 and 178 for complexes (1) and (2), respectively). The antitrypanosomal activity seems to be independent of the nature of the isomer (alpha or beta) complex (1) being slightly more active against the parasite, and complex (2) presenting higher therapeutic safety. Treatment with both complexes at nanomolar concentrations generated important changes in mitochondria and reservosome of the parasite, which are essential organelles for their survival. A reduction in mitochondrial membrane potential after treatment with both complexes was detected. Mitochondria impairment after treatment was confirmed for complex (2) by the observation of alterations and abnormal swelling and disposition of the mitochondria around the kinetoplast and changes in arrangement of kinetoplast were also observed. In addition, the formation of spicules in the lumen of reservosomes was detected after treatments with both complexes. Thus, both complexes tested affected organelles involved with essential cell function as energy conversion, nutrient digestion and reserve of the parasite. These complexes have relevant potential to be further evaluated in CD since there is no effective current treatment for the chronic phase of this disease and unfortunately trypanosomatid diseases continue to cause significant morbidity and mortality, especially among the impoverished. Despite the *in vitro* efficacy of these complexes, many questions remain unanswered regarding the molecular mechanisms involved in their action against *T. cruzi*. However, these findings open interesting perspectives for investigating *in vitro* the efficacy of metallic complexes against the intracellular amastigote life cycle form of the parasite and, after that, against infective trypomastigote form *in vitro* and in *in vivo* infection models, as well as for a more complete description of the mechanism of action of these complexes.

Conflicts of interest

There are no conflicts to declare.

Acknowledgements

All authors are grateful for the financial support received from Coordenação de Aperfeiçoamento de Pessoal de Nível Superior

(CAPES), finance code 001; Conselho Nacional de Desenvolvimento Científico e Tecnológico (CNPq); and Fundação Carlos Chagas Filho de Amparo à Pesquisa do Estado do Rio de Janeiro (FAPERJ).

The LDRX at the Universidade Federal Fluminense (UFF) is thanked for the data collection of complex (1).

We also thank Eliandro Joaci de Lima and Luís Otávio da Silva Pacheco for the technical assistance.

References

- 1 C. Chagas, Nova tripanosomiase humana: estudos sobre a morfologia e o ciclo evolutivo do *Schizotrypanum cruzi* n. gen., n.sp., agente etiológico de nova entidade mórbida do homem, *Mem. Inst. Oswaldo Cruz*, 1909, **1**, 159–218, DOI: 10.1590/S0074-02761909000200008.
- 2 World Health Organization, [(accessed on 31 October 2020)], 2020. Available online: https://www.who.int/neglected_diseases/diseases/en/.
- 3 J. C. Dias, V. Amato Neto and E. J. Luna, Alternative transmission mechanisms of *Trypanosoma cruzi* in Brazil and proposals for their prevention, *Rev. Soc. Bras. Med. Trop.*, 2011, **44**(3), 375–379, DOI: 10.1590/s0037-86822011005000032.
- 4 P. J. Hotez, E. Dumonteil, L. Woc-Colburn, J. A. Serpa, S. Bezek, M. S. Edwards, C. J. Hallmark, L. W. Musselwhite, B. J. Flink and M. E. Bottazzi, Chagas Disease: “The New HIV/AIDS of the Americas”, *PLoS Neglected Trop. Dis.*, 2012, **6**, e1498, DOI: 10.1371/journal.pntd.0001498.
- 5 A. R. De Lima, M. C. Navarro, R. Arteaga and V. Contreras, Cultivation of *Trypanosoma cruzi* epimastigotes in low glucose axenic media shifts its competence to differentiate at metacyclic trypomastigotes, *Exp. Parasitol.*, 2008, **119**, 336–342, DOI: 10.1016/j.exppara.2008.03.003.
- 6 S. Goldenberg and A. R. Avila, Aspects of *Trypanosoma cruzi* stage differentiation, *Adv. Parasitol.*, 2011, **75**, 285–305, DOI: 10.1016/B978-0-12-385863-4.00013-7.
- 7 World Health Organization, *Research priorities for Chagas disease, human African trypanosomiasis and leishmaniasis. WHO: technical report of the TDR Disease Reference Group on Chagas Disease, Human Africa Trypanosomiasis and Leishmaniasis*, World Health Organization, Geneva, 2012. (WHO Technical Report Series, 975).
- 8 World Health Organization, *Sustaining the drive to overcome the global impact of neglected tropical diseases: second WHO report in neglected tropical diseases*, World Health Organization, Geneva, 2013.
- 9 J. R. Coura and J. C. Dias, Epidemiology, control and surveillance of Chagas disease: 100 years after its discovery, *Mem. Inst. Oswaldo Cruz*, 2009, **104**, 31–40, DOI: 10.1590/S0074-02762009000900006.
- 10 World Health Organization, *Chagas disease (American trypanosomiasis)*, World Health Organization, WHO Fact sheet No. 340. Geneva, 2016.
- 11 A. Rassi Jr., A. Rassi and J. Marcondes de Rezende, American trypanosomiasis (Chagas disease), *Infect. Dis.*

- Clin. North Am.*, 2012, **26**, 275–291, DOI: 10.1016/j.idc.2012.03.002.
- 12 World Health Organization, Chagas disease in Latin America: an epidemiological update based on 2010 estimates, *Wkly. Epidemiol. Rec.*, 2015, **90**, 33–44.
- 13 M. Castillo-Riquelme, Chagas Disease in Non-Endemic Countries, *Lancet Global Health*, 2017, **5**(4), e379–e380, DOI: 10.1016/S2214-109X(17)30090-6.
- 14 M. Boiani, L. Piacenza, P. Hernández, L. Boiani, H. Cerecetto, M. González and A. Denicola, Mode of action of nifurtimox and N-oxide-containing heterocycles against *Trypanosoma cruzi*: is oxidative stress involved?, *Biochem. Pharmacol.*, 2010, **79**, 1736–1745, DOI: 10.1016/j.bcp.2010.02.009.
- 15 I. Molina, F. Salvador, A. Sánchez-Montalvá, B. Treviño, N. Serre, A. Sao Avilés and B. Almirante, Toxic Profile of Benznidazole in Patients with Chronic Chagas Disease: Risk Factors and Comparison of the Product from Two Different Manufacturers, *Antimicrob. Agents Chemother.*, 2015, **59**(10), 6125–6131, DOI: 10.1128/AAC.04660-14.
- 16 C. J. Forsyth, S. Hernandez, W. Olmedo, A. Abuhamidah, M. I. Traina, D. R. Sanchez, J. Soverow and S. K. Meymandi, Safety Profile of Nifurtimox for Treatment of Chagas Disease in the United States, *Clin. Infect. Dis.*, 2016, **63**(8), 1056–1062, DOI: 10.1093/cid/ciw477.
- 17 R. Docampo and S. N. Moreno, Free radical metabolites in the mode of action of chemotherapeutic agents and phagocytic cells on *Trypanosoma cruzi*, *Rev. Infect. Dis.*, 1984, **6**(2), 223–238, DOI: 10.1093/clinids/6.2.223.
- 18 R. Docampo, Sensitivity of parasites to free radical damage by antiparasitic drugs, *Chem.-Biol. Interact.*, 1990, **73**(1), 1–27, DOI: 10.1016/0009-2797(90)90106-w.
- 19 J. D. Maya, S. Bollo, L. J. Nuñez-Vergara, J. A. Squella, Y. Repetto, A. Morello, J. Perie and G. Chauvière, *Trypanosoma cruzi*: effect and mode of action of nitroimidazole and nitrofurans derivatives, *Biochem. Pharmacol.*, 2003, **65**(6), 999–1006, DOI: 10.1016/s0006-2952(02)01663-5.
- 20 V. Sueth-Santiago, D. Decote-Ricardo, A. Morrot, C. G. Freire-de-Lima and M. E. Challenges, in the chemotherapy of Chagas disease: Looking for possibilities related to the differences and similarities between the parasite and host, *World J. Biol. Chem.*, 2017, **8**(1), 57–80, DOI: 10.4331/wjbc.v8.i1.57.
- 21 E. G. Díaz de Toranzo, J. A. Castro, B. M. Franke de Cazzulo and J. J. Cazzulo, Interaction of benznidazole reactive metabolites with nuclear and kinetoplastic DNA, proteins and lipids from *Trypanosoma cruzi*, *Experientia*, 1988, **44**(10), 880–881, DOI: 10.1007/bf01941187.
- 22 A. Moncayo and A. C. Silveira, Current epidemiological trends for Chagas disease in Latin America and future challenges in epidemiology, surveillance and health policy, *Mem. Inst. Oswaldo Cruz*, 2009, **104**(Suppl 1), 17–30, DOI: 10.1590/s0074-02762009000900005.
- 23 J. Bermudez, C. Davies, A. Simonazzi, J. P. Real and S. Palma, Current drug therapy and pharmaceutical challenges for Chagas disease, *Acta Trop.*, 2016, **156**, 1–16, DOI: 10.1016/j.actatropica.2015.12.017.
- 24 S. Caldas, I. S. Caldas, A. B. Cecílio, L. D. Diniz, A. Talvani, I. Ribeiro and M. T. Bahia, Therapeutic responses to different anti-*Trypanosoma cruzi* drugs in experimental infection by benznidazole-resistant parasite stock, *Parasitol*, 2014, **141**, 1628–1637, DOI: 10.1017/S0031182014000882.
- 25 J. H. McKerrow, P. S. Doyle, J. C. Engel, L. M. Podust, S. A. Robertson, R. Ferreira, T. Saxton, M. Arkin, I. D. Kerr, L. S. Brinen and C. S. Craik, Two approaches to discovering and developing new drugs for Chagas disease, *Mem. Inst. Oswaldo Cruz*, 2009, **104**, 263–269, DOI: 10.1590/S0074-02762009000900034.
- 26 C. B. Moraes, M. A. Giardini, H. Kim, C. H. Franco, A. M. Araujo-Junior, S. Schenkman, E. Chatelain and L. H. Freitas-Junior, Nitroheterocyclic compounds are more efficacious than CYP51 inhibitors against *Trypanosoma cruzi*: implications for Chagas disease drug discovery and development, *Sci. Rep.*, 2014, **4**, 4703, DOI: 10.1038/srep04703.
- 27 I. Molina, J. Gómez i Prat, F. Salvador, B. Treviño, E. Sulleiro, N. Serre, D. Pou, S. Roure, J. Cabezas, L. Valerio, A. Blanco-Grau, A. Sánchez-Montalvá, X. Vidal and A. Pahissa, Randomized trial of posaconazole and benznidazole for chronic Chagas' disease, *N. Engl. J. Med.*, 2014, **370**(20), 1899–1908, DOI: 10.1056/NEJMoa1313122.
- 28 J. A. Urbina, Recent clinical trials for the etiological treatment of chronic chagas disease: advances, challenges and perspectives, *J. Eukaryotic Microbiol.*, 2014, **62**(1), 149–156, DOI: 10.1111/jeu.12184.
- 29 L. S. Sargenito, M. H. Branquinha and A. L. S. Santos, Funding for Chagas Disease: A 10-Year (2009–2018) Survey, *Trop. Med. Infect. Dis.*, 2020, **5**(2), 88, DOI: 10.3390/tropicalmed5020088.
- 30 D. Gambino, Potentiality of vanadium compounds as anti-parasitic agents, *Coord. Chem. Rev.*, 2011, **255**(19–20), 2193–2203, DOI: 10.1016/j.ccr.2010.12.028.
- 31 C. Fernandes, A. Horn Jr., B. F. Lopes, E. S. Bull, N. F. B. Azeredo, M. M. Kanashiro, F. V. Borges, A. J. Bortoluzzi, B. Szpoganicz, A. B. Pires, R. W. A. Franco, J. C. A. Almeida, L. L. F. Maciel, J. A. L. C. Resende and G. Schenk, Induction of apoptosis in leukemia cell lines by new copper(II) complexes containing naphthyl groups via interaction with death receptors, *J. Inorg. Biochem.*, 2015, **153**, 68–87, DOI: 10.1016/j.jinorgbio.2015.09.014.
- 32 M. Vieites, P. Smircich, B. Parajón-Costa, J. Rodríguez, V. Galaz, C. Olea-Azar, L. Otero, G. Aguirre, H. Cerecetto, M. González, A. Gómez-Barrio, B. Garat and D. Gambino, Potent *in vitro* anti-*Trypanosoma cruzi* activity of pyridine-2-thiol N-oxide metal complexes having an inhibitory effect on parasite-specific fumarate reductase, *J. Biol. Inorg. Chem.*, 2008, **13**, 723–735, DOI: 10.1007/s00775-008-0358-7.
- 33 D. A. Paixão, C. D. Lopes, Z. A. Carneiro, L. M. Sousa, L. P. de Oliveira, N. P. Lopes, M. Pivatto, J. D. S. Chaves, M. V. de Almeida, J. Ellena, M. B. Moreira, A. V. G. Netto, R. J. de Oliveira, S. Guillard, S. de Albuquerque and W. Guerra, *In vitro* anti-*Trypanosoma cruzi* activity of ternary

- copper(II) complexes and *in vivo* evaluation of the most promising complex, *Biomed. Pharmacother.*, 2019, **109**, 157–166, DOI: 10.1016/j.biopha.2018.10.057.
- 34 M. F. Mosquillo, L. Bilbao, F. Hernández, I. Machado, D. Gambino, B. Garat and L. Pérez-Díaz, Effect of a new anti-T. cruzi metallic compound based on palladium, *BioMetals*, 2018, **31**(6), 961–974, DOI: 10.1007/s10534-018-0140-4.
- 35 C. D. Lopes, B. Possato, A. P. S. Gaspari, R. J. Oliveira, U. Abram, J. P. A. Almeida, F. R. Rocho, A. Leitão, C. A. Montanari, P. I. S. Maia, J. S. Silva, S. Albuquerque and Z. A. Carneiro, Organometallic gold(III) complex [Au(Hdamp)(L14)] + (L1 = SNS-donating thiosemicarbazone) as a candidate to new formulations against Chagas disease, *ACS Infect. Dis.*, 2019, **5**(10), 1698–1707, DOI: 10.1021/acscinfed.8b00284.
- 36 L. C. Batista, F. S. de Souza, V. M. de Assis, S. H. Seabra, A. J. Bortoluzzi, M. N. Rennó, A. Horn Jr., R. A. DaMatta and C. Fernandes, Antiproliferative activity and conversion of tachyzoite to bradyzoite of *Toxoplasma gondii* promoted by new zinc complexes containing sulfadiazine, *RSC Adv.*, 2015, **5**, 100606–100617, DOI: 10.1039/C5RA17690E.
- 37 J. A. Portes, C. S. Motta, N. F. Azeredo, C. Fernandes, A. Horn Jr., W. de Souza, R. A. DaMatta and S. H. Seabra, *In vitro* treatment of *Toxoplasma gondii* with copper(II) complexes induces apoptosis-like and cellular division alterations, *Vet. Parasitol.*, 2017, **245**, 141–152, DOI: 10.1016/j.vetpar.2017.04.002.
- 38 J. A. Portes, N. F. B. Azeredo, P. G. T. Siqueira, T. G. De Souza, C. Fernandes, A. Horn Jr., D. R. S. Candela, W. de Souza, R. A. DaMatta and S. H. Seabra, A new iron(III) complex-containing sulfadiazine inhibits the proliferation and induces cystogenesis of *Toxoplasma gondii*, *Parasitol. Res.*, 2018, **117**(9), 2795–2805, DOI: 10.1007/s00436-018-5967-7.
- 39 R. R. Gagne, C. A. Koval and G. C. Lisensky, Ferrocene as an internal standard for electrochemical measurements, *Inorg. Chem.*, 1980, **19**(9), 2854–2855, DOI: 10.1021/ic50211a080.
- 40 Bruker APEX3, SAINT and SADABS, Bruker AXS Inc., Madison, Wisconsin, USA, 2016.
- 41 G. M. Sheldrick, SHELXT – Integrated space-group and crystalstructure determination, *Acta Crystallogr., Sect. A: Found. Adv.*, 2015, **71**, 3–8, DOI: 10.1107/S2053273314026370.
- 42 G. M. Sheldrick, Chemistry and structure, *Acta Crystallogr., Sect. C: Struct. Chem.*, 2015, **71**, 3–8, DOI: 10.1107/S2053229614026540.
- 43 O. V. Dolomanov, L. J. Bourhis, R. J. Gildea, J. A. K. Howard and H. Puschmann, OLEX2: a complete structure solution, refinement and analysis program, *J. Appl. Crystallogr.*, 2009, **42**, 339–341, DOI: 10.1107/S0021889808042726.
- 44 C. Bannwarth, S. Ehlert and S. Grimme, GFN2-xTB—An Accurate and Broadly Parametrized Self-Consistent Tight-Binding Quantum Chemical Method with Multipole Electrostatics and Density-Dependent Dispersion Contributions, *J. Chem. Theory Comput.*, 2019, **15**(3), 1652–1671, DOI: 10.1021/acs.jctc.8b01176.
- 45 S. Grimme, C. Bannwarth and P. Shushkov, A Robust and Accurate Tight-Binding Quantum Chemical Method for Structures, Vibrational Frequencies, and Noncovalent Interactions of Large Molecular Systems Parametrized for All spd-Block Elements ($Z = 1–86$), *J. Chem. Theory Comput.*, 2017, **13**(5), 1989–2009, DOI: 10.1021/acs.jctc.7b00118.
- 46 P. Pracht, F. Bohle and S. Grimme, Automated exploration of the low-energy chemical space with fast quantum chemical methods, *Phys. Chem. Chem. Phys.*, 2020, **22**, 7169–7192, DOI: 10.1039/C9CP06869D.
- 47 J. P. Perdew, K. Burke and M. Ernzerhof, Generalized Gradient Approximation Made Simple, *Phys. Rev. Lett.*, 1996, **77**(18), 3865–3868, DOI: 10.1103/PhysRevLett.77.3865.
- 48 K. G. Dyall, Relativistic quadruple-zeta and revised triple-zeta and double-zeta basis sets for the 4p, 5p, and 6p elements, *Theor. Chem. Acc.*, 2006, **115**, 441–447, DOI: 10.1007/s00214-006-0126-0.
- 49 E. Van Lenthe, J. G. Snijders and E. J. Baerends, The zero-order regular approximation for relativistic effects: The effect of spin-orbit coupling in closed shell molecules, *J. Chem. Phys.*, 1996, **105**, 6505, DOI: 10.1063/1.472460.
- 50 F. Neese, “The ORCA program system” Wiley In order to gain further understanding of the probable structure of complex (2), DFT calculation were applied using the known X-ray structure parameters for complex (1), *Wiley Interdiscip. Rev.: Comput. Mol. Sci.*, 2012, **2**(1), 73–88.
- 51 F. Neese, Software update: the ORCA program system, version 4.0, *Wiley Interdiscip. Rev.: Comput. Mol. Sci.*, 2017, **8**(1), e1327.
- 52 N. Trotsko, A. Bekier, A. Paneth, M. Wujec and K. Dzitko, Synthesis and *in vitro* Anti-Toxoplasma gondii Activity of Novel Thiazolidin-4-one Derivatives, *Molecules*, 2019, **24**(17), 3029, DOI: 10.3390/molecules24173029.
- 53 T. L. Riss and R. A. Moravec, Use of multiple assay endpoints to investigate the effects of incubation time, dose of toxin, and plating density in cell-based cytotoxicity assays, *Assay Drug Dev. Technol.*, 2004, **2**(1), 51–62, DOI: 10.1089/154065804322966315.
- 54 S. T. De Macedo-Silva, T. L. De Oliveira Silva, J. A. Urbina, W. De Souza and J. C. Rodrigues, Antiproliferative, Ultrastructural, and Physiological Effects of Amiodarone on Promastigote and Amastigote Forms of *Leishmania amazonensis*, *Mol. Biol. Int.*, 2011, **2011**, 876021, DOI: 10.4061/2011/876021.
- 55 R. O. Moreira, S. R. Morcelli, M. M. Kanashiro, J. A. L. C. Resende, L. L. F. Maciel, J. C. A. Almeida, L. R. Gahan, A. Horn Jr. and C. Fernandes, Modulating the antitumoral activity by the design of new platinum(II) compounds: Synthesis, characterization, DFT, ultrastructure and mechanistic studies, *J. Inorg. Biochem.*, 2019, **194**, 200–213, DOI: 10.1016/j.jinorgbio.2018.12.016.
- 56 G. L. Parrilha, S. S. Ferreira, C. Fernandes, G. C. Silva, N. M. F. Carvalho, O. A. C. Antunes, V. Drago, A. J. Bortoluzzi and A. Horn Jr., Properties of (m-Oxo)di-iron Complexes and Catalytic Activity Toward Cyclohexane

- Oxidation, *J. Braz. Chem. Soc.*, 2010, **21**(4), 603–613, DOI: 10.1590/S0103-50532010000400004.
- 57 G. L. Parrilha, C. Fernandes, A. J. Bortoluzzi, B. Szpoganicz, M. S. Silva, C. T. Pich, H. Terenzi and A. Horn Jr., A new μ -oxo di-iron complex with suitable features to mimic metal-hydroxylase activity: X-ray molecular structure, aqua solution behavior and nuclease activity of the complex $[\text{Fe}(\text{HPCINOL})(\text{SO}_4)]_2\text{-}\mu\text{-oxo}$, *Inorg. Chem. Commun.*, 2008, **11**, 643–647, DOI: 10.1016/j.inoche.2008.02.019.
- 58 J. Bernstein, R. E. Davis, L. Shimoni and N. L. Chang, Patterns in Hydrogen Bonding: Functionality and Graph Set Analysis in Crystals, *Angew. Chem., Int. Ed. Engl.*, 1995, **34**(15), 1555–1573, DOI: 10.1002/anie.199515551.
- 59 K. S. Murray, Binuclear oxo-bridged iron(III) complexes, *Coord. Chem. Rev.*, 1974, **12**(1), 1–35, DOI: 10.1016/S0010-8545(00)80384-7.
- 60 N. Mardirossian and M. Head-Gordon, Thirty years of density functional theory in computational chemistry: an overview and extensive assessment of 200 density functionals, *Mol. Phys.*, 2017, **115**(19), 2315–2372, DOI: 10.1080/00268976.2017.1333644.
- 61 S. M. Blinder, Basic Concepts of Self-Consistent-Field Theory, *Am. J. Phys.*, 1965, **33**, 431, DOI: 10.1119/1.1971665.
- 62 A. B. Caballero, C. Marín, A. Rodríguez-Diéguez, I. Ramírez-Macías, E. Barea, M. Sánchez-Moreno and J. M. Salas, *In vitro* and *in vivo* antiparasitic activity against *Trypanosoma cruzi* of three novel 5-methyl-1,2,4-triazolo[1,5-a]pyrimidin-7(4H)-one-based complexes, *J. Inorg. Biochem.*, 2011, **105**(6), 770–776, DOI: 10.1016/j.jinorgbio.2011.03.015.
- 63 G. Scalese, I. Machado, C. Fontana, G. Risi, G. Salinas, L. Pérez-Díaz and D. Gambino, New heteroleptic oxidovanadium(V) complexes: synthesis, characterization and biological evaluation as potential agents against *Trypanosoma cruzi*, *J. Biol. Inorg. Chem.*, 2018, **23**(8), 1265–1281, DOI: 10.1007/s00775-018-1613-1.
- 64 L. Friggeri, L. Scipione, R. Costi, M. Kaiser, F. Moraca, C. Zamperini, B. Botta, R. Di Santo, D. De Vita, R. Brun and S. Tortorella, New Promising Compounds with *in Vitro* Nanomolar Activity against *Trypanosoma cruzi*, *ACS Med. Chem. Lett.*, 2013, **4**(6), 538–541, DOI: 10.1021/ml400039r.
- 65 G. Bringmann, B. Hertlein-Amslinger, I. Kajahn, M. Dreyer, R. Brun, H. Moll, A. Stich, K. N. Ioset, W. Schmitz and L. H. Ngoc, Phenolic analogs of the N,C-coupled naphthylisoquinoline alkaloid ancistrocladinium A, from *Ancistrocladus cochinchinensis* (Ancistrocladaceae), with improved antiprotozoal activities, *Phytochemistry*, 2011, **72**(1), 89–93, DOI: 10.1016/j.phytochem.2010.10.006.
- 66 C. Fonseca-Berzal, A. Ibáñez-Escribano, F. Reviriego, J. Cumella, P. Morales, N. Jagerovic, J. J. Nogal-Ruiz, J. A. Escario, P. B. Da Silva, Mde. N. Soeiro, A. Gómez-Barrio and V. J. Arán, Antichagasic and trichomonacidal activity of 1-substituted 2-benzyl-5-nitroindazolin-3-ones and 3-alkoxy-2-benzyl-5-nitro-2H indazoles, *Eur. J. Med. Chem.*, 2016, **115**, 295–310, DOI: 10.1016/j.ejmech.2016.03.036.
- 67 H. M. McBride, M. Neuspiel and S. Wasiak, Mitochondria: More Than Just a Powerhouse, *Curr. Biol.*, 2006, **16**(14), R551–R560, DOI: 10.1016/j.cub.2006.06.054.
- 68 R. F. S. Menna-Barreto and S. L. De Castro, The Double-Edged Sword in Pathogenic Trypanosomatids: The Pivotal Role of Mitochondria in Oxidative Stress and Bioenergetics, *BioMed Res. Int.*, 2014, **2014**(ID 614014), 1–14, DOI: 10.1155/2014/614014.
- 69 N. Cunha-e-Silva, C. Sant'Anna, M. G. Pereira, I. Porto-Carreiro, A. L. Jeovanio and W. De Souza, Reserosomes: multipurpose organelles?, *Parasitol. Res.*, 2006, **99**(4), 325–327, DOI: 10.1007/s00436-006-0190-3.
- 70 C. Sant'anna, M. G. Pereira, L. Lemgruber, W. De Souza and N. L. Cunha e Silva, New insights into the morphology of *Trypanosoma cruzi* reserosome, *Microsc. Res. Tech.*, 2008, **71**, 599–605, DOI: 10.1002/jemt.20592.
- 71 M. J. Soares, T. Souto-Padrón and W. De Souza, Identification of a large pre-lysosomal compartment in the pathogenic protozoan *Trypanosoma cruzi*, *J. Cell Sci.*, 1992, **102**, 157–167.
- 72 J. J. Cazzulo, M. C. Cazzulo Franke, J. Martinez and B. M. Franke De Cazzulo, Some kinetic properties of a cysteine proteinase (cruzipain) from *Trypanosoma cruzi*, *Biochim. Biophys. Acta*, 1990, **1037**(2), 186–191, DOI: 10.1016/0167-4838(90)90166-d.
- 73 M. G. Pereira, E. S. Nakayasu, C. Sant'Anna, N. N. De Cicco, G. C. Atella, W. De Souza, I. C. Almeida and N. Cunha-e-Silva, *Trypanosoma cruzi* epimastigotes are able to store and mobilize high amounts of cholesterol in reserosome lipid inclusions, *PLoS One*, 2011, **6**(7), e22359, DOI: 10.1371/journal.pone.0022359.

3.2. Trabalho II

Em processo de submissão para *Antimicrobial Agents and Chemotherapy* - AAC

Dinuclear Fe(III) coordination compounds at nanomolar concentration reduce the *in vitro* growth and changes the structural organization of *Trypanosoma cruzi* amastigotes

Felipe Figueirôa Moreira^a, Juliana de Araujo Portes^b, Christiane Fernandes^c, Adolfo Horn Júnior^c, Wanderley de Souza^b, Renato Augusto DaMatta^{a*}, Sergio Henrique Seabra^{a*}.

^aLaboratório de Biologia Celular e Tecidual, Centro de Biociências e Biotecnologia, Universidade Estadual do Norte Fluminense Darcy Ribeiro (UENF), Campos dos Goytacazes, RJ, Brazil.

^bLaboratório de Ultraestrutura Celular Hertha Meyer, Instituto de Biofísica Carlos Chagas Filho, Universidade Federal do Rio de Janeiro (UFRJ), RJ, Brazil.

^cDepartamento de Química, Universidade Federal de Santa Catarina (UFSC), Florianópolis, SC, Brazil.

* Corresponding authors: Sergio Henrique Seabra: E-mail - seabrash@uenf.br; Renato Augusto DaMatta: E-mail - renato@uenf.br.

ABSTRACT

Chagas disease is a neglected tropical disease caused by the protozoan pathogen *Trypanosoma cruzi*. The disease is a major public health problem affecting about 6 to 7 million people worldwide, mostly in Latin America. Only two antiquated nitroheterocyclic drugs, benznidazole and nifurtimox, are available for the treatment of Chagas disease and there is no vaccine for preventing the infection. These drugs require prolonged treatment, are effective only in the acute phase of the disease, and have severe toxic effects. Therefore, new drugs are urgently needed. It has been shown that coordination compounds are effective against intracellular protozoans such as *Leishmania* spp., *Toxoplasma gondii* and *T. cruzi*. Herein, we tested the *in vitro* effect on *T. cruzi* amastigotes (Dm28c strain) of two μ -oxo Fe(III) dinuclear complexes: [(HL1)(Cl)Fe(μ -O)Fe(Cl)(HL2)(Cl)₂·(CH₃CH₂OH)₂·H₂O (1) and [(HL2)(Cl)Fe(μ -O)Fe(Cl)(HL2)] (Cl)₂·H₂O (2). Parasites were treated with the complexes and the outcome was analyzed. Complex (1) exhibited the lowest IC₅₀ values, which were 61.29 ± 4.21 and 107.48 ± 6.60 nM for 72 and 96 h of treatment, respectively. Complex (2) showed IC₅₀ values of 50.64 ± 2.20 and 173.00 ± 5.60 nM for the same treatment times. Light microscopy images revealed that

treatments with the Fe(III) complexes for 96 h caused amastigotes to change to a spindle-form inside the host cells. Low cytotoxicity to the host cell LLC-MK2 was found for both complexes, resulting in impressive selectivity indexes of 167.28 for complex (1) and 454.28 for complex (2), after 96 h of treatment. Ultrastructural analysis of the parasite after treatment with the complexes showed that the mitochondria outer membrane presented swelling and abnormal disposition around the kinetoplast. In addition, altered nucleus structure, with heterochromatin concentrated in patches at the nuclear envelope were observed. Furthermore, treatment with both complexes reduced the mitochondrial membrane potential of the parasite as seen by JC-1 dye. The complexes showed low nanomolar IC₅₀ values affecting mitochondria and nucleus, essential organelles for the survival of the parasite. The possible mechanism of action could be the induction of an apoptotic-like cell death process. The low IC₅₀ and the high selectivity index show that both complexes act as a new prototype of drugs against *T. cruzi* and may be used for further development in drug discovery to treat Chagas disease.

1. INTRODUCTION

Chagas disease (CD) is a chronic degenerative disease described over a century ago and caused by the protozoan *Trypanosoma cruzi* (Chagas, 1909). This disease is a major public health burden because it is estimated that 6–7 million people, globally, are infected with *T. cruzi* and many more are exposed to risk of infection, mostly in Latin America (WHO, 2019; Rassi Jr. *et al.*, 2012). Routes of primary infection consist of direct transmission by triatomine vector, consumption of food contaminated with feces of infected triatomines, transfusion of blood from infected donors, and vertical transmission from infected mothers to their newborns illness (Coura *et al.*, 2015). Clinically, CD displays 2 phases, acute and chronic. The initial, acute phase of infection with *T. cruzi* lasts for 4–8 weeks, and the chronic phase persists for the host's lifespan (Dias, 1984; WHO, 2019). The initial, acute phase is characterized by high parasitemia, where the parasite assumes the trypomastigote form and invades cells of the liver, gut, spleen, lymphatic ganglia, CNS, and skeletal and cardiac muscles tissue (Rassi Jr. *et al.*, 2010). The acute phase is usually asymptomatic or might present a mild febrile illness, complicating the diagnosis. About 30% of infected patients develop chronic CD, in which the parasites cause damage to target organs (Perez *et al.*, 2015).

Challenges still exist concerning CD, such as the difficulty for early diagnosis and in finding efficient antitrypanosomal drugs for the treatment, since current treatment requires

extended durations, have side effects and are unable to eliminate all parasites in some patients (Chatelain, 2014; Dias *et al.*, 2016). Only two old nitroheterocyclic drugs, benznidazole (Rochagan, Roche) and nifurtimox (Lampit, Bayer), are available for the treatment of CD and there is no vaccine for preventing the infection. These treatments were developed over 40 years ago and benznidazole is the only drug that is approved by US Food and Drug Administration to treat *T. cruzi* infection (CDC, 2019). These drugs require prolonged treatment (60 to 90 days), are effective only in the acute phase of the disease, and have severe toxic effects (Molina *et al.*, 2015; Forsyth *et al.*, 2016; Kratz *et al.*, 2018).

In recent years, our group has been developing, characterizing and testing coordination compounds containing the first row transition metal ions (Cu(II), Co(II), Zn(II) and Fe(III)) as a promising class of chemical with potential to be applied in the chemotherapy of distinct diseases, including neglected diseases such as Toxoplasmosis (Portes *et al.*, 2015), Leishmaniasis (Rocha *et al.*, 2023) and CD (Moreira *et al.*, 2021). We reported anti-*Toxoplasma* activity and ultrastructural analyzes of two Cu(II) complexes (Portes *et al.*, 2017). These complexes had also exhibited relevant antitumor activity (Fernandes *et al.*, 2015). Both complexes, which do not present Sulfadiazine (SDZ⁻) coordinated to the Cu(II) center, irreversibly control the growth of the parasite *T. gondii in vitro* that causes toxoplasmosis, resulting in IC₅₀ values of 3.57 and 0.78 μmol L⁻¹, after 48 h of treatment. It was observed that these compounds induce conversion of part of the parasites from the tachyzoite form to bradyzoite, with their subsequent death. The comparison between the IC₅₀ values for the compounds under investigation indicates better efficiency when compared with SDZ alone, suggesting an effect of the nature of the metal and the ligand on the anti-*Toxoplasma* activity (Portes *et al.*, 2017). Zn and Fe(III) complexes, containing SDZ⁻ coordinated to the metal center, also exhibited anti-*Toxoplasma* activity *in vitro* (Batista *et al.*, 2015; Portes *et al.*, 2018). Recently, we reported the anti-*Toxoplasma* activity and DFT studies of water-soluble complexes (Fe, Cu, Zn) containing the ligand N-2[(pyridine-2-ylmethyl)amino)ethanol. Among all compounds investigated, the Fe(III) complex [Fe(HL1)Cl₃] showed the best anti-*Toxoplasma* activity (Cardoso *et al.*, 2022).

We also evaluated the effects of two Co(II) coordination compounds *in vitro* antiproliferative activity against the promastigote form of *Leishmania amazonensis*, that causes Leishmaniasis, showing an IC₅₀ value for complex **(1)** of 4.90 (24 h), 3.50 (48 h) and 3.80 μmol L⁻¹ (72 h), and for complex **(2)** of 2.09, 4.20 and 2.80 μmol L⁻¹, respectively. Complex **(1)** was able to elevate mitochondrial membrane potential of the

parasites after treatment. Transmission electron microscopy revealed typical apoptotic condensation of chromatin, altered kinetoplast and mitochondria structures, suggesting that apoptosis-like cell death of the protozoa is probably mediated by an apoptotic mechanism associated with mitochondrial dysfunction (Rocha *et al.*, 2023).

In 2021 we reported the antichagasic activity of two isomeric Fe(III) complexes against *T. cruzi* epimastigotes at the nanomolar range concentration, showing low cytotoxicity to the host cells LLC-MK2, resulting in a high selectivity index. Treatment with both complexes, at nanomolar concentrations, generated important changes in essential organelles for parasite survival. After treatment with complex (2), mitochondria presented swelling and abnormal disposition around the kinetoplast and still changes in arrangement of kinetoplast. In addition, the formation of spicules in the lumen of reservosomes was detected after treatments with both complexes (Moreira *et al.*, 2021). Here, we tested the effect of both complexes on intracellular amastigotes of *T. cruzi* in LLC-MK2 host cells.

2. MATERIALS AND METHODS

2.1. Metallocomplexes

The compounds used were Fe- α -Nafttol BMPA and Fe- β -Nafttol BMPA, which have an iron centers and the organic ligand BMPA, and were named as complex (1) and complex (2), respectively. These compounds were synthesized and chemically characterized previously (MOREIRA *et al.*, 2021). They were diluted in dimethylsulfoxide (DMSO) solvent and added directly to the culture medium. The DMSO concentration did not exceed 0.01%, avoiding interference with the viability of the parasites and host cells.

2.2. Host cells culture

LLC-MK2 cells (ATCC® CCL-7™, Rockville, MD, USA) were cultured in 25 cm² cell culture flasks (SPL Life Sciences) in Dulbecco's Modified Eagle Medium (DMEM) (Sigma Aldrich, USA), supplemented with 10% or 5% fetal bovine serum (FBS) (Thermo Fisher Scientific, USA). The cultures were maintained at 37 °C under an atmosphere of 5% CO₂. Every 48 h or after the formation of confluent monolayers, cultures were treated with trypsin/EDTA solution (Sigma-Aldrich, USA) to obtain subcultures.

2.3. Cell viability

The viability of host cells after treatment with the compounds was evaluated based on the reduction of MTT [3-(4,5-dimethylthiazol-2-yl)-2,5-diphenyltetrazolium bromide] (Sigma

Aldrich, USA) (KUMAR *et al.*, 2018). In 96-well plates, 1×10^5 cells per well were grown in DMEM supplemented with 5% FBS. After 24 h, the cells were washed and treated with compounds at different concentrations. As a negative control, cells were cultured under the same conditions without the addition of compounds. As a positive control, cells were treated with 10% Triton X-100.

After 24 h of treatment, 15 μ l of MTT solution (5 mg/ml in DMEM) was added over the cells in each well of the plate, incubated for 4 h at 37 °C and 5% CO₂. The formed formazan crystals were solubilized by the addition of 100 μ l of DMSO. A 100 μ l volume of supernatant from each well was transferred to a new 96-well plate and read at 570 nm in a microplate reader VersaMax (Molecular Devices) using SoftMax Pro 6.0 software. Data were plotted using GraphPad Prism 5.0 software. The data presented were representative of at least three independent experiments.

2.4. Epimastigotes culture

T. cruzi (strain Dm28c) epimastigotes forms were maintained *in vitro* in 25 cm² cell culture flasks in Liver Infusion Tryptose (LIT) culture medium (DIFCO) (CAMARGO, 1964) supplemented with 10% FBS and hemin (20 μ g/mL). The cultures were maintained at 28 °C and every 72 or 96 h, when the parasites were in the exponential growth phase, subcultures of these cells were performed.

2.5. Metacyclogenesis

Epimastigotes of *T. cruzi* (strain Dm28c) were maintained as previously described (item 2.4) for 168 h reaching the transition between the logarithmic and stationary phases of growth. After this period, the parasites were transferred to Triatomine Artificial Urine (TAU) medium for 2 h at 28 °C and then to TAU-3AAG medium for 120 h (JORGE & CASTRO, 2000). At the end of this process, metacyclic trypomastigotes were recovered from the middle portion of the culture supernatant, centrifuged (1500 g, at 5 °C, for 15 min), resuspended in DMEM and counted with a Neubauer chamber.

2.6. Infection of host cells with trypomastigotes

Metacyclic trypomastigotes of *T. cruzi* (strain Dm28c), obtained from *in vitro* metacyclogenesis, were used to infect LLC-MK2 host cells. These cells were previously cultivated (1×10^4) for 24 h over sterile coverslips in a 24-well plate, and infected using a ratio of 10:1 (parasite:host cell). After 2 h of interaction, cells were washed with PBS to

remove non-internalized parasites and further cultured for 24 h with DMEM supplemented with FBS. After this time of infection, it was possible to observe amastigotes inside the host cells. Infected cultures had their DMEM supplemented with 5% FBS changed every 48 h. Similar procedure was performed with cells cultured in 25 cm² culture flasks for electron microscopy analysis.

2.7. Amastigote antiproliferative assay

After 24 h of infection, compounds were added to host cells infected with amastigotes at concentrations of 0, 5, 50, 100, 500 nM and 1 μM and maintained for up to 96 h of culture at 37 °C and 5% CO₂. Assays were in duplicates and at least three independent experiments were performed.

2.8. Bright field light microscopy

Infected and treated host cells were fixed in a 4% formaldehyde solution in PBS for 1 h, washed with PBS, stained with 10% Giemsa in distilled water for 10 min, and dehydrated through a graded series of acetone-xylene. Slides were mounted by placing the coverslips over a drop of Entellan. Slides were observed in the light microscope Axioplan - ZEISS. The infection index (I.I.) were obtained by quantifying the number of infected cells and the number of parasites per cell, using the following calculation: I.I.= % infected cells x mean number of parasites per infected cell. For the determination of the IC₅₀ (growth inhibitory concentration at 50%) of the compounds against amastigotes, the values of I.I. obtained with the five different concentrations used were plotted and a non-linear curve analysis performed using the Sigma Plot 8.0 program (Systat Software Inc., Chicago, IL, USA). For the significance tests, the data were analyzed by the Two-way ANOVA quantitative analysis of variance with Bonferroni's multiple comparison post-test using the Graph Pad Prism 5.0 program, Version 5.0 (San Diego, CA, USA). The results of the IC₅₀ calculations are presented as means ± SD of three independent biological replicates. The selectivity index (SI) was calculated by dividing the CC₅₀ (concentration that inhibits the proliferation of host cells by 50% of the host cells) by the IC₅₀ (PORTES *et al.*, 2017).

2.9. Electron Microscopy Analysis

For analysis of the parasites' ultrastructure, infected cells that were treated or not with the compounds cultured for 72h in 25 cm² culture flasks (120 nM and 200 nM of complexes (1) and (2), respectively), were fixed for 1 h in a solution containing 2.5% glutaraldehyde

and 4% recently prepared formaldehyde in 0.1 mol L⁻¹ sodium cacodylate buffer, pH 7.4. After fixation, cells were mechanically removed from the culture flasks with a cell scraper and washed twice with PBS and post-fixed for 1 h in the dark with a solution containing 1% osmium tetroxide (OsO₄) and 1.6% ferrocyanide in 0.1 M sodium cacodylate buffer. Subsequently, the parasites were washed in the same buffer, dehydrated in a graded series of acetone, and embedded in Epon. Ultrathin sections were stained with uranyl acetate and lead citrate and observed under a JEOL JEM 1400 Plus transmission electron microscope (MOREIRA *et al.*, 2021).

2.10. Mitochondrial membrane potential by fluorescence microscopy

The mitochondrial membrane potential of infected host cells and parasites treated or not with the compounds [120 nM and 200 nM of complexes **(1)** and **(2)**, respectively;] for 96 h) was investigated using the fluorescent marker JC-1. The parasites were incubated with 40 µg/ml of JC-1 in DMEM at 37 °C for 20 min (Macedo-Silva *et al.*, 2011) and were analyzed using a Zeiss LSM-710 confocal laser scanning microscope. Quantification of the mitochondrial membrane potential was performed by measurement of fluorescence intensity in ZEN Microscopy Software for each experimental condition in triplicates of three independent experiments. Parasites presenting red fluorescence labeled mitochondria were considered with active mitochondrial membrane potential.

3. RESULTS

The effect of the Fe(III) complexes was investigated against intracellular amastigotes growth for 96 h. No significant difference was found at 24 and 48 h, but after 72 h and 96 h of treatment a concentration-dependent inhibition of the growth of the parasite was detected (Figure 1). In the presence of 5 nM of complex **(1)** after 72 h of treatment, the infection index of amastigotes corresponded to 60% of the untreated group (control). At the same treatment time with 50, 100, 500 nM and 1 µM, the percentage of infection index was 36, 18, 3 and 2%, respectively, compared to the control group (Figure 1a). At 96 h of treatment, with the same treatment concentrations the infection index was 41, 39, 13, 1 and 1% of the control group, respectively (Figure 1a). A similar trend was observed for complex **(2)** (Figure 1b), indicating that the nature of the isomer (alpha or beta) presented slight influence on the anti-amastigotal activity. In the presence of 5 nM of complex **(2)** after 72 h of treatment, the infection index of amastigotes corresponded to 60% of the control group (Figure 1b). After the same treatment time with 50, 100, 500 nM and 1 µM,

the infection index was 50, 38, 6 and 3%, respectively, compared to the control group. At 96 h of treatment, the infection index was 68, 56, 28, 15 and 1% of the control group, respectively, for the same treatment concentrations (Figure 1b).

Complex **(1)** presented IC_{50} values of 61.29 ± 4.21 and 107.48 ± 6.60 nM for 72 and 96 h of treatment, respectively. Complex **(2)** also presented a low IC_{50} values of 50.64 ± 2.20 and 173.00 ± 5.60 nM for the same treatment times. The IC_{50} values of complexes **(1)** and **(2)** are promising when compared to some other metal complexes reported in the literature. The cytotoxicity of iron complexes to LLC-MK2 was evaluated after 72 and 96 h of treatment to obtain the CC_{50} value on mammalian cells and the SI of the compounds. Complex **(1)** presented CC_{50} values of 29.26 ± 0.44 and 17.98 ± 0.24 μ M for 72 and 96 h of treatment, respectively. Complex **(2)** also presented low CC_{50} values of 189.1 ± 15.8 and 78.59 ± 3.56 μ M for the same treatment times. Based on these data, the selectivity indexes values were 477.4 and 167.28 for complex **(1)**, and 3734.2 and 454.28 for complex **(2)**, against amastigotes, for 72 and 96 h of treatment, respectively (Table 1).

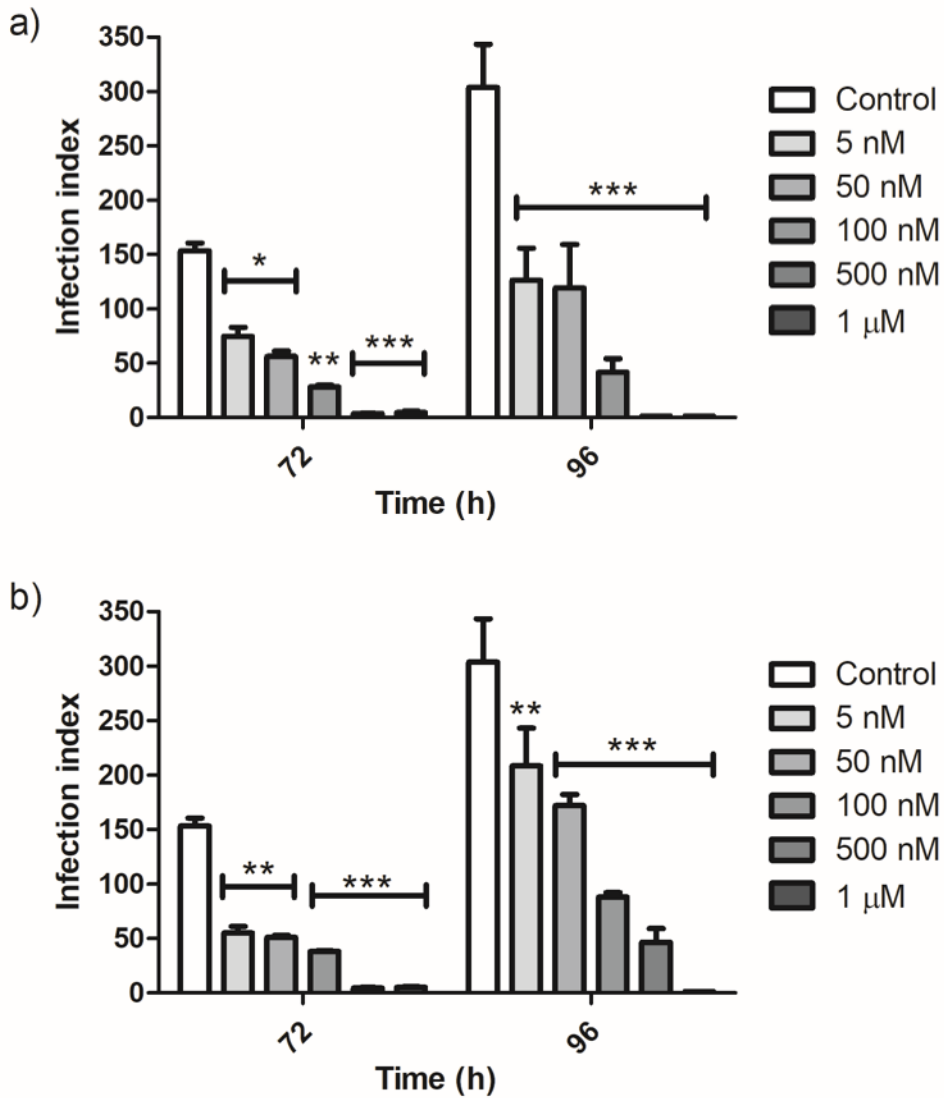


Figure 1. Antiproliferative effects of the Fe(III) (a) complex (1) and (b) complex (2) on amastigote of *Trypanosoma cruzi* in LLC-MK2 host cell line. After 24 h of infection, different concentrations of the complexes (1) and (2) were added to the cultures and the infection index evaluated at 72 h and 96 h. Mean and standard deviation of three independent experiments. * $P \leq 0.05$ ** $P \leq 0.01$ and *** $P \leq 0.001$ in relation to the control.

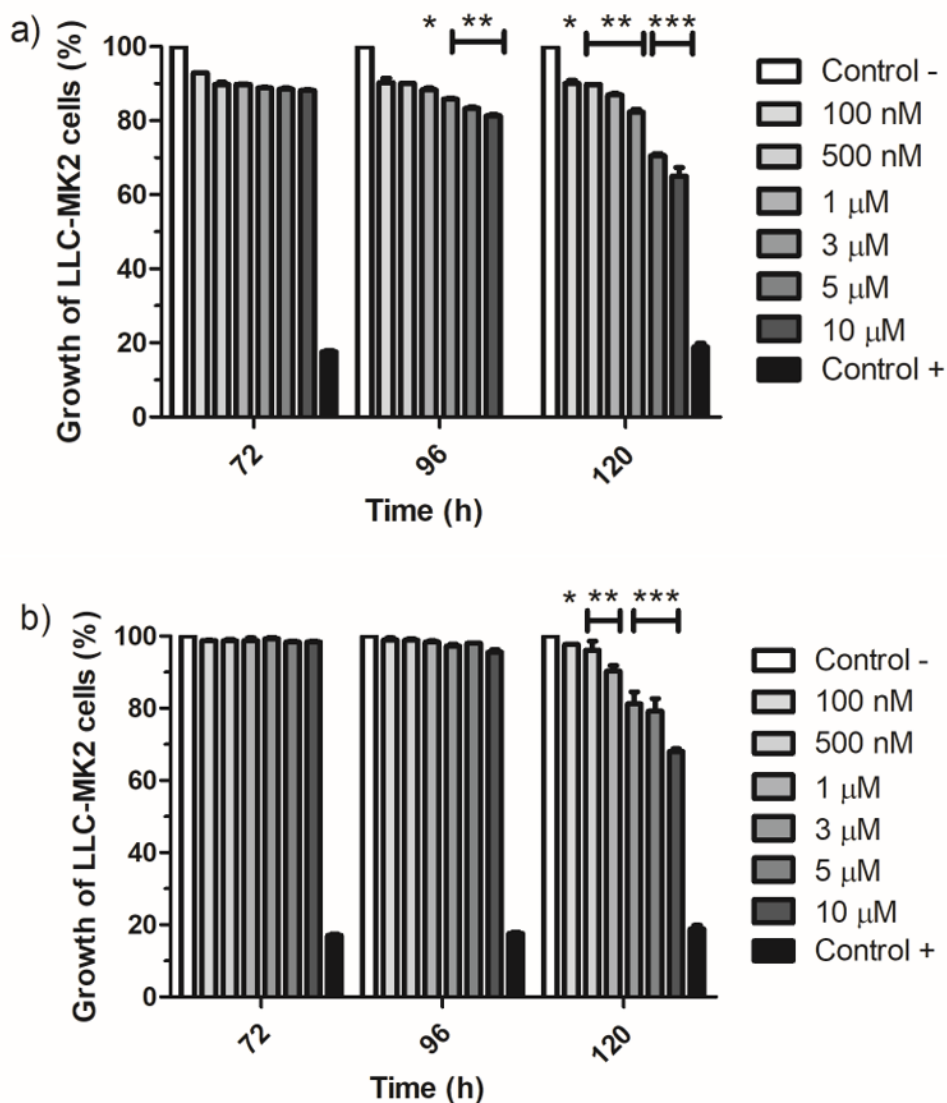


Figure 2. Cytotoxic effects of Fe(III) complexes on LLC-MK2 cells. Percentage of growth of LLC-MK2 cells treated with different concentrations of (a) complex (1) and (b) complex (2). Negative control: cells were cultured in DMEM medium with FBS without complexes. Positive control: cells were cultured with 10% Triton X-100 in DMEM medium. * $P \leq 0.05$ ** $P \leq 0.01$ and *** $P \leq 0.001$ in relation to the control (-).

Table 1. Cytotoxicity to amastigotes of *Trypanosoma cruzi* and to LLC-MK2 host cell line and Selective Index of the iron complexes

	IC ₅₀ (nM) <i>T. cruzi</i> amastigote		CC ₅₀ (μM) LLCMK2		SI	
	72 h	96 h	72 h	96 h	72 h	96 h
Complex (1)	61.29 ± 4.21	107.48 ± 6.60	29.26 ± 0.44	17.98 ± 0.24	477.40	167.28
Complex (2)	50.64 ± 2.20	173.00 ± 5.60	189.10 ± 15.8	78.59 ± 3.56	3734.20	454.28

IC₅₀: concentration that inhibits 50% of the proliferation of the replicative form.

CC₅₀: concentration that inhibits the proliferation of 50% of the host cells.

SI: selectivity index.

Light microscopy images revealed that treatments with the Fe(III) complexes for 96 h affected the characteristic organization of amastigotes inside the host cells. As expected, in untreated cells, numerous parasites were distributed throughout the cytoplasm (Figures 3A and 3B). However, after treatment with complex (1) (Figure 3C and 3D) and complex (2) (Figure 3E and 3F), number of parasites drastically reduced, confirming that the Fe(III) complexes lowered the growth of *T. cruzi*. In addition, treatment generated amastigotes with a fusiform shape (Figure 3C to 3F).

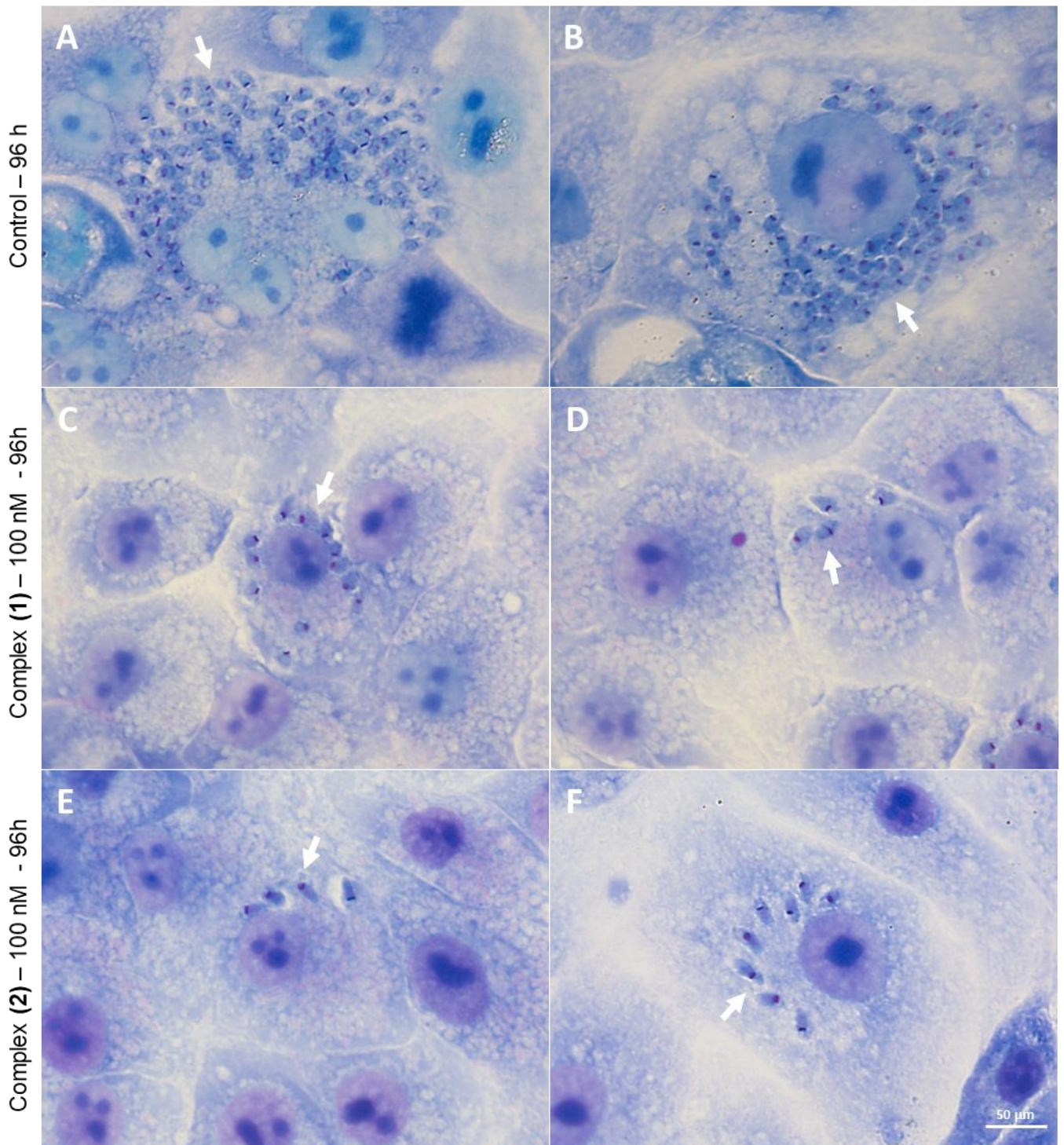


Figure 3. Bright field light microscopy of amastigote of *Trypanosoma cruzi* (arrows) in LLC-MK2 host cell line treated or not with Fe(III) complexes **(1)** and **(2)**. Non-treated parasites (A and B) cultured for 96 h. Parasites were treated for 96h with complex **(1)** (C and D) and complex **(2)** (E and F), both at 100 nM. After treatment, parasite numbers clearly reduced and they became elongated. Bars: 50 μ m

Transmission electron microscopy showed that untreated parasites presented normal ultrastructure, with well-arranged and preserved organelles, such as plasma membrane, nucleus, kinetoplast and mitochondria (Figure 4A and 4B). However, after treatment with complex **(1)** for 72 h (Figure 4C, D and E) and complex **(2)** for 72h (Figure 4F, G and H) parasites displayed an elongated shape (Figure 4C and F), their nucleus structure was altered with heterochromatin concentrated in patches at the nuclear envelope (Figures 4D, E and G), and the mitochondria swelled as seen by the abnormal disposition of their membrane around the kinetoplast (Figures 4E and 4H).

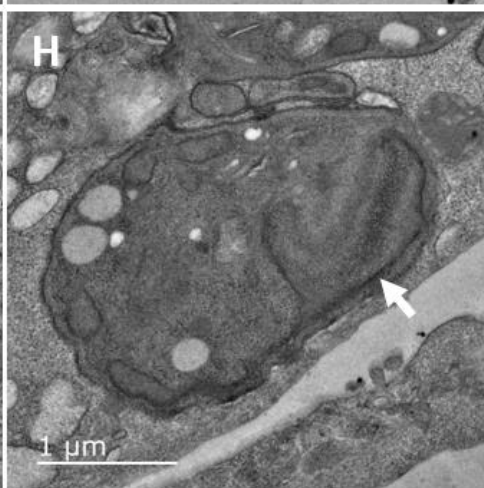
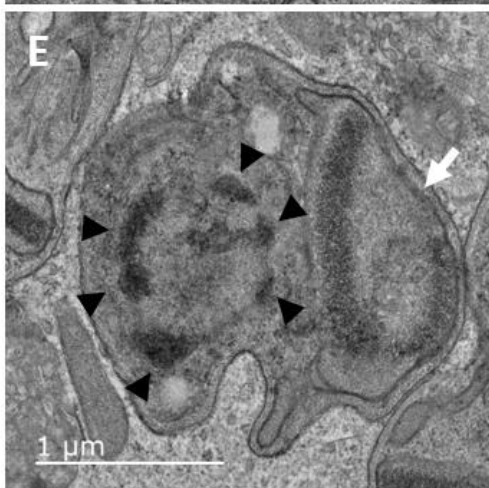
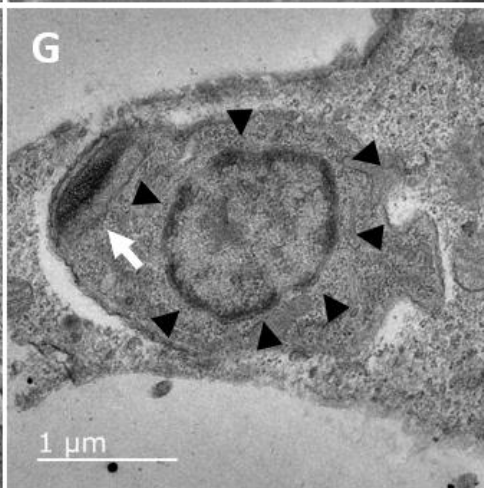
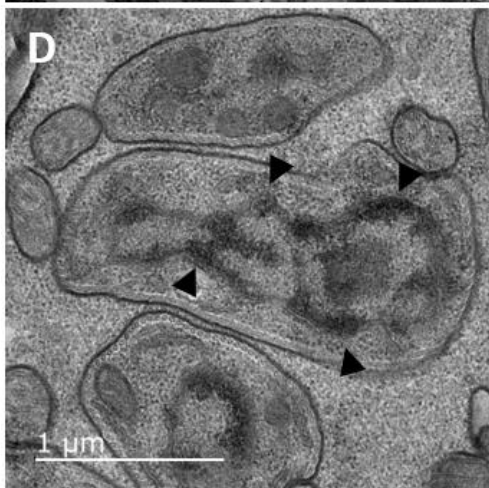
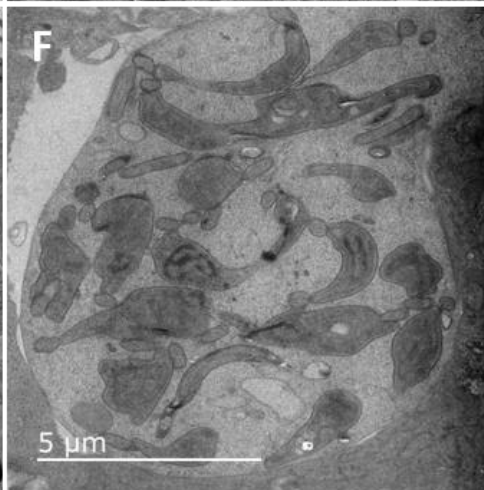
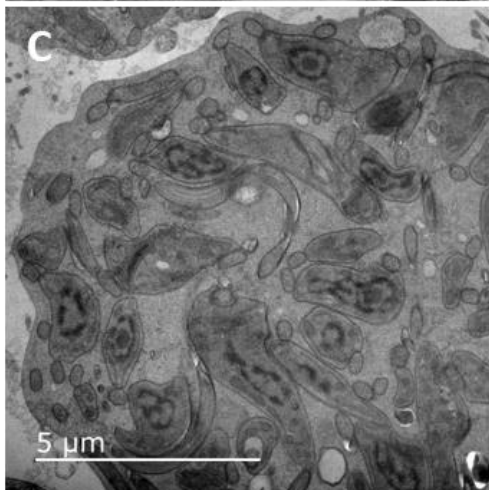
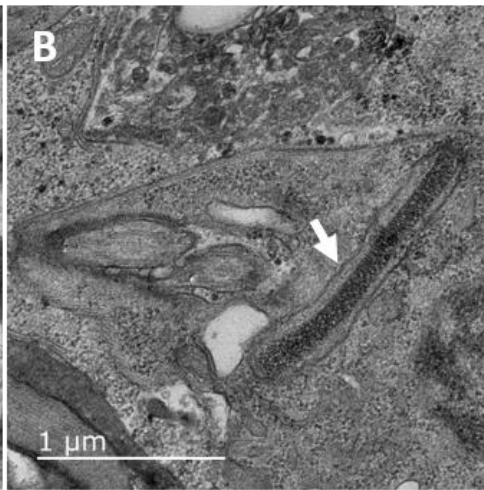
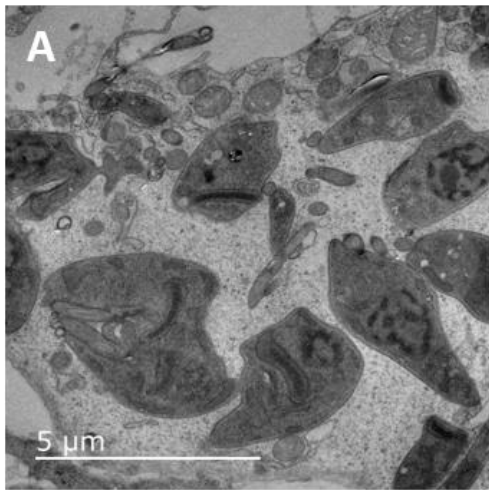


Figure 4. Transmission electron microscopy images of intracellular amastigote of *Trypanosoma cruzi* in LLC-MK2 host cell line treated or not with Fe(III) complexes **(1)** and **(2)**. (A and B) Untreated cells present parasites with normal ultrastructure of organelles such as the mitochondria membrane around the kinetoplast and nuclear chromatin. Parasites treated with complex **(1)** at 120 nM for 72 h (C, D and E) and complex **(2)** at 200 nM for 72h (F, G and H). Note that treatment induced swelling and abnormal disposition around the kinetoplast of the parasite mitochondria membrane (arrows) and altered nucleus structure, with heterochromatin concentrated in patches at the nuclear envelope (arrowhead). Bars: 5 μ m and 1 μ m.

Confocal laser scanning microscopy images showed significant loss of mitochondrial membrane potential in parasites treated with complexes **(1)** and **(2)** (at concentrations of 120 nM and 200 nM, respectively), and subsequently incubated with the mitochondrial functional marker JC-1. Untreated parasites presented normal mitochondrial function (Fig. 5A, B and C). After treatment with complex **(1)** for 96 h (Figure 5D, E and F) the reduction in mitochondrial membrane potential reached 15% (Figure 5J), when compared to the control. Parasites treated with complex **(2)** for 96h (Figure 5G, H and I), showed a more expressive reduction reaching 31% (Figure 5J). Thus, treatment with the compounds directly interfere with energy metabolism of the parasite.

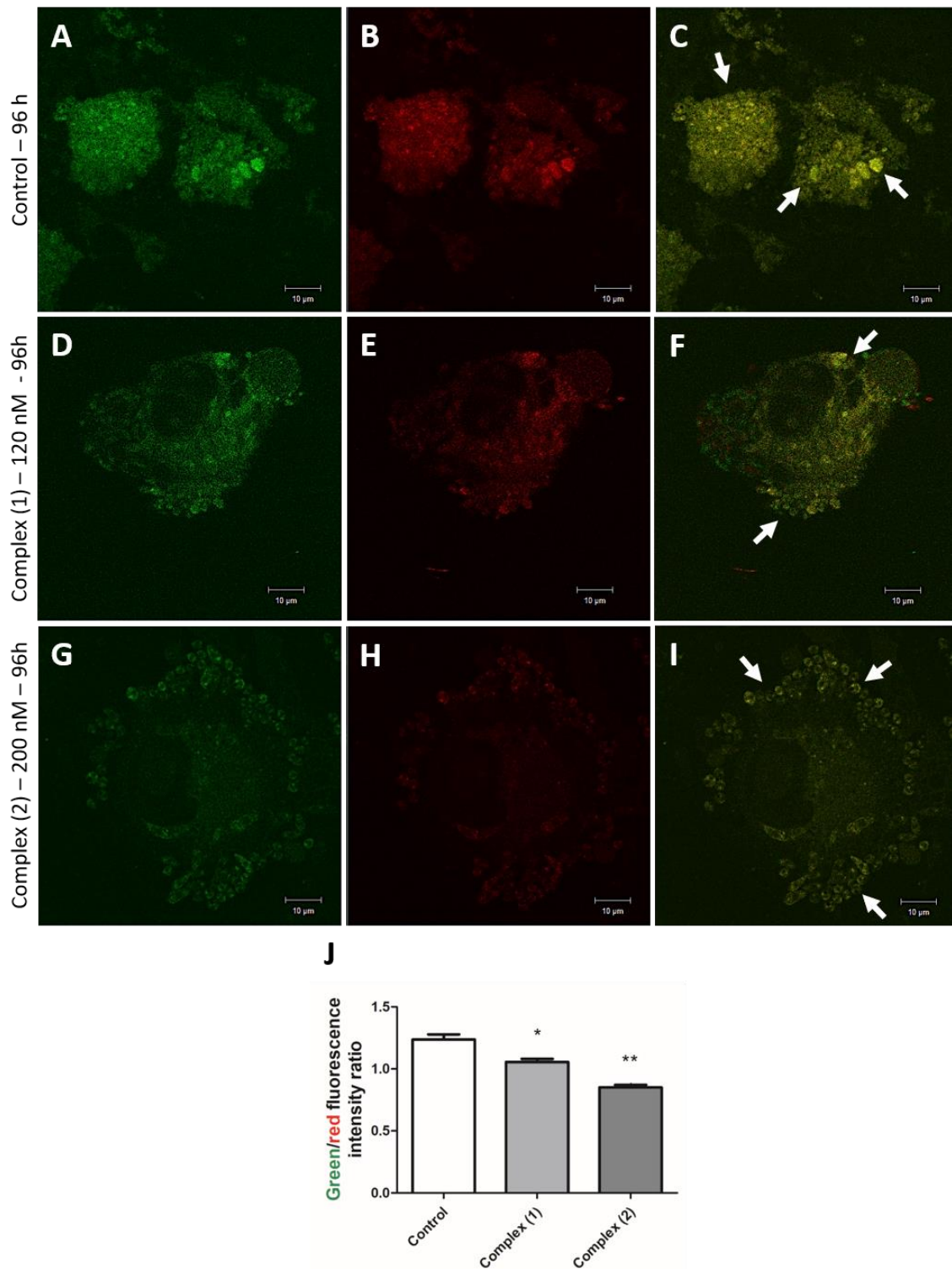


Figure 5. Mitochondrial membrane potential, revealed by JC-1 labeling, of amastigote forms of *Trypanosoma cruzi* in LLC-MK2 host cells treated or not with Fe(III) complexes (1) and (2). Parasites were treated for 96 h with complexes (1) and (2) at 120 nM and 200 nM, respective, and were visualized by light microscopy. Non-treated parasites (arrows) show normal mitochondrial membrane potential (A, B and C) and parasites (arrows) treated with complex (1) (D, E and F) or complex (2) (G, H and I) lost mitochondrial membrane potential as seen by low red JC-1 fluorescence. Bars: 10 µm. Ratio between the intensity of the green fluorescence with the red fluorescence of amastigotes JC-1 labeled

showing the status of the mitochondrial membrane potential after treatment with complexes (1) and (2). * $P \leq 0.05$ ** $P \leq 0.01$ in relation to the control.

4. DISCUSSION

Based on the need to develop and test new drugs to treat CD, we show here that dinuclear Fe(III) complexes (1) and (2) are effective in the treatment of *T. cruzi* amastigotes. The complexes showed low nanomolar IC₅₀ values, with a concentration-dependent inhibition of the growth of the parasite. Cytotoxicity test of the iron complexes for LLC-MK2 host cell resulted in high CC₅₀ values and, consequently, high SI for both complexes. The Fe(III) complexes also affected the characteristic organization of parasites inside the host cells, generating amastigotes with a fusiform shape. Ultrastructural analysis of the parasites treated with the complexes, in addition to confirming the elongation of their structure, also showed heterochromatin in the periphery of the nuclear envelope and swelled mitochondria. The treatment with both complexes was also able to reduce the mitochondrial membrane potential of the amastigotes. These findings show that Fe(III) complexes in nanomolar concentrations are capable of killing *T. cruzi* amastigotes, generating mitochondrial alterations and suggesting cell death by an apoptosis-like mechanism.

Compounds of metallic nature already present high antitripanosomal activity. Palladium and platinum complexes showed IC₅₀ values in the nanomolar range (67–200 nM) against epimastigotes of the Tulahuen 2 strain (Vieites *et al.*, 2008). Copper complex were also able to control the amastigote infection of the CL Brener strain with an IC₅₀ ranging from 0.3 to 418 μ M (Paixão *et al.*, 2019). We previously chemically characterized complexes (1) and (2) and showed an IC₅₀ values in the nanomolar scale (97–122 nM) after treatment of *T. cruzi* epimastigotes (Y strain) (Moreira *et al.*, 2021). These results corroborate and reinforce the importance of the IC₅₀ values present here against intracellular amastigote form of *T. cruzi* (Dm28c). These results showing that these complexes were able to penetrate the host cell plasma membrane and reach the parasite maintaining their efficiency.

Evaluations of the cytotoxicity of complexes (1) and (2) in LLC-MK2 cells were performed up to 120 hours of treatment. Both complexes showed low cytotoxicity to the host cell for treatments of 96h; significant toxicity was detected by 120h of treatment and in concentrations above 1000 times the IC₅₀ values for the parasite. Low values of IC₅₀ and high values of CC₅₀ resulted in high selectivity indexes (167 and 454, complexes (1) and (2), respectively). Thus, indicating high therapeutic safety for these drugs as prototypes. Benzimidazole SI values are reported varying from 1 (Caballero *et al.*, 2011) to 11.26 (Fonseca-Berzal *et al.*, 2016) depending on the cell lineage. For complexes (1) and (2) the SI was about 15 and 40 times higher, respectively, which indicates an efficient selectivity index against the pathogenic agent and demonstrating that they are safer than this current drug. While complex (1) is slightly more active against the parasite, complex (2) has a better SI.

We have shown that amastigotes of *T. cruzi* when treated with complex (1) or (2) undergo morphological changes, as seen in light microscopy images, losing their rounded shape and presenting themselves with a fusiform shape. Possibly this is due to a strategy of the

parasite to differentiate itself in order to survive, but additional tests still need to be performed. In addition, amastigotes also show ultrastructural changes as the mitochondria swelled as seen by the abnormal disposition of their membrane around the kinetoplast and their nucleus structure was altered with heterochromatin concentrated in patches at the nuclear envelope. Ultrastructural changes such as mitochondrial swelling and heterochromatin concentrated in patches at the nuclear envelope have already been reported as typical morphological characteristics of cell death promoted by apoptosis-like in trypanosomes and mammalian cells (Salvesen & Dixit, 1997; Deolindo *et al.*, 2010; Rocha *et al.*, 2023).

The ultrastructural alterations observed in mitochondria after treatment with both complexes were probably impairing the function of this organelle. This was confirmed by analyzing the mitochondrial membrane potential with the JC-1 marker, a lipophilic cationic fluorescent dye, which is used to monitor mitochondrial potential (Macedo-Silva *et al.*, 2011; Moreira *et al.*, 2021). JC-1 assay showed significant loss of mitochondrial membrane potential in parasites treated with complexes (1) and (2). Trypanosomatids presents a single mitochondria, an organelle that plays an important role in energy metabolism, and the dysfunction of this organelle can lead to parasite death (Pedra-Rezende *et al.*, 2022). These results showed that both complexes were capable of affecting a central organelle of the parasite possibly impairing energy metabolism and other functions of the mitochondria.

5. CONCLUSION

As previously described against epimastigotes forms of *T. cruzi* (Moreira *et al.*, 2021), complexes (1) e (2) were active against *T. cruzi* amastigotes at concentrations in the nanomolar range, showing low cytotoxicity to the host cells LLC-MK2, resulting in a high selectivity index for both complexes. Treatment with both complexes at nanomolar concentrations generated important changes in mitochondria and nuclear heterochromatin of the parasite, suggesting cell death of the parasite promoted by apoptosis-like. A reduction in mitochondrial membrane potential after treatment with both complexes was detected. Thus, both complexes affected an organelle involved with essential cell function. The antitrypanosomal activity of Fe(III) complexes, previously demonstrated in epimastigotes forms, was also presented, for the first time, against amastigotes forms of the parasite, leading to a lethal action due to the imbalance of the energetic system. These findings open interesting perspectives for investigating the efficacy of metallic complexes against trypanomastigote form in *in vivo* models, as well as for a more complete description of the mechanism of action of these complexes against amastigotes.

6. REFERENCES

- BATISTA, L. C.; DE SOUZA, F. S.; DE ASSIS, V. M.; SEABRA, S. H.; BORTOLUZZI, A. J.; RENNÓ, M. N.; HORN JR., A.; DAMATTA, R. A.; FERNANDES, C.. Antiproliferative activity and conversion of tachyzoite to bradyzoite of *Toxoplasma gondii* promoted by new zinc complexes containing sulfadiazine, RSC Adv.. v. 5, p. 100606–100617, 2015. DOI: 10.1039/C5RA17690E

- CABALLERO, A. B.; MARÍN, C.; RODRÍGUEZ-DIÉGUEZ, A.; RAMÍREZMACÍAS, I.; BAREA, E.; SÁNCHEZ-MORENO, M.; SALAS, J. M. In vitro and in vivo antiparasital activity against *Trypanosoma cruzi* of three novel 5-methyl-1,2,4-triazolo[1,5-a]pyrimidin7(4H)-one-based complexes, *J. Inorg. Biochem.* v. 105(6), p. 770–776, 2011. DOI: 10.1016/j.jinorgbio.2011.03.015
- CAMARGO, E. P. Growth and differentiation in *Trypanosoma cruzi*. I. Origin of. *Rev. Inst. Med. Trop. Sao Paulo.* v. 12, p. 93–100, 1964. PMID: 14177814
- CARDOSO, A.P.; MADUREIRA, L.M.P.; SEGAT, B. B.; JENNIFER, N.C.; CARGNELUTTI, R.; CANDELA, D. R.S.; MARIANO, D. L.; PARREIRA, R.L.T.; HORN JR., A.; SEABRA, S. H.; DAMATTA, R.A.; MOREIRA, F. F.; MOREIRA, R. V.; CARAMORI, G. F.; FERNANDES, C. Development, structural, spectroscopic and in silico investigation of new complexes relevant as antitoxoplasma metallopharmacs, *J. Mol. Struct.* v. 1265, p. 133380, 2022. <https://doi.org/10.1016/j.molstruc.2022.133380>.
- CDC, Centers for Disease Control and Prevention, Antiparasitic Treatment. 2019. https://www.cdc.gov/parasites/chagas/health_professionals/tx.html.
- CHAGAS, C. Nova tripanosomíase humana: estudos sobre a morfologia e o ciclo evolutivo do *Schizotrypanum cruzi* n. gen., n.sp., agente etiológico de nova entidade mórbida do homem. *Mem. Inst. Oswaldo Cruz.* v. 1, p. 159–218, 1909. DOI: 10.1590/S0074-02761909000200008.
- Chatelain, E. Chagas disease drug discovery: toward a new era. *J. Biomol. Screen.* v. 20, p. 22–35, 2014. DOI: 10.1177/1087057114550585
- COURA JR. The main sceneries of Chagas disease transmission. The vectors, blood and oral transmissions - A comprehensive review. *Mem. Inst. Oswaldo Cruz.* v. 110, p. 277–282, 2015.
- DEOLINDO, P.; TEIXEIRA-FERREIRA, A.S.; DAMATTA, R.A.; ALVES, E.W. L-amino acid oxidase activity present in fractions of *Bothrops jararaca* venom is responsible for the induction of programmed cell death in *Trypanosoma cruzi*. *Toxicon.* v. 56, p. 944–955, 2010. <https://doi.org/10.1016/j.toxicon.2010.06.019>
- DIAS JCP, RAMOS AN JR, GONTIJO ED, LUQUETTI A, SHIKANAI-YASUDA MA, COURA JR, TORRES RM, MELO JRDC, DE ALMEIDA EA, DE OLIVEIRA W JR, SILVEIRA AC, DE REZENDE JM, PINTO FS, FERREIRA AW, RASSI A, FRAGATA FILHO AA, DE SOUSA AS, CORREIA D, JANSEN AM, ANDRADE GMQ, BRITTO CFDPDC, PINTO AYDN, RASSI A JR, CAMPOS DE, ABAD-FRANCH F, SANTOS SE, CHIARI E, HASSLOCHER-MORENO AM, MOREIRA EF, MARQUES DSDO, SILVA EL, MARINETO JA, GALVÃO LMDC, XAVIER SS, VALENTE SADS, CARVALHO NB, CARDOSO AV, SILVA RAE, DA COSTA VM, VIVALDINI SM, OLIVEIRA SM, VALENTE VDC, LIMA MM, ALVES RV. 2016. 2nd Brazilian consensus on Chagas disease, 2015. *Rev. Soc. Bras. Med. Trop.* v. 49, p. 3-60, 2016. doi: 10.1590/0037-8682-0505-2016
- DIAS, J.C.P. Acute Chagas' disease. *Mem Inst Oswaldo Cruz.* v. 79 (suppl), p. 85-91, 1984.
- FERNANDES, C.; HORN JR., A.; LOPES, B. F.; BULL, E. S.; AZEREDO, N. F. B.; KANASHIRO, M. M.; BORGES, F. V.; BORTOLUZZI, A. J.; SZPOGANICZ, B.; PIRES, A. B.; FRANCO, R. W. A.; ALMEIDA, J. C. A.; MACIEL, L. L. F.; RESENDE, J. A. L. C.; SCHENK, G.. Induction of apoptosis in leukemia cell lines by new copper(II) complexes containing naphthyl groups via interaction with death receptors, *J. Inorg. Biochem.* v. 153, p. 68–87, 2015. DOI: 10.1016/j.jinorgbio.2015.09.014.
- FONSECA-BERZAL, C.; IBÁÑEZ-ESCRIBANO, A.; REVIRIEGO, F.; CUMELLA, J.; MORALES, P.; JAGEROVIC, N.; NOGAL-RUIZ, J. J.; ESCARIO, J. A.; DA SILVA, P. B.;

- SOEIRO, MDE. N.; GÓMEZBARRIO, A.; ARÁN, V. J. Antichagasic and trichomonacidal activity of 1-substituted 2-benzyl-5-nitroindazolin-3-ones and 3-alkoxy-2-benzyl-5-nitro-2H indazoles, *Eur. J. Med. Chem.* v. 115, p. 295–310, 2016. DOI: 10.1016/j. ejmech.2016.03.036.
- FORSYTH, C. J.; HERNANDEZ, S.; OLMEDO, W.; ABUHAMIDAH, A.; TRAINA, M. I.; SANCHEZ, D. R.; SOVEROW, J.; MEYMANDI, S. K. Safety Profile of Nifurtimox for Treatment of Chagas Disease in the United States, *Clin. Infect. Dis.* v. 63(8), p. 1056–1062, 2016. DOI: 10.1093/cid/ciw477.
- JORGE, T.C.A.; CASTRO, S.L. Doença de chagas: manual para experimentação animal [online]. Rio de Janeiro: **Editora FIOCRUZ**, 2000. 368 p. Antropologia e Saúde collection. ISBN 85-85676-75-2. Available from SciELO Books <<http://books.scielo.org>>.
- KRATZ, J.M.; GARCIA BOURNISSEN, F.; FORSYTH, C.J.; SOSA-ESTANI, S. Clinical and pharmacological profile of benzimidazole for treatment of Chagas disease. *Expert Rev. Clin. Pharmacol.* v. 11, p. 943-957, 2018. DOI: 10.1080/17512433.2018.1509704
- KUMAR, P.; NAGARAJAN, A.; UCHIL, P.D. Analysis of Cell Viability by the MTT Assay. *Cold Spring Harb Protoc.* v. 6, 2018. doi: 10.1101/pdb.prot095505. PMID: 29858338.
- MACEDO-SILVA, S. T.; DE OLIVEIRA SILVA, T. L.; URBINA, J. A.; DE SOUZA, W.; RODRIGUES, J. C. Antiproliferative, Ultrastructural, and Physiological Effects of Amiodarone on Promastigote and Amastigote Forms of *Leishmania amazonensis*, *Mol. Biol. Int.*, 876021, 2011. DOI: 10.4061/2011/876021
- MOLINA, I.; SALVADOR, F.; SÁNCHEZ-MONTALVÁ, A.; TREVIÑO, B.; SERRE, N.; SAO AVILÉS, A.; ALMIRANTE, B. Toxic Profile of Benzimidazole in Patients with Chronic Chagas Disease: Risk Factors and Comparison of the Product from Two Different Manufacturers, *Antimicrob. Agents Chemother.* v. 59(10), p. 6125–6131, 2015. DOI: 10.1128/AAC.04660-14.
- MOREIRA FF, PORTES JA, BARROS AZEREDO NF, FERNANDES C, HORN A JR, SANTIAGO CP, SEGAT BB, CARAMORI GF, MADUREIRA LMP, CANDELA DRS, MARQUES MM, LAMOUNIER CAMARGOS RESENDE JA, DE SOUZA W, DAMATTA RA, SEABRA SH. Development of new dinuclear Fe(III) coordination compounds with in vitro nanomolar antitrypanosomal activity. *Dalton Trans.* v. 14;50(35), p. 12242-12264, 2021. doi: 10.1039/d1dt01048d. PMID: 34519725.
- PAIXÃO, D. A.; LOPES, C. D.; CARNEIRO, Z. A.; SOUSA, L. M.; DE OLIVEIRA, L. P.; LOPES, N. P.; PIVATTO, M.; CHAVES, J. D. S.; DE ALMEIDA, M. V.; ELLENA, J.; MOREIRA, M. B.; NETTO, A. V. G.; DE OLIVEIRA, R. J.; GUILARDI, S.; DE ALBUQUERQUE, S.; GUERRA, W. In vitro anti-Trypanosoma cruzi activity of ternary copper(II) complexes and in vivo evaluation of the most promising complex, *Biomed. Pharmacother.* v. 109, p. 157– 166, 2019 DOI: 10.1016/j.biopha.2018.10.057.
- PEDRA-REZENDE, Y.; BOMBAÇA, A.C.S.; MENNA-BARRETO, R.F.S. Is the mitochondrion a promising drug target in trypanosomatids? *Mem Inst Oswaldo Cruz.* v. 21, p. 117:e210379, 2022. DOI: 10.1590/0074-02760210379. PMID: 35195164; PMCID: PMC8862782.
- PEREZ, C.J.; LYMBERY, A.J.; THOMPSON, R.C.A. Reactivation of chagas disease: implications for global health. *Trends Parasitol.* v. 31 (11), p. 595-603, 2015. DOI: 10.1016/j.pt.2015.06.006
- PORTES, J. A.; AZEREDO, N. F. B.; SIQUEIRA, P. G. T.; DE SOUZA, T. G.; FERNANDES, C.; HORN JR., A.; CANDELA, D. R. S.; DE SOUZA, W.; DAMATTA, R. A.; SEABRA, S. H. A new iron(III) complex-containing sulfadiazine inhibits the proliferation and induces cystogenesis of *Toxoplasma gondii*, *Parasitol. Res.* v. 117(9), p. 2795–2805, 2018. DOI: 10.1007/s00436-018-5967-7

- PORTES, J. A.; MOTTA, C. S.; AZEREDO, N. F.; FERNANDES, C.; HORN JR., A.; DE SOUZA, W.; DAMATTA, R. A.; SEABRA, S. H. In vitro treatment of *Toxoplasma gondii* with copper(II) complexes induces apoptosis-like and cellular division alterations, *Vet. Parasitol.* v. 245, p. 141–152, 2017. DOI: 10.1016/j. vetpar.2017.04.002.
- PORTES, J.A.; SOUZA, T.G.; DOS SANTOS, T.A.; DA SILVA, L.L.; RIBEIRO, T.P.; PEREIRA, M.D.; HORN, A.JR.; FERNANDES, C.; DAMATTA, R.A.; DE SOUZA, W.; SEABRA, S.H.; Reduction of *Toxoplasma gondii* Development Due to Inhibition of Parasite Antioxidant Enzymes by a Dinuclear Iron(III) Compound. *Antimicrobial Agents Chemotherapy*, [S.l.], v. 59, n. 12, p. 7374-7386, 2015.
- RASSI JR., A.; RASSI A.; MARCONDES DE REZENDE, J. American trypanosomiasis (Chagas disease). *Infect. Dis. Clin. North Am.* v. 26, p. 275–291, 2012. DOI: 10.1016/j. idc.2012.03.002.
- RASSI JR., A.; RASSI, A.; MARIN-NETO, J.A. Chagas disease. *Lancet*, 375 (9723), p. 1388-1402, 2010. DOI: 10.1016/S0140-6736(10)60061-X
- ROCHA SM, HORN A JR, R DE M L TERRA A, REZENDE LM, MOREIRA FF, DAMATTA RA, XAVIER FR, CERVO R, CARGNELUTTI R, MOORKKANNUR SN, OWENBY G, PRABHAKAR R, SEABRA SH, FERNANDES C. In vitro anti-*Leishmania* activity of new isomeric cobalt(II)complexes and in silico insights: Mitochondria impairment and apoptosis-like cell death of the parasite. *J Inorg Biochem.* v. 240:112088, 2023. doi: 10.1016/j.jinorgbio.2022.112088. Epub 2022 Dec 9. PMID: 36630792.
- SALVESEN, G.S.; DIXIT, V.M. Caspases: intracellular signaling by proteolysis. *Cell*, v. 91, p. 443-446, 1997. DOI: 10.1016/s0092-8674(00)80430-4
- VIEITES, M.; SMIRCICH, P.; PARAJÓN-COSTA, B.; RODRÍGUEZ, J.; GALAZ, V.; OLEAZAR, C.; OTERO, L.; AGUIRRE, G.; CERECETTO, H.; GONZÁLEZ, M.; GÓMEZ-BARRIO, A.; GARAT, B.; GAMBINO, D. Potent in vitro anti-*Trypanosoma cruzi* activity of pyridine-2- thiol N-oxide metal complexes having an inhibitory effect on parasite-specific fumarate reductase, *J. Biol. Inorg. Chem.* v. 13, p. 723–735, 2008. DOI: 10.1007/s00775-008-0358-7.
- WHO: World Health Organization, Chagas disease (American trypanosomiasis). 2019. https://www.who.int/neglected_diseases/news/Chagas-Preventing-mother-to-child-transmission/en/.

4. DISCUSSÃO

Tomando como base a necessidade de desenvolver e testar novos fármacos para tratar a DC, mostramos aqui a eficácia dos complexos dinucleares de Fe(III) (**1**) e (**2**) no tratamento de epimastigotas e amastigotas de *T. cruzi*, apresentando desempenho promissor no desenvolvimento de uma nova terapia. Os complexos apresentaram baixos valores de IC₅₀ na escala nanomolar, com inibição do crescimento do parasito dose-dependente. O teste de citotoxicidade dos complexos de Fe para célula hospedeira LLC-MK2 resultou em altos valores de CC₅₀ e, conseqüentemente, alto índice de seletividade (IS) para ambos os complexos. Os complexos de Fe(III) também afetaram a organização característica dos parasitos dentro das células hospedeiras, gerando amastigotas com formato fusiforme. A análise ultraestrutural dos parasitos tratados com os complexos, além de confirmar o alongamento de sua estrutura, também mostrou heterocromatina na periferia do envelope nuclear, mitocôndrias inchadas e formação de espículas no interior dos reservossomos. O tratamento com ambos os complexos também foi capaz de reduzir o potencial de membrana mitocondrial de epimastigotas e amastigotas. Esses achados mostram que complexos de Fe(III) em concentrações nanomolares são capazes de eliminar epimastigotas e amastigotas de *T. cruzi*, gerando alterações em organelas importantes para a sobrevivência do parasito e sugerindo morte celular por um mecanismo semelhante à apoptose.

Compostos de natureza metálica possuem uma significativa importância no desenvolvimento farmacológico, devido às diversas aplicações em diferentes áreas, principalmente contra agentes infecciosos. As estratégias na terapia contra *T. cruzi* se baseiam em três princípios: coordenação de um ligante metálico com atividade tripanocida, coordenação de compostos metálicos intercalantes de DNA e de compostos inibidores diretos de enzimas do parasito (FRICKER *et al.*, 2008). Estudos mostram que a utilização de compostos em coordenação à metais trazem benefício e agregam vantagens aos fármacos, que se tornam mais ativos que os compostos sozinhos (não coordenados à metais) e mais eficazes que fármacos da clínica, como os compostos de Pt e Pd, que foram mais ativos em testes *in vitro* contra a forma epimastigota de *T. cruzi* do que o Nifurtimox (OTERO *et al.*, 2006; VIEITES *et al.*, 2011).

Os compostos com núcleo de Fe estudados aqui, apresentaram baixos valor de IC₅₀, em concentrações na escala nanomolar (50–173 nM), para os testes *in vitro* contra as formas epimastigota (cepa Y) e amastigotas (cepa Dm28C) de *T. cruzi*. PORTES e

colaboradores (2015), também mostraram o efeito de complexos com núcleo de Fe sobre taquizoítas de *Toxoplasma gondii in vitro*, por até seis dias de tratamento. Este composto apresentou um valor de IC₅₀ na faixa de micromolar, provocando alterações no citoplasma e na membrana que indicam morte por um mecanismo similar a apoptose, além de induzir cistogênese. Esse composto provocou o aumento de produção de espécies reativas de oxigênio nas células infectadas e tratadas, e foi capaz de reduzir a atividade de enzimas antioxidantes importantes para o parasito. Apesar de atingir o parasito *T. gondii*, o composto apresentou baixa citotoxicidade para as células hospedeiras, assim como vimos neste trabalho com os compostos testados. Os valores de IC₅₀ dos complexos de Fe (III) (1) e (2) são promissores quando comparados a alguns outros complexos metálicos relatados na literatura. Caballero e colaboradores (2011) mostraram em seu trabalho valores de IC₅₀ na faixa micromolar de três diferentes complexos metálicos (24,4 µM a 31,2 µM) e o medicamento Benznidazol (15,8 µM) após 72 h de tratamento para epimastigotas (cepa Maracay) (CABALLERO *et al.*, 2011); os valores observados para agentes à base de V também estão na faixa de 6,2 µM - 10,5 µM, enquanto o IC₅₀ observado para Nifurtimox é de 2,8 µM após 120 h de tratamento para epimastigotas (cepa CL Brener) (SCALESE *et al.*, 2018). Alguns outros complexos de natureza metálica foram ativos com valores de IC₅₀ na faixa nanomolar, semelhantes aos compostos que estamos relatando. Os complexos de Pd e Pt apresentaram IC₅₀ de 67 - 200 nM contra epimastigotas (cepa Tulahuen 2) (VIEITES *et al.*, 2008) e o complexo de Cu também foi capaz de controlar a infecção de amastigotas (cepa CL Brener) com um IC₅₀ variando de 0,3 a 418 µM (PAIXÃO *et al.*, 2019).

Estudos com compostos de natureza química não metálica também mostram alta atividade, como novos derivados 4-minopiridínicos, derivados azólicos e imidazóis 1 e 3-5, que apresentaram valores de IC₅₀ na faixa de concentração em nanomolar (5,0 a 36,0 nM) contra amastigotas (cepa Tulahuen C2C4). Os enantiômeros (S)-1, (S)-3 e (S)-5 mostraram uma atividade mil vezes maior do que o medicamento de referência Benznidazol (FRIGGERI *et al.*, 2013). Vários estudos revelam a atividade tripanocida de alcalóides. Neste contexto, os derivados da quinolina têm recebido grande atenção, como o 4'-Odemethylancistrocladinium A, um alcalóide naphthylyisoquinoline isolado da casca e das folhas de *Ancistrocladus ochinchinensis*, que apresentou excelente efeito contra amastigotas de *T. cruzi*, apresentando um IC₅₀ igual a 0,03 µM, sendo cerca de 70 vezes mais potente que o Benznidazol (BRINGMANN *et al.*, 2011). Portanto, esses complexos podem ter potencial como drogas anti-*Trypanosoma*.

No primeiro trabalho exposto aqui, caracterizamos quimicamente os complexos de Fe(III) **(1)** e **(2)** e mostramos valores de IC₅₀ na escala nanomolar após o tratamento de epimastigotas de *T. cruzi* (cepa Y). Esses resultados corroboram e reforçam a importância dos valores de IC₅₀, também na escala nanomolar presentes no segundo trabalho contra a forma intracelular amastigota de *T. cruzi* (cepa Dm28c). Esses resultados mostram que esses complexos foram capazes de penetrar na membrana plasmática da célula hospedeira e atingir o parasito mantendo sua eficiência.

As avaliações da citotoxicidade dos complexos de Fe(III) **(1)** e **(2)** em células LLC-MK2 foram realizadas em até 120 horas de tratamento. Ambos os complexos apresentaram baixa citotoxicidade para a célula hospedeira para tratamentos de 96h; toxicidade significativa foi detectada a partir de 120h de tratamento e em concentrações 1000 vezes acima dos valores de IC₅₀ para o parasito. Valores baixos de IC₅₀ e altos valores de CC₅₀ resultaram em altos IS (167 e 454, complexos **(1)** e **(2)**, respectivamente). Assim, indicando alta segurança terapêutica para esses fármacos, não oferecendo risco ao hospedeiro e agindo de forma mais seletiva contra o parasito. Os valores de IS para o Benznidazol são relatados variando de 1 (CABALLERO *et al.*, 2011) a 11,26 (FONSECA-BERZAL *et al.*, 2016), dependendo da linhagem celular. Para os complexos **(1)** e **(2)** o IS foi cerca de 15 e 40 vezes maior, respectivamente, o que indica um IS eficiente contra o agente patogênico e assim demonstrando que são mais seguros que a droga de escolha para o tratamento atual para a DC. Enquanto o complexo **(1)** se mostrou um pouco mais ativo contra o parasito, o complexo **(2)** tem um IS melhor.

Investigamos aqui o efeito dos compostos de Fe(III) **(1)** e **(2)** sobre a ultraestrutura do parasito, utilizando a microscopia eletrônica de transmissão, que permite a observação detalhada de organelas e outras estruturas celulares. Esse tipo de análise pode auxiliar no esclarecimento de questões relacionadas a mecanismos de ação desses quimioterápicos como já foi visto em alguns trabalhos (CARDOSO *et al.*, 2022; ROCHA *et al.*, 2023). Com isso podemos observar alterações importantes em epimastigotas e amastigotas de *T. cruzi* após o tratamento com ambos os complexos em organelas essenciais para a sobrevivência dos parasitos como mitocôndrias, reservossomos e núcleo. Mostramos que tanto epimastigotas quanto em amastigotas de *T. cruzi*, quando tratadas com o complexo **(1)** ou **(2)** sofrem alterações em suas mitocôndrias gerando inchaço e disposição anormal de sua membrana ao redor do cinetoplasto, que por sua vez também apresentou menor condensação em seu arranjo. As mitocôndrias são organelas essenciais envolvidas na conversão de energia, ciclo celular, sinalização e morte celular. A mitocôndria deste

parasito encontra-se intimamente associada ao cinetoplasto (ou DNA mitocondrial), e abriga diferentes enzimas do metabolismo oxidante e energético e devido as diferenças entre as mitocôndrias de mamíferos e tripanosomatídeos, esta organela é um excelente alvo para intervenções terapêuticas (MENNA-BARRETO *et al.*, 2014). Portanto, nosso trabalho mostra que os complexos são capazes de atingir um alvo farmacológico de destaque, possivelmente gerando impacto no metabolismo energético dos parasitos.

Outra organela que apresentou alterações ultraestruturais foram os reservossomos dos epimastigotas de *T. cruzi*, como o rompimento desta organela e o surgimento de cristais em seu lúmen. Os reservossomos são organelas lisossômicas essenciais para o metabolismo energético, que estão presentes na parte posterior dos epimastigotas de *T. cruzi* e estão presentes de forma exclusiva nessas formas. Estas organelas são estruturas de membrana arredondada com reservas lipídicas em seu lúmen com aspecto elétron denso (SANT'ANNA *et al.*, 2008; SOARES *et al.*, 1992). Proteases do lisossomo, como a cruzipaina, principal cisteína protease de *T. cruzi* (CAZZULO *et al.*, 1990), estão concentradas nos reservossomos, para digerir o material endocitado, embora os reservossomos também sejam capazes de armazenar macromoléculas, como o colesterol, para mobilização futura quando necessário (PEREIRA *et al.*, 2011). As alterações nos reservossomos de epimastigotas, causadas pelo tratamento com os complexos de Fe mostradas nesse trabalho, possivelmente causaram um desequilíbrio na endocitose, digestão e reserva de nutrientes, afetando conseqüentemente o metabolismo energético do parasito.

O núcleo de amastigotas tratadas com ambos os complexos também sofreu alterações em sua heterocromatina, ficando concentrada em manchas no envelope nuclear. Alterações ultraestruturais, como inchaço mitocondrial e heterocromatina concentrada em manchas no envelope nuclear, já foram relatadas anteriormente como características morfológicas típicas de morte celular promovida por apoptose em tripanossomatídeos e células de mamíferos (SALVESEN & DIXIT, 1997; DEOLINDO *et al.*, 2010; ROCHA *et al.*, 2023). Portanto, podemos inferir que o mecanismo de morte celular dos parasitos provocado pelos complexos de Fe possivelmente é por apoptose *like*.

Os danos mitocondriais observados nas análises ultraestruturais de epimastigotas e amastigotas após o tratamento com ambos os complexos indicam prejuízos na função dessa organela. Isso foi confirmado pela análise do potencial de membrana mitocondrial com o marcador JC-1, um marcador de viabilidade mitocondrial fluorescente catiônico lipofílico,

usado para monitorar o potencial de membrana mitocondrial. As mitocôndrias concentram JC-1 de acordo com seu potencial de membrana interna. Em baixas concentrações JC-1 é um monômero que emite fluorescência verde (530 nm) e em concentrações mais altas quando se acumula em mitocôndrias ativas, JC-1 forma J-agregados, emitindo fluorescência vermelha (590 nm), indicando o estado mitocondrial energizado (MACEDO-SILVA *et al.*, 2011). Os tripanossomatídeos apresentam uma única mitocôndria, organela que desempenha importante papel no metabolismo energético, e cuja disfunção pode levar à morte do parasito (PEDRA-REZENDE *et al.*, 2022). Esses resultados mostraram que ambos os complexos foram capazes de afetar uma organela central do parasito, prejudicando o metabolismo energético e outras funções da mitocôndria de epimastigotas e amastigotas de *T. cruzi*.

Apesar da eficácia *in vitro* desses compostos metálicos de Fe, muitas questões permanecem sem resposta a respeito dos mecanismos moleculares envolvidos na ação dos mesmos contra *T. cruzi*. Porém, estes resultados abrem perspectivas interessantes para a investigação da eficácia dos compostos em modelo de infecção *in vivo*, bem como para uma descrição mais completa do mecanismo de ação dos compostos sobre o parasito.

5. CONCLUSÃO

Foram apresentados dois novos complexos de Fe (III), complexos (1) e (2). Ambos os complexos foram ativos contra epimastigotas e amastigotas de *T. cruzi* em concentrações na faixa nanomolar, apresentando baixa citotoxicidade para as células hospedeiras LLC-MK2, resultando em um alto índice de seletividade para ambos os complexos. A atividade anti-*Trypanosoma* parece ser independente da natureza do isômero (alfa ou beta) sendo complexo (1) ligeiramente mais ativo contra o parasito, e complexo (2) apresentando maior segurança terapêutica.

O tratamento com ambos os complexos em concentrações nanomolares gerou alterações importantes nas mitocôndrias, reservossomos e núcleo, organelas essenciais para sobrevivência do parasito. As alterações nas mitocôndrias de formas epimastigotas e amastigotas após o tratamento com ambos os complexos incluíram inchaço mitocondrial e disposição anormal da membrana externa ao redor do cinetoplasto e também alterações no arranjo do cinetoplasto. Os danos mitocondriais observados por ultraestrutura corroboram a redução no potencial de membrana mitocondrial detectado após o tratamento de ambas as formas do parasito com os complexos. Além disso, a formação de espículas no lúmen dos reservossomos de epimastigotas foi detectada após tratamentos com ambos os complexos. E nas amastigotas, os complexos foram capazes de gerar alterações nucleares, com a condensação da heterocromatina no envoltório nuclear, sugerindo morte celular do parasito semelhante a apoptose. Assim, ambos os complexos testados afetaram organelas envolvidas com funções celulares essenciais na conversão de energia, digestão de nutrientes e reserva do parasito.

Esses complexos têm potencial relevante para serem avaliados como futuros fármacos na terapia contra DC, uma vez que não há tratamento atual eficaz para a fase crônica dessa doença e, infelizmente, as doenças causadas por tripanossomatídeos continuam causando morbidade e mortalidade significativas, especialmente entre os mais pobres. Apesar da eficácia *in vitro* desses complexos, os mecanismos moleculares envolvidos em sua ação contra *T. cruzi* ainda necessitam de investigação. No entanto, esses achados abrem perspectivas interessantes para investigar a eficácia de complexos metálicos contra a forma tripomastigota infecciosa *in vitro* e em modelos de infecção *in vivo*, bem como para uma descrição mais completa do mecanismo de ação desses complexos.

6. REFERÊNCIAS BIBLIOGRÁFICAS

- ALSFORD S, HORN D. Trypanosomatid histones. **Mol Microbiol.** v. 53(2), p. 365-72, 2004.
- ALVES, C.R.; ALBUQUERQUE-CUNHA, J.M.; MELLO, C.B. *Trypanosoma cruzi*: attachment to perimicrovillar membrane glycoproteins of *Rhodnius prolixus*. **Experimental Parasitology**, [S.l.], v. 116, p. 44-52, 2007.
- BATISTA, L. C.; DE SOUZA, F. S.; DE ASSIS, V. M.; SEABRA, S. H.; BORTOLUZZI, A. J.; RENNÓ, M. N.; HORN JR., A.; DAMATTA, R. A.; FERNANDES, C.. Antiproliferative activity and conversion of tachyzoite to bradyzoite of *Toxoplasma gondii* promoted by new zinc complexes containing sulfadiazine, **RSC Adv.** v. 5, p. 100606–100617, 2015.
- BERN, C.; MONTGOMERY, S.P.; KATZ, L.; CAGLIOTI, S.; SHAMER, S. Chagas disease and the US blood supply. **Current Opinion in Infectious Disease**, [S.l.], v. 21, p. 476-482, 2008.
- BORGES, L.J.H.; BULL, É.S.; FERNANDES, C.; HORN, A. JR.; AZEREDO, N.F.; RESENDE, J.A.L.C.; FREITAS, W.R.; CARVALHO, E.C.Q.; LEMOS, L.S.; JERDY, H.; KANASHIRO, M.M. In vitro and in vivo studies of the antineoplastic activity of copper (II) compounds against human leukemia THP-1 and murine melanoma B16-F10 cell lines. **European Journal of Medicinal Chemistry**, [S.l.], v. 123, p. 128-140, 2016.
- BOSCARDIN, S.; TORRECILHAS, A.; MANARIN, R.; REVELLI, S.; GONZALEZ-REY, E.; TONELLI, R.; SILBER, A. Chagas' disease: an update on immune mechanism and therapeutic strategies. **Journal of Cellular and Molecular Medicine**, [S.l.], v. 14, p. 1-42, 2009.
- BRASIL. Vigilância em Saúde no Brasil 2003–2019. **Bol. Epidemiológico.** 2019:1–156. <https://portalarquivos2.saude.gov.br/images/pdf/2019/setembro/25/boletim-especial-21ago19-web.pdf>
- BRENNER, Z.; ANDRADE, Z.; BARRAL-NETO, M. *Trypanosoma cruzi* e Doença de Chagas, Rio de Janeiro: Guanabara Koogan, v. 2, 2000.
- BRUIJNINCX, C.A.; SADLER, P.J. New trends for metal complexes with anticancer activity. **Current Opinion in Chemical Biology**, [S.l.], v. 12, p. 1–10, 2010.

- BUCKNER, F.S.; GRIFFIN, J.H.; WILSON, A.J.; VAN VOORHIS, W.C. Potent anti-*Trypanosoma cruzi* activities of oxidosqualene cyclase inhibitors. **Antimicrobial Agents and Chemotherapy**, [S.l.], v. 45, p. 1210-1215, 2001.
- CABALLERO, A. B.; MARÍN, C.; RODRÍGUEZ-DIÉGUEZ, A.; RAMÍREZMACÍAS, I.; BAREA, E.; SÁNCHEZ-MORENO, M.; SALAS, J. M. In vitro and in vivo antiparasital activity against *Trypanosoma cruzi* of three novel 5-methyl-1,2,4-triazolo[1,5-a]pyrimidin7(4H)-one-based complexes, **J. Inorg. Biochem.** v. 105(6), p. 770–776, 2011.
- CARDOSO, A.P.; MADUREIRA, L.M.P.; SEGAT, B. B.; JENNIFER, N.C.; CARGNELUTTI, R.; CANDELA, D. R.S.; MARIANO, D. L.; PARREIRA, R.L.T.; HORN JR., A.; SEABRA, S. H.; DAMATTA, R.A.; MOREIRA, F. F.; MOREIRA, R. V.; CARAMORI, G. F.; FERNANDES, C. Development, structural, spectroscopic and in silico investigation of new complexes relevant as antitoxoplasma metallopharmacs, **J. Mol. Struct.** v. 1265, p. 133380, 2022.
- CARDOSO, A.P.; MADUREIRA, L.M.P.; SEGAT, B. B.; JENNIFER, N.C.; CARGNELUTTI, R.; CANDELA, D. R.S.; MARIANO, D. L.; PARREIRA, R.L.T.; HORN JR., A.; SEABRA, S. H.; DAMATTA, R.A.; MOREIRA, F. F.; MOREIRA, R. V.; CARAMORI, G. F.; FERNANDES, C. Development, structural, spectroscopic and in silico investigation of new complexes relevant as antitoxoplasma metallopharmacs, **J. Mol. Struct.** v. 1265, p. 133380, 2022.
- CARVALHO, T.M.U.; DE SOUZA, W. Early events related with the behaviour of *Trypanosoma cruzi* within an endocytic vacuole in mouse peritoneal macrophages. **Cell Structure and Function**, [S.l.], v. 14, n. 4, p. 383–392, 1989.
- CASSOLA A. RNA Granules Living a Post-transcriptional Life: the Trypanosomes' Case. **Curr Chem Biol.** v. 5(2), p. 108-17, 2011.
- CASTRO, D.P.; SEABRA, S.H.; GARCIA, E.S.; DE SOUZA, W.; AZAMBUJA, P. *Trypanosoma cruzi*: ultrastructural studies of adhesion, lysis and biofilm formation by *Serratia marcescens*. **Experimental Parasitology**, [S.l.], v. 117, p. 201-207, 2007.
- CAZZULO, J.J.; CAZZULO FRANKE, M.C.; MARTINEZ, J.; FRANKE DE CAZZULO, B.M. Some kinetic properties of a cysteine proteinase (cruzipain) from *Trypanosoma cruzi*. **Biochimica Biophysica Act**, v. 1037, p. 186–191, 1990.

- CDC, **Centers for Disease Control and Prevention**, Antiparasitic Treatment. 2019. https://www.cdc.gov/parasites/chagas/health_professionals/tx.html.
- CHAGAS, C. Nova tripanosomíase humana: estudos sobre a morfologia e o ciclo evolutivo do *Schizotrypanum cruzi* n. gen., n.sp., agente etiológico de nova entidade mórbida do homem. **Mem. Inst. Oswaldo Cruz**. v. 1, p. 159–218, 1909.
- CHAMOND, N.; COATNOAN, N.; MINOPRIO, P. Immunotherapy of *Trypanosoma cruzi* infections. **CurrentDrug Targets - Immune, Endocrine & Metabolic Disorders**, [S.l.], v. 2, p. 247-254, 2002.
- CINQUE, G.M.; SZAJNMAN, S.H.; ZHONG, L.; DOCAMPO, R.; SCHVARTZAPEL, A.J.; RODRIGUEZ, J.B.; GROS, E.G. Structure-activity relationship of new growth inhibitors of *Typanosoma cruzi*. **Journal of Medicinal Chemistry**, [S.l.], v. 41, p. 1540-1554, 1998.
- COURA, J.R. Chagas disease: what is known and what is need - a background article. **Memórias do Instituto Oswaldo Cruz**, Rio de Janeiro, v.102, suppl. 1, p. 113-122, 2007.
- COURA, J.R.; BORGES-PEREIRA, J. **Memórias do Instituto Oswaldo Cruz**, Rio de Janeiro, v.106, 641, 2011.
- DE SOUZA W, ATTIAS M, RODRIGUES JC. Particularities of mitochondrial structure in parasitic protists (Apicomplexa and Kinetoplastida). **Int J Biochem Cell Biol**. v. 41(10), p. 2069-80, 2009.
- DE SOUZA W, SOUTO-PADRÓN T. The paraxial structure of the flagellum of trypanosomatidae. **J Parasitol**. v. 66(2), p. 229-36, 1980.
- DE SOUZA W. Basic cell biology of *Trypanosoma cruzi*. **Curr Pharm Des**. v. 8(4), p. 269-85, 2002.
- DE SOUZA W. Cell biology of *Trypanosoma cruzi*. **Int Rev Cytol**. v. 86, p. 197-283, 1984.
- DEOLINDO, P.; TEIXEIRA-FERREIRA, A.S.; DAMATTA, R.A.; ALVES, E.W. L-amino acid oxidase activity present in fractions of *Bothrops jararaca* venom is responsible for the induction of programmed cell death in *Trypanosoma cruzi*. **Toxicon**. v. 56, p. 944–955, 2010.

- DIAS, J.C.P. Globalização, iniquidade e doença de Chagas. **Caderno de Saúde Pública**, Rio de Janeiro, v. 23, suppl.1, p. s13-s22, 2007
- DIAS, J.C.P.; SCHOFIELD, C.J. The evolution of Chaga's Disease (American Trypanosomiasis) Control after 90 Years since Carlos Chagas Discovery. **Memórias do Instituto Oswaldo Cruz**, Rio de Janeiro, v. 94, p. 103-121, 1999.
- DIAS, J.P.; BASTOS, C.; ARAÚJO, E.; MASCARENHAS, A.V.; MARTINS NETTO, E.; GRASSI, F. Acute Chagas disease outbreak associated with oral transmission. **Revista Sociedade Brasileira de Medicina Tropical**, Uberaba, v. 41, p. 296-300, 2008.
- DOCAMPO, R.; STOPPANI, A.O. Genetation of superoxide anion and hydrogen peroxide induced by nifurtimox in *Trypanosoma cruzi*. **Archives of Biochemistry and Biophysics**, [S.l.], v. 197, p. 317-321, 1979.
- ELIAS MC, FARIA M, MORTARA RA, et al. Chromosome localization changes in the *Trypanosoma cruzi* nucleus. **Eukaryot Cell**. v. 1(6), p. 944-53, 2002.
- FAIRLAMB, A.H. Future prospects for the chemotherapy of Chaga's disease. **Medicina**, Buenos Aires, v. 59, p. 179, 1999.
- FERNANDES, C.; HORN JR., A.; LOPES, B. F.; BULL, E. S.; AZEREDO, N. F. B.; KANASHIRO, M. M.; BORGES, F. V.; BORTOLUZZI, A. J.; SZPOGANICZ, B.; PIRES, A. B.; FRANCO, R. W. A.; ALMEIDA, J. C. A.; MACIEL, L. L. F.; RESENDE, J. A. L. C.; SCHENK, G.. Induction of apoptosis in leukemia cell lines by new copper(II) complexes containing naphthyl groups via interaction with death receptors, **J. Inorg. Biochem.** v. 153, p. 68–87, 2015
- FIDALGO LM, GILLE L. Mitochondria and trypanosomatids: targets and drugs. **Pharm Res.** v. 28(11), p. 2758-70, 2011.
- FONSECA-BERZAL, C.; IBÁÑEZ-ESCRIBANO, A.; REVIRIEGO, F.; CUMELLA, J.; MORALES, P.; JAGEROVIC, N.; NOGAL-RUIZ, J. J.; ESCARIO, J. A.; DA SILVA, P. B.; SOEIRO, MDE. N.; GÓMEZBARRIO, A.; ARÁN, V. J. Antichagasic and trichomonacidal activity of 1-substituted 2-benzyl-5-nitroindazolin-3-ones and 3-alkoxy-2-benzyl-5-nitro-2H indazoles, **Eur. J. Med. Chem.** v. 115, p. 295–310, 2016.
- FRICKER SP, MOSI RM, CAMERON BR, BAIRD I, ZHU Y, ANASTASSOV V, COX J, DOYLE PS, HANSELL E, LAU G, LANGILLE J, OLSEN M, QIN L, SKERLJ R,

- WONG RS, SANTUCCI Z, MCKERROW JH. Metal compounds for the treatment of parasitic diseases. **J Inorg Biochem.** v. 102, p. 1839-1845, 2008.
- FRICKER, S.P. Metal based drugs: from serendipity to design. **Dalton Transactions**, [S.l.], v. 43, p. 4903-4917, 2007.
- FRIGGERI, L.; SCIPIONE, L.; COSTI, R.; KAISER, M.; MORACA, F.; ZAMPERINI, C.; BOTTA, B.; DI SANTO, R.; DE VITA, D.; BRUN, R.; TORTORELLA, S. New Promising Compounds with in Vitro Nanomolar Activity against *Trypanosoma cruzi*, **ACS Med Chem Lett.** v. 4(6), p. 538-541, 2013.
- G. SCALESE, I. MACHADO, C. FONTANA, G. RISI, G. SALINAS, L. PÉREZ-DÍAZ, D. GAMBINO, New heteroleptic oxidovanadium(V) complexes: synthesis, characterization and biological evaluation as potential agents against *Trypanosoma cruzi*, **J. Biol. Inorg. Chem.** v. 23(8), p. 1265-1281, 2018.
- GARCIA, E.S.; RATCLIFFE, N.A.; WHITTEN, M.M.; GONZALEZ, M.S.; AZAMBUJA, P. Exploring the role of insect host factors in the dynamics of *Trypanosoma cruzi*-*Rhodnius prolixus* interactions. **Journal of Insect Physiology**, [S.l.], v. 53, p. 11-21, 2007.
- GRUENBERG J. The endocytic pathway: a mosaic of domains. **Nat Rev Mol Cell Biol.** v. 2(10), p. 721-30, 2001
- GUERRA, W.; AZEVEDO, E.A.; MONTEIRO, A.R.S.; BUCCIARELLI-RODRIGUEZ, M.; CHARTONE-SOUZA, E.; NASCIMENTO, A.M.A.; FONTES, A.P.S.; LE MOYEC, L.; PEREIRA-MAIA, E.C. Synthesis, characterization, and antibacterial activity of three palladium(II) complexes of tetracyclines. **Journal of Inorganic Biochemistry**, [S.l.], v. 99, p. 2348-2354, 2005.
- JANZEN CJ, FERNANDEZ JP, DENG H, DIAZ R, HAKE SB, CROSS GA. Unusual histone modifications in *Trypanosoma brucei*. **FEBS Lett.** v. 580(9), p. 2306-10, 2006.
- MACEDO-SILVA, S. T.; DE OLIVEIRA SILVA, T. L.; URBINA, J. A.; DE SOUZA, W.; RODRIGUES, J. C. Antiproliferative, Ultrastructural, and Physiological Effects of Amiodarone on Promastigote and Amastigote Forms of *Leishmania amazonensis*, **Mol. Biol. Int.**, 876021, 2011.

- MARTINS-MELO, F.R.; RAMOS JÚNIOR, A.N.; ALENCAR, C.H.; HEUKELBACH, J. Prevalence of Chagas disease in Brazil: a systematic review and meta-analysis. **Acta Tropica**, Rio de Janeiro, v. 130, p. 167-74, 2014.
- MENDES, I.C.; MOREIRA, J.P.; ARDISSON, J.D.; DOS SANTOS, R.G.; DA SILVA, P.R.O.; GARCIA, I.; CASTIÑEIRAS, A.; BERALDO, H. Organotin(IV) complexes of 2-pyridineformamide-derived thiosemicarbazones: Antimicrobial and cytotoxic effects. **European Journal of Medicinal Chemistry**, [S.l.], v. 43, p. 1454-1461, 2005.
- MENNA-BARRETO, R.F.S.; DE CASTRO, S.L. The Double-Edged Sword in Pathogenic Trypanosomatids: The Pivotal Role of Mitochondria in Oxidative Stress and Bioenergetics, **BioMed Research International**. v. 2014, p. 1-14, 2014.
- MONCAYO, A.; ORTIZ YANINE, M.I. An update on Chagas disease (human American trypanosomiasis). **Annals of Tropical Medicine and Parasitology**, [S.l.], v. 100, p. 663-677, 2006.
- MONTEIRO AC, ABRAHAMSON M, LIMA AP, et al. Identification, characterization and localization of chagasin, a tight-binding cysteine protease inhibitor in *Trypanosoma cruzi*. **J Cell Sci**. v. 114(Pt 21), p. 3933-42, 2001.
- MOREIRA FF, PORTES JA, BARROS AZEREDO NF, FERNANDES C, HORN A JR, SANTIAGO CP, SEGAT BB, CARAMORI GF, MADUREIRA LMP, CANDELA DRS, MARQUES MM, LAMOUNIER CAMARGOS RESENDE JA, DE SOUZA W, DAMATTA RA, SEABRA SH. Development of new dinuclear Fe(III) coordination compounds with in vitro nanomolar antitrypanosomal activity. **Dalton Trans**. v. 14;50(35), p. 12242-12264, 2021.
- MOREL, C.M. Chagas disease, from discovery to control- and beyond: history, myths and lessons to take home. **Memórias do Instituto Oswaldo Cruz**, Rio de Janeiro, v. 94, p. 3-16, 1999.
- MORRIS JC, DREW ME, KLINGBEIL MM, et al. Replication of kinetoplast DNA: an update for the new millennium. **Int J Parasitol**. v. 31(5-6), p. 453-8, 2001.
- NEVES, D.P. **Parasitologia Humana**, São Paulo: Atheneu, v. 11, 2005.

- NÓBREGA, A.A.; GARCIA, M.H.; TATTO, E.; OBARA, M.T.; COSTA, E.; SOBEL, J.; ARAUJO, W.N. Oral transmission of Chagas Disease by consumption of açai Palm Fruit, Brasil. **Emerging Infectious Diseases**, [S.l.], v. 15, p. 653-655, 2009.
- NOGUEIRA, N.F.S.; GONZALEZ, M.S.; GOMES, J.E. *Trypanosoma cruzi*: involvement of glycoinositolphospholipids in the attachment to the luminal midgut surface of *Rhodnius prolixus*. **Experimental Parasitology**, [S.l.], v. 116, p. 120-128, 2007.
- NUNES, M.C.; DONES, W.; MORILLO, C.A.; ENCINA, J.J.; RIBEIRO, A.L. Chagas disease: an overview of clinical and epidemiological aspects. **Journal of the American College of Cardiology**, [S.l.], v. 62(9), p. 767-776, 2013.
- NWAKA, S.; HUDSON, A. Innovative lead discovery strategies for tropical diseases. **Nature Reviews Drug Discovery**, [S.l.], v. 5, p. 941-955, 2006.
- ORVIG, C.; ABRAMS, M.J. Medicinal inorganic chemistry: introduction. **Chemical Reviews**, [S.l.], v. 99(9), p. 2201-2204, 1999.
- PAIXÃO, D. A.; LOPES, C. D.; CARNEIRO, Z. A.; SOUSA, L. M.; DE OLIVEIRA, L. P.; LOPES, N. P.; PIVATTO, M.; CHAVES, J. D. S.; DE ALMEIDA, M. V.; ELLENA, J.; MOREIRA, M. B.; NETTO, A. V. G.; DE OLIVEIRA, R. J.; GUILARDI, S.; DE ALBUQUERQUE, S.; GUERRA, W. In vitro anti-*Trypanosoma cruzi* activity of ternar copper(II) complexes and in vivo evaluation of the most promising complex, **Biomed. Pharmacother.** v. 109, p. 157– 166, 2019.
- PARUSSINI F, GARCÍA M, MUCCI J, et al. Characterization of a lysosomal serine carboxypeptidase from *Trypanosoma cruzi*. **Mol Biochem Parasitol.** v. 131(1), p. 11-23, 2003.
- PEDRA-REZENDE, Y.; BOMBAÇA, A.C.S.; MENNA-BARRETO, R.F.S. Is the mitochondrion a promising drug target in trypanosomatids? **Mem Inst Oswaldo Cruz.** v. 21, p. 117:e210379, 2022.
- PEREIRA, M.G.; NAKAYASU, E.S.; SANT'ANNA, C.; DE CICCO, N.N.; ATELLA, G.C.; DE SOUZA, W.; ALMEIDA, I.C.; CUNHA-E-SILVA, N. *Trypanosoma cruzi* epimastigotes are able to store and mobilize high amounts of cholesterol in reservosome lipid inclusions. **PLoS ONE**, v. 6, e22359, 2011.
- PÉREZ-REBOLLEDO, A.; AYALA, J.D.; DE LIMA, G.M.; MARCHINI, N.; BOMBIERI, G.; ZANI, C.L.; SOUZA-FAGUNDES, E.M.; BERALDO, H. Structural

studies and cytotoxic activity of N(4)-phenyl-2-benzoylpyridine thiosemicarbazone Sn(IV) complexes. **European Journal of Medicinal Chemistry**, [S.l.], v. 40, p. 467-472, 2005.

PORTES, J.A.; AZEREDO, N.F.; SIQUEIRA, P.G.T.; SOUZA, T.G.; FERNANDES, C.; HORN, A.JR.; CANDELA, D.R.S.; DE SOUZA, W.; DAMATTA, R.A.; SEABRA, S.H.; A new iron(III) complex-containing sulfadiazine inhibits the proliferation and induces cystogenesis of *Toxoplasma gondii*. **Parasitology Research**, v. 117, p. 2795-2805, 2018.

PORTES, J.A.; MOTTA, C.S.; AZEREDO, N.F.; FERNANDES, C.; HORN, A.JR.; DE SOUZA, W.; DAMATTA, R.A.; SEABRA, S.H.; *In vitro* treatment of *Toxoplasma gondii* with copper(II) complexes induces apoptosis-like and cellular division alterations. **Veterinary Parasitology**, v. 245, p. 141-152, 2017.

PORTES, J.A.; SOUZA, T.G.; DOS SANTOS, T.A.; DA SILVA, L.L.; RIBEIRO, T.P.; PEREIRA, M.D.; HORN, A.JR.; FERNANDES, C.; DAMATTA, R.A.; DE SOUZA, W.; SEABRA, S.H.; Reduction of *Toxoplasma gondii* Development Due to Inhibition of Parasite Antioxidant Enzymes by a Dinuclear Iron(III) Compound. **Antimicrobial Agents Chemotherapy**, [S.l.], v. 59, n. 12, p. 7374-7386, 2015.

RASSI JR., A.; RASSI, A.; MARIN-NETO, J.A. Chagas disease. **Lancet**, 375 (9723), p. 1388-1402, 2010.

RASSI JÚNIOR, A.; RASSI, A.; DE REZENDE, J.M. American trypanosomiasis (Chagas disease). **Infectious Disease Clinics of North America**, [S.l.], v. 26, p. 275-291, 2012.

RASSI JÚNIOR, A.; RASSI, A.; MARIN-NETO, J.A. Chagas Disease. **The Lancet**, Reino Unido, v. 375, p. 1387-1402, 2010.

ROCHA SM, HORN A JR, R DE M L TERRA A, REZENDE LM, MOREIRA FF, DAMATTA RA, XAVIER FR, CERVO R, CARGNELUTTI R, MOORKKANNUR SN, OWENBY G, PRABHAKAR R, SEABRA SH, FERNANDES C. In vitro anti-Leishmania activity of new isomeric cobalt(II) complexes and in silico insights: Mitochondria impairment and apoptosis-like cell death of the parasite. **J Inorg Biochem**. v. 240:112088, 2023.

- SALVESEN, G.S.; DIXIT, V.M. Caspases: intracellular signaling by proteolysis. **Cell**, v. 91, p. 443-446, 1997.
- SANT'ANNA, C.; PEREIRA, M.G.; LEMGRUBER, L.; DE SOUZA, W.; CUNHA E SILVA, N.L. New insights into the morphology of *Trypanosoma cruzi* reservosome. **Microscopy Research and Technique**, v. 71, p. 599–605, 2008.
- SANTOS CC, SANT'ANNA C, TERRES A, et al. Chagasin, the endogenous cysteine-protease inhibitor of *Trypanosoma cruzi*, modulates parasite differentiation and invasion of mammalian cells. **J Cell Sci**. v. 118(Pt 5), p. 901-15, 2005.
- SCHOFIELD, C.J.; JANNIN, J.; SALVATELLA, R. The future of Chagas Disease control. **Trends in Parasitology**, [S.l.], v. 22, p. 583-588, 2006.
- SILVEIRA, A.C.; DIAS, J.C.P. O controle da transmissão vetorial. **Revista Sociedade Brasileira de Medicina Tropical**, Uberaba, v. 44, p. 52-63, 2011.
- SOARES MJ, DE SOUZA W. Cytoplasmic organelles of trypanosomatids: a cytochemical and stereological study. **J Submicrosc Cytol Pathol**. v. 20(2), p. 349-61, 1988.
- SOARES, M.J.; SOUTO-PADRON, T.; DE SOUZA, W. Identification of a large pre-lysosomal compartment in the pathogenic protozoon *Trypanosoma cruzi*. **Journal of Cell Science**, v. 102, p.157–167, 1992.
- TANOWITZ, H.B.; KIRCHHOFF, L.V.; SIMON, D.; MORRIS, S.A.; WEISS, L.M. & WITTNER, M. Chagas' Disease. **Clinical Microbiology Reviews**, [S.l.], v. 5, p. 400-419, 1992.
- TEIXEIRA DE, BENCHIMOL M, CREPALDI PH, DE SOUZA W. Interactive multimedia to teach the life cycle of *Trypanosoma cruzi*, the causative agent of Chagas disease. **PLoS Negl Trop Dis**. v. 6(8), p. 1749, 2012.
- TEIXEIRA, A.R.L.; NITZ, N.; GUIMARO, M.C.; GOMES, C.; SANTOS-BUCH, C.A. Chagas disease. **Postgraduate Medical Journal**, [S.l.], v. 82(974), p. 788-798, 2006.
- TONG, W.; LOWIS, D.R.; PERKINS, R.; CHEN, Y.; WELSH, W.J.; GODDETTE, D.W.; HERITAGE, T.W.; SHEEHAN, D.M. Evaluation of quantitative structure-activity relationship methods for large-scale prediction of chemicals binding to the estrogen receptor. **Journal of Chemical Information and Computer Sciences**, Washington, v. 38, p. 669-677, 1998.

- VAN HELLEMOND JJ, OPPERDOES FR, TIELENS AG. The extraordinary mitochondrion and unusual citric acid cycle in *Trypanosoma brucei*. **Biochem Soc Trans.** v. 33(5), p. 967-71 2005.
- VAN RIJT S.H.; SADLER, P.J. Current applications and future potential for bioinorganic chemistry in the development of anticancer drugs. **Drug Discov Today**, [S.l.], v. 14, p. 1089–1097, 2009.
- VERONESI, R. Doenças Infecciosas e parasitárias. **Guanabara Koogan**, Rio de Janeiro, v. 8, p. 1082, 1991.
- VIEITES, M.; SMIRCICH, P.; PARAJÓN-COSTA, B.; RODRÍGUEZ, J.; GALAZ, V.; OLEA-AZAR, C.; OTERO, L.; AGUIRRE, G.; CERECETTO, H.; GONZÁLEZ, M.; GÓMEZ-BARRIO, A.; GARAT, B.; GAMBINO, D. Potent in vitro anti-*Trypanosoma cruzi* activity of pyridine-2- thiol N-oxide metal complexes having an inhibitory effect on parasite-specific fumarate reductase, **J. Biol. Inorg. Chem.** v. 13, p. 723–735, 2008.
- VIOTTI, R.; VIGLIANO, C.; LOCOCO, B.; ALVAREZ, M.G.; PETTI, M.; BERTOCCHI, G.; ARMENTI, A. Side effects of benznidazole as treatment in chronic Chagas disease: fears and realities. **Expert Reviews of Anti-infective Therapy**, [S.l.], v. 7, p. 157-163, 2009.
- WHO, Chagas disease (American trypanosomiasis). **World Health Organization** Fact sheet No. 340. Geneva: World Health Organization, 2016.
- WHO. Chagas disease (American trypanosomiasis). **World Health Organization**, Geneva, Fact Sheet N°: 340, p. 1-4, 2015.
- WHO. Chagas disease (American trypanosomiasis). **World Health Organization**, Geneva, Fact Sheet, [https://www.who.int/news-room/fact-sheets/detail/chagas-disease-\(american-trypanosomiasis\)](https://www.who.int/news-room/fact-sheets/detail/chagas-disease-(american-trypanosomiasis)), 2022.
- WRIGHT, G.D.; SUTHERLAND, A.D. New strategies for combating multidrug-resistant bacteria. **Trends in molecular medicine**, [S.l.], v. 13(6), p. 260-267, 2007.
- YOSHIDA, N. Molecular mechanisms of *Trypanosoma cruzi* infection by oral route. **Memórias do Instituto Oswaldo Cruz**, Rio de Janeiro, v. 104, p. 101–107, 2009.